A GEOSTATISTICALLY BASED METHOD FOR DESIGNING BATCH DIVERSION IN MATRIX ACIDIZING

A Dissertation

by

ROBERT MARK SHIRLEY

Submitted to the Office of Graduate and Professional Studies of
Texas A&M University
in partial fulfillment of the requirements for the degree of

DOCTOR OF PHILOSOPHY

Chair of Committee,	Alfred Daniel Hill
Co-Chair of Committee,	Ding Zhu
Committee Members,	Nobuo Morita
	Victor Ugaz
Head of Department,	Jeffrey Spath

August 2019

Major Subject: Petroleum Engineering

ABSTRACT

Since the inception and use of matrix acidizing to stimulate wells, the oil and gas industry has continued to develop new and improved fluids and materials for chemical diversion. However, the effects of chemical diversion are still inconsistent, difficult to diagnose, and difficult to predict. This dissertation seeks to develop a method for designing batch diversion treatments of the recently developed diverting agent, Polylactic Acid (PLA), even when the permeability profile of the well that is being stimulated is unknown.

In the last decade, there have been several publications describing the use of PLA as a diverting agent in multistage matrix acidizing treatments. The aliphatic polyester is particularly useful as a diverting agent because it hydrolyzes in the presence of heat and water, leaving no residue in the formation, thus negating the need for any clean-up fluids. Most of the publications about PLA diversion focus on the physical and chemical attributes of the diverter and attempt to demonstrate its effectiveness via field trials, but few have investigated how PLA creates resistance to fluid flow.

In this study, the mechanisms by which PLA can cause diversion during a multistage treatment are analyzed using laboratory experiments. The results from these experiments are used to develop a model that describes how local injectivity is affected based on the amount of diverter that is deposited. This model is then incorporated into a near wellbore simulator and validated using published results. Finally, a geostatistical tool, sequential indicator simulation, is used to characterize the near wellbore permeability

profile using permeability profiles from neighboring wells. This kriging-based interpolation technique is used because permeability profiles are seldom known with a high degree of accuracy, but it is more common to know the statistical distribution of the permeability based on neighboring wells.

These experiments and simulations have revealed that PLA causes diversion very differently if it fills wormholes versus if it builds a filter cake at the surface. A greater resistance to flow can be achieved if the diverter bridges the wormhole opening and builds a filter cake on the sand face as opposed to filling the wormholes. It is also shown that even if PLA fills the wormhole, further acid injection causes the dominant wormholes to continue to propagate. The simulations have also shown that the use of PLA as a diverter can create a more uniform skin factor profile, but it can worsen the total skin factor.

The method to design batch PLA diversion treatments, when the permeability distribution along the well is not known, was applied to a well in a synthetic reservoir that contains real well log data. The method was able to identify an optimal batch size of PLA based on the predicted cumulative well production. The results also demonstrate that the location of the high permeability streaks relative to the heel and toe have an impact on whether the application of diversion could improve the cumulative production of the well or not. Finally, the results show that if there is a mix of limestone and dolomite along the well, if the dolomite has a low permeability relative to the limestone, a diversion treatment tends to have a more significant impact on the cumulative production.

DEDICATION

To Jesus Christ, my closest friend, and ever-present help in times of need

and to my wife and my daughter, who are the favorite part of my life.

ACKNOWLEDGEMENTS

I would like to thank my committee chair and co-chair, Prof. Hill and Prof. Zhu, for their guidance and support. In particular, I would like to thank Dr. Hill for all the time he spent discussing ideas and my results with me; despite having several large projects and even being department head for a majority of my degree, he always found time to help me. I would like to thank Dr. Zhu for challenging me to think differently and approach presentations and discussions with more patience and thought. I would also like to thank them for allowing me to do collaborative research with Texas A&M Qatar. I would like to thank Dr. Da Motta for all that he taught me through our daily meetings during my stay in Qatar, and for being a part of my committee for some time. I would also like to thank my committee members, Prof. Ugaz, and Prof. Morita, for their contributions and assistance.

Additionally, I would like to thank my family and, especially, my father and mother, Gordon and Angela, for their love, encouragement and strong belief in my potential.

Finally, I would like to thank my wife, Candice, for all the selfless sacrifices she has made to join me in chasing this dream.

CONTRIBUTORS AND FUNDING SOURCES

Contributors

This work was supervised by a dissertation committee consisting of Professor A. D. Hill (advisor), Professor D. Zhu (co-advisor) and Professor N. Morita of the Department of Petroleum Engineering and Professor V. Ugaz of the Department of Chemical Engineering.

Funding Sources

Graduate study was supported by the Acid Stimulation Research Project (ASRP) Sponsors and by the Harold Vance Department of Petroleum Engineering.

This work was also made possible in part by a diversity fellowship from the Office of Graduate and Professional Studies (OGAPS).

NOMENCLATURE

I_{ani}	Anisotropy ratio
χ	Acid dissolving power
$\overline{k}$	Average permeability of the well
C_{da}	Concentration of diverting agent (volume of particles/volume of suspension)
C	Covariance
A	Cross-sectional area to flow
ρ_{da}	Density of the diverting agent particles
ΔP	Drawdown pressure
E	Expected value
λ	Kriging weights
L	Length of the treatment interval
l_{PLA}	Length of the wormholes filled by PLA
m_{cake}	Mass of filter cake
m_{PW}	Mass of PLA particles in the wormholes
h	Payzone thickness
k	Permeability
k*	Permeability at an unsampled location
k_s	Permeability of the damaged region
k_{cake}	Permeability of the filter cake
k_i	Permeability of the ith grid

φ_{cake}	Porosity of the filter cake
ΔP	Pressure drop
ΔP_{cake}	Pressure drop across a filter cake
r_s	Radius of the damaged region
r_w	Radius of the wellbore
r_{wh}	Radius of the wormholed region
I	Random indicator variable
γ	Semi-variance
s_{cake}	Skin factor due to a filter cake
s_{PLA}	Skin factor due to a multistage treatment of acid and PLA
s_i	Skin factor of the ith grid
α	Specific cake resistance
l_{cake}	Thickness of the filter cake
l	Thickness of the porous medium
s_{total}	Total skin factor of the well
μ	Viscosity
V_{acid}	Volume of acid injected
V_{cake}	Volume of filter cake
V_{pc}	Volume of particles deposited in a filter cake
V_{pw}	Volume of PLA filter cake in the wormholes
V_w	Volume of wormholes created
q	Volumetric flow rate

q_i Volumetric flow rate of the ith grid

B_o Volumetric formation factor

y_b Well spacing (or distance to the drainage boundary in the y-direction)

TABLE OF CONTENTS

Page

LIST OF FIGURES

Page

LIST OF TABLES

Page

1. INTRODUCTION AND OBJECTIVES

When fluid is pumped into a well, a majority of the fluid tends to flow into zones with the highest permeability, or least formation damage. Diversion techniques are used to allow stimulation fluids to fully contact the open well intervals and by extension treat the entire well. The diversion techniques that are used in matrix acidizing can be categorized into four groups: mechanical isolation, rate and pressure, coiled tubing, or chemical diversion techniques.

1.1 Types of Diversion Used in Matrix Acidizing

Mechanical isolation techniques control the point of fluid entry into the formation by limiting where fluid can flow within the wellbore or where fluid can exit the wellbore. These techniques include the use of packers, plugs, ball sealers, perforation wash tools, and sliding sleeves. These methods can be seen as the surest ways to evenly distribute acid into the formation along the well. However, they can be costly and time-consuming. Furthermore, if there are any issues during their deployment or use, mechanical intervention or workover may be required to resolve these issues.

Rate and pressure techniques include limited entry treatment, maximum pressure differential and injection rates (MAPDIR), and controlled acid jetting. The limited entry technique was first postulated by Lagrone and Rasmussen (1962). This technique involves limiting the number and diameter of perforations and injecting fluid at a high rate. The perforations act as chokes that can create restrictions to flow where needed. MAPDIR was developed by Paccaloni (1993). This technique suggests pumping the highest injection

rate possible without fracturing the formation. This technique is not like the other diversion techniques, in the sense that it does not alter the relative flow of the stimulation fluid in the high or low permeability regions. However, it achieves the highest possible injection rates into the low permeability regions (without mechanically diverting flow) and thus attempts to attain complete stimulation coverage. This technique negates the need for any chemicals or mechanical tools, and it removes any risk of permanently damaging the formation, but it comes at the cost of higher volumes of stimulation fluid. Controlled acid jetting combines limited entry liners with MAPDIR (Hansen and Nederveen 2002). In acid jetting, small orifices or nozzles are used to create high-velocity jets of acid that impinge on the borehole wall. This is typically done using perforated drill pipe, pre-drilled liners, open hole perforations or specialized tools.

Coiled tubing has become a widely accepted and routinely used placement technique in matrix acidizing. Instead of conventional bullheading (i.e., pumping the stimulation fluid down the tubing and into the casing), acid can be delivered through coiled tubing. The coiled tubing can be moved along the well during the treatment to alter where the acid is delivered in the wellbore. This technique is useful because it does not directly expose the wellhead and completion tubulars to corrosive acid solutions. However, coiled tubing is limited by how far within the well it can reach, and it limits the acid injection rate because the coiled tubing diameter is smaller than that of the drill pipe or production tubing. More importantly, it has been shown that the movement of the tubing does not affect the distribution of acid into the formation (Eckerfield, 2000). Once fluid enters the wellbore from the coiled tubing, the majority of the fluid flows through the path of least

resistance into the formation, even if the fluid must flow through the wellbore to the high permeability zones.

Chemical diverting agents include foams, viscous fluids, and particulates. Foam is a dispersion of gas in a liquid. The liquid film that separates the bubbles in the foam reduces the gas mobility, which in turn, lowers the liquid saturation and the liquid relative permeability (Zhou and Rossen, 1995). Viscous fluids cause diversion by creating a bank of viscous fluid in the high permeability zones and the existing wormholes so that there is increased resistance to subsequent stimulation fluids. Particulate diversion, which is the primary focus of this dissertation, works by creating a relatively low permeability filter cake in the wormholes or on the sandface. The filter cake induces a pressure drop and resistance to subsequent flow wherever it is deposited. The magnitude of the restriction to fluid flow is related to the amount of the diverting agent that has been deposited at that location. The local flow restrictions result in a redistribution of the flow of acid into the formation along the well and allow a greater proportion of the acid to flow into low permeability/highly damaged zones. Chemical diverters can be very effective, relatively cheap and quick, but they typically carry a risk of negatively affecting the subsequent production of the well if they are not fully removed prior to production.

1.2 Polylactic Acid

Over the past 80 years, there have been several forms of chemical diverters used for matrix acidizing treatments. One of the more recent diverting agents to be used is Polylactic Acid (PLA). PLA is an aliphatic polyester that hydrolytically degrades in the

presence of water to form a carboxylic acid and an alcohol. The ester bonds in the macromolecular main chains are continually broken to form the monomer, lactic acid. The hydrolysis reaction is illustrated in Figure 1-1.

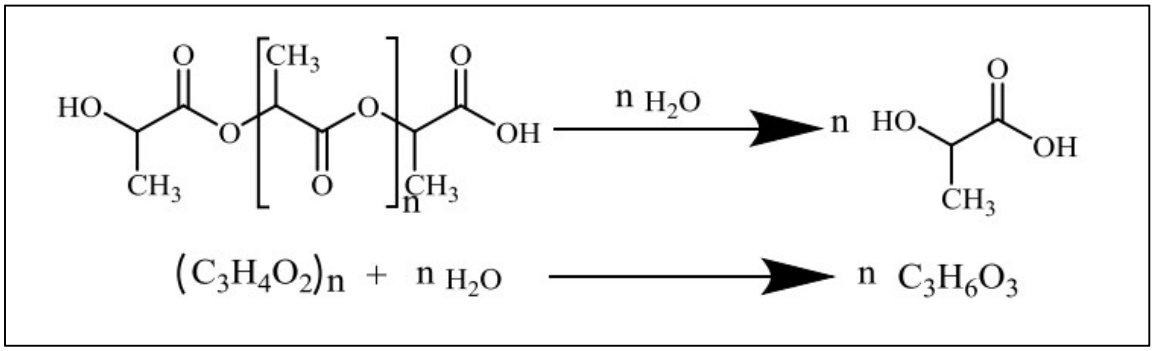

Figure 1-1: Hydrolysis of PLA (Adapted from Jin et al., 2017)

Both PLA and its monomer, lactic acid, are biodegradable and non-toxic. PLA can be manufactured from corn. Lactic acid (milk acid) is produced in our bodies. Since PLA's degradation products are water soluble and do not leave any residue, there is no need for clean-up fluids to be pumped after the acidizing treatment. PLA is also suitable for use as a diverting agent because it is stable under pumping conditions and insoluble in water. PLA can be manufactured in a variety of shapes and sizes and is even used in multi-modal size distributions (see Figure 1-2). The degradation rate of PLA varies based on a vast number of factors such as its molecular weight, the degree of crystallinity, pH, temperature, brine and acid concentration (Willberg and Dismuke 2009, B. Reddy and J. Cortez 2014). This allows PLA to be engineered for its specific application.

Figure 1-2: Different forms of PLA (Granular, Powder, and Fiber) (Adapted from Yoshimura et al., 2014)

Several recently published papers have described 'novel degradable diverting agents.' Since they also degrade in the presence of heat and water to form lactic acid, we can generally assume that this refers to the use of PLA (Van Domelen, 2017). Several field applications using PLA in matrix acidizing treatments have been carried out in multiple countries, and it has been shown that PLA, in its different forms, can be used to create a uniform skin profile along the well (Reddy and Cortez, 2014).

1.3 Use of Geostatistics in Reservoir Characterization

Reservoir characterization refers to describing reservoir characteristics using all of the available data. A wide variety of data can be used such as core and log data, tracer data, well tests, production data, and even seismic data. This data can be useful in describing a variety of reservoir properties such as facies distribution, depositional environment, and reservoir porosity and permeability. Having more data available can lead to a better reservoir description.

Reservoir heterogeneity refers to spatial variations in reservoir properties. The wells that are considered candidates for diversion during a matrix acidizing stimulation typically have highly heterogeneous permeability (ranging from a few milli-darcies to several darcies) and can even contain different lithologies (limestone, dolomite, and anhydrite) (Thabet et al., 2009). Permeability and lithology, among other properties, are extremely important in determining whether diversion should be used, what type of diversion is most suitable and how to optimize a diversion treatment. Moreover, the information that is needed to determine the near wellbore permeability such as production logs or core data is seldom known for a well before its stimulation. It is more common to know the statistical distribution of permeability from neighboring wells. Hence, geostatistical tools can be useful tools for describing the unknown reservoir permeability.

Geostatistical tools account for the spatial relationships of properties when estimating a given property at an unsampled location (i.e., there is no observed data for that location). Geostatistical techniques take advantage of the fact that in many natural phenomena, variables that are close together tend to be more similar than variables spaced far apart. As distance increases between two measurements, their similarity decreases. The main advantages of geostatistical tools for interpolation of reservoir properties are that: the spatial relationships can be customized for the property being estimated; they can provide estimation errors and uncertainty estimates; they perform declustering of the input data; and they honor the input or sampled data. The disadvantages of these techniques are that large amounts of sampled data may be required; they involve subjective decision

making; and they can be more computationally expensive than simpler interpolation methods.

Geostatistical techniques are applied in three steps: 1) assumption of stationarity 2) spatial modeling of the data and 3) estimation of the property at unsampled locations. Statistical stationarity of order "r" implies that moments up to order "r" are independent of location. Hence, a random function is second-order stationary if its mean (1^{st} moment) and covariance/variogram (2^{nd} moment) are finite and independent of location, i.e., its 2^{nd} order probability density function is invariant under translation.

The next step is to develop a spatial relationship for the variable. As the distance between successive measurements increases, the similarity between the measurements decreases. This similarity, or lack of similarity, can be mathematically defined using a variogram. A variogram is a plot of the semi-variance, γ, versus separation distance between pairs of data, h, also called lag. Semi-variance measures the dissimilarity between two values as shown in Eq. 1-1.

$$\gamma(X,Y) = \frac{1}{2}E((X-Y)^2) \tag{1-1}$$

Since the similarity of two measurements decreases with increasing lag distance, the semi-variance increases with increasing lag distance. A typical variogram is as shown in Figure 1-3.

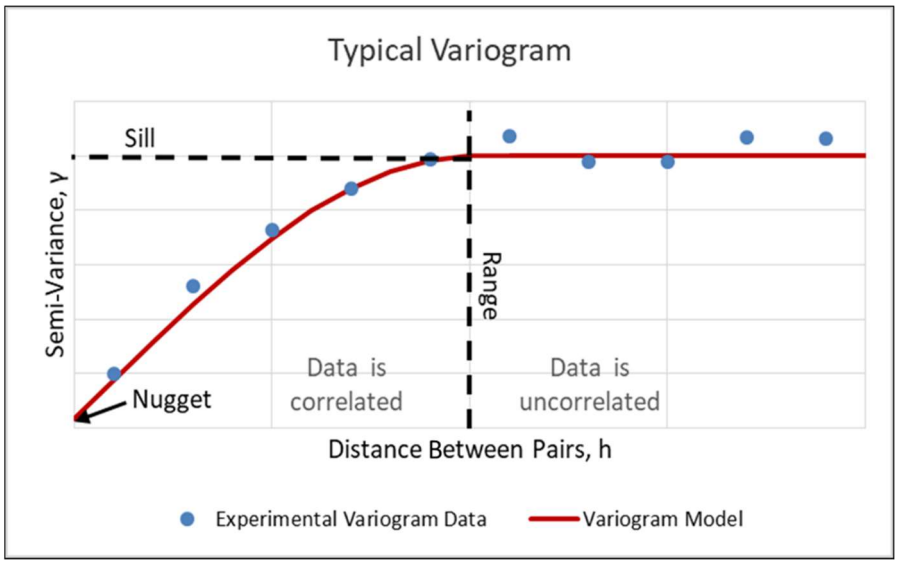

Figure 1-3: A typical variogram illustrating its various components

The final stage of the geostatistical process is to estimate the variable at the unknown locations. The variogram is used to weigh the influence of the known sample data on the estimate of the variable at an unknown location. The most common technique for estimation is called kriging. Conditional simulation is also often used along with kriging to create multiple possible and equally probable realizations.

1.4 Kriging

Kriging was developed by Danny Krige, a South African geoscientist who used the kriging tools in gold mines. The mathematical validity was later developed by Georges Matheron (Matheron 1965). Kriging estimates a property at an unknown location, k*, as a linear combination of the available measurements of the property k from the nearby available samples (see Eq 1-2).

$$k^* = \sum_{i=1}^{n} \lambda_i \, k_i \qquad (1\text{-}2)$$

In other words, kriging estimates the unsampled value as a weighted combination of the sampled values. The weights assigned to the neighboring value, λ_i, are calculated using algorithms that minimize the estimation variance and create an unbiased estimate. The weights are calculated using the covariance between the known data points and the covariance between the known and unknown data (which are obtained from the variogram model). All kriging types use this basic approach with minor variations. For example, in 'Simple Kriging,' the algorithm that is used to calculate the kriging weights is given by Eq. 1-3.

$$\begin{bmatrix}\text{Covariance among} \\ \text{known data points}\end{bmatrix} [\lambda] = \begin{bmatrix}\text{Covariance between known} \\ \text{and unknown data}\end{bmatrix} \qquad (1\text{-}3)$$

In the proposed method for designing the optimal diverter batch size, Indicator Kriging was used along with conditional simulation (the combination of these techniques is called Sequential Indicator Simulation, SIS) to create the permeability realizations of a reservoir. This method was used because, unlike kriging methods that assume a Gaussian distribution of the property being estimated, indicator kriging does not have any underlying assumptions about the data distribution and can preserve connectivity of extreme values. When simulating the permeability in a reservoir, connectivity of high permeability may represent channels while connectivity of low permeability zones may

represent barriers to flow so this kriging method is often preferred for permeability estimation.

Sequential Indicator Simulation is carried out as follows:

1. Select some thresholds, k, of the property being estimated, Z.
2. Carry out indicator transformation on the known data points for each threshold. The random indicator variable $I(Z_k; x)$ is associated with the random function $Z(x)$ for the threshold value Z_k as shown in Eq 1-4:

$$I(Z_k; x) = \begin{cases} 0 \text{ if } Z(x) > Z_k \\ 1 \text{ if } Z(x) \leq Z_k \end{cases} \quad (1\text{-}4)$$

3. Compute indicator variograms at each threshold. An indicator variogram is created in the same way as a typical variogram, but the transformed property values are used instead of the actual property values.
4. At an unknown location, estimate the cumulative probability of that threshold by carrying out indicator kriging (Indicator Kriging uses the same procedure as Simple Kriging but uses the transformed property values and indicator variograms).
5. Compute a cumulative density function (CDF) using the cumulative probabilities at each threshold.
6. Sample a value from the CDF that was created for the unknown location and include this point as a part of the conditioning data (or known data points).
7. Repeat steps 4-6 until all locations have been estimated.

1.5 Research Objectives

The primary objective of this research was to develop a method for selecting the optimal size of PLA diverter batches based on the geostatistical characterization of the near wellbore formation. To do this, several intermediate objectives were also met:

1. Determine the mechanisms by which PLA causes diversion using laboratory experiments.
2. Use the experimental results to create a model that mathematically describes how PLA can induce additional pressure drop to the fluid flow into the formation where PLA is deposited.
3. Implement the PLA pressure drop model in a near wellbore simulator.
4. Combine geostatistically-based, near wellbore permeability characterization with the diversion model to determine the optimal size of diverter batches during a stimulation treatment.

2. LITERATURE REVIEW

2.1 History of Diversion in Matrix Acidizing

Ever since acid has been used to stimulate and remove formation damage from wells, our industry has sought after various means to achieve equal zonal coverage of the well during stimulation. Table 2-1 below shows the history of the development of diverting agents (Harrison, 1972, Glasbergen et al., 2006, Chang et al., 2007, Kalfayan and Martin, 2009, Van Domelen, 2017).

Table 2-1: History of diverting agents for matrix acidizing

Year	Event or Diverting Agent/ Technique	Description
1896	Invention of acidizing technique of stimulation	The first patent issued to Herman Frasch.
1932	Oil industry started to use HCl acid to stimulate wells	
1936	Soap solution	The soap solution reacts with calcium chloride to form an oil soluble precipitate.
1937	Gels	Locust bean gum creates a gel with calcium or sodium chloride that can blank off zones.

Table 2-1: Continued

Year	Event or Diverting Agent/ Technique	Description
1935-1940	Sulfuric acid	Sulfuric acid reacts with calcium carbonate in the formation to form an insoluble calcium sulfate precipitate.
1935-1940	Heavy calcium chloride brine	Heavy calcium chloride brine was used in vertical wells to prevent acid from entering the formation water by diverting acid up the hole.
1935-1940	Cellophane	Cellophane was mixed with locust bean gum to form a plug at the bottom of vertical wells. This was done to prevent acid from entering formation water.
1935-1940	Rubber packers	Packers were used to mechanically limit fluid from entering formation water in a vertical well.
1944	Fluid interface detecting tools	A method was developed to determine and alter the location of acid in the wellbore. Acid was pumped through the tubing and oil was pumped in the casing. A fluid interface detection tool was run on wireline to determine the location of the interface between oil and acid in the wellbore. More acid or oil was pumped to move the interface in the desired direction.
1945-1950	Open hole hook packers	Open hole hook packers have side door choke assemblies that allow selective treatment above or below the packer.
1945	Straddle packers	Hydraulically inflated packers are used to allow treatment above, below or in between packers without moving the packers.

Table 2-1: Continued

Year	Event or Diverting Agent/ Technique	Description
1947	Emulsions	Locust bean gum can be used as an emulsifier to create a high viscosity fluid.
1951	Coiled tubing	Coiled tubing is used to control where acid enters the wellbore by injecting acid through tubing that is run through the wellbore or production casing.
1951	Acid-kerosene emulsion	A mixture of lime, kerosene, a fatty acid, and calcium chloride salt create an emulsion. The stimulation acid can be mixed in with this emulsion for the treatment.
1954	Mothballs (Naphthalenes)	Crushed mothballs were mixed with viscous acid suspensions. They were thought to be an ideal blocking agent for many wells because the naphthalene mothballs are oil soluble and they sublime at 175°F.
1954	Oyster shells	Oyster shells were used with oil external phase emulsions as a blocking material.
1955	Crushed limestone and sodium tetraborate	Crushed limestone and sodium tetraborate (Borax) were used as blocking agents. However, Borax was found to be poisonous so its use was discontinued and rock salt was used instead.
1956	Gilsonite	Gilsonite (a form of asphalt) is oil soluble, and it softens at 195°F and melts at 300°F, so it is suitable for oil reservoirs in that temperature range. In wells that do not produce liquid hydrocarbons, a post-flush of xylene can be performed to remove the gilsonite.

Table 2-1: Continued

Year	Event or Diverting Agent/ Technique	Description
1956	High viscosity gels/fluids	Guar Gum's high viscosity is ideal for use as a carrier of the particulate diverting agents and as a gelling agent. Hydroxyethyl cellulose (HEC) was later used instead of guar gum for this application since HEC has better clean up characteristics.
1956	Ball Sealers	Rubber balls were used to seal off perforations. A variety of ball sealer materials were subsequently used: solid nylon balls, aluminum balls, rubber covered aluminum balls, rubber covered phenolic balls, and Permeable plastic consolidated walnut shell balls.
1961	Limited Entry	A technique was developed that limits the spacing and the diameter of perforations. When acid is injected at a high rate, the sized perforations act as chokes and add local restrictions to flow.
1962	Swellable synthetic polymer	Solid inert synthetic swellable polymers were used as particulate diverters because of their ability to swell 30-40 times its original shape; the polymers are pliable, deformable and degradable.

Table 2-1: Continued

Year	Event or Diverting Agent/ Technique	Description
1964	Plug and Perf	The method (which was first called Pine Island Fracturing Technique) involves perforating the lowest or furthest zone and stimulating the well. A plug is then inserted to block off the stimulated zone, and another section of the well is perforated and treated. This is repeated until the entire well is treated. At its inception, the plugs were made of pea gravel and sand, and as many as six stages were used.
1965	Baffle rings	These baffle rings are installed in the casing string and are designed to accept a "giant ball sealer" that acts as like a cement plug.
1965	Wax-Polymer Particulates / Wax beads (Unibeads)	A wax-polymer blend, which was a refinery by-product, was used as a blocking material. It was useful because of its oil solubility.
1966	Chicken feed	Chicken feed was used as a blocking material in dry gas wells. It is a mixture of ground grains that completely degrade in water, brine or acid.

Table 2-1: Continued

Year	Event or Diverting Agent/ Technique	Description
1967	Temperature surveying between diversion stages (Temp-Trol)	Temp-Trol is a method that uses temperature surveys to determine the amount of diverter that is needed during the stimulation treatment. A temperature survey is run at the end of each diversion and acidizing stage. During each survey, the length of the interval that has been treated (cooled intervals) is compared to the length of the interval that has not been treated to determine the amount of diverting agent that is needed in subsequent stages.
1965-1970	Paraformaldehyde	This diverting agent was designed for high temperature (250-350°F) dry gas wells. Paraformaldehyde is soluble in oil and water so it can be removed using a post-flush fluid. One disadvantage of using Paraformaldehyde is that if it is used with guar gum it breaks down the breaker in the fluid.
1969	Benzoic acid flakes	Benzoic acid flakes are suitable for use as a particulate diverting agent because it is soluble in oil and water. Its solubility in water depends on both pH and temperature.
1969	Foam	Foam is a dispersion of gas in a liquid. The liquid film that separates the bubbles in the foam reduces the gas mobility, which in turn lowers the liquid saturation and the liquid relative permeability.

Table 2-1: Continued

Year	Event or Diverting Agent/ Technique	Description
1965-1971	Oil soluble resins	These sticky, heavy hydrocarbon solids are useful as particulate diverters because they are completely soluble in oil and leave no formation damage. Also, they can penetrate gravel packs.
1993	MAPDIR	The maximum pressure differential and injection rate (MAPDIR) technique is not a typical diversion technique in that it does not prevent or lessen flow from entering high permeability zones. MAPDIR uses the maximum possible injection rate without fracturing the formation; this maximizes the flow rate that can enter low permeability zones. In this sense, it still creates full zonal coverage. This method negates the need for any diverting agent or mechanical tools but comes at the cost of higher acid usage.
1997	Viscoelastic Surfactants (VES) Systems	VES is a specialized surfactant with an ionically bonded head and a covalently bonded tail. VES causes an increase in viscosity as the acid is neutralized thus causing diversion after a zone has been treated.
2001	Self Viscosifying Acids (SVA)	SVA is composed of three components: A gelling agent (typically a polyacrylamide), a cross-linking agent and a breaker. The crosslinker that is used does not work at low pH, i.e. before neutralization. As the SVA reacts with the formation, the crosslinker becomes active and drastically increases the fluid viscosity.

Table 2-1: Continued

Year	Event or Diverting Agent/ Technique	Description
2004	Relative permeability modifiers	Relative permeability modifiers are polymers that adsorb on the pore walls and disproportionally affect the permeability of one phase compared to another. They had been previously used for water control during production for several years (since 1982).
2006	Polylactic Acid (PLA)	Polylactic acid is an ester that degrades in the presence of water negating the need for any cleanup fluid.

Chang et al. (2007) noted that as an industry we have learned several key lessons about what is desirable in a diverting agent method or material based on the history of the applications as shown in Table 2-1:

- The diverting agent must not cause permanent damage to the formation and must be compatible with the formation and its fluids. During 1935-1940, sulfuric acid was developed as a diverter. It was effective in diverting fluid by creating a precipitate with carbonate formations. However, since the precipitate could not be removed, it created permanent damage. Thus the use of sulphuric acid as a diverting agent was discontinued.
- The diverting agent materials or fluid must be safe and non-toxic. In 1955, sodium tetraborate (Borax) was developed as a diverter. However, Borax was quickly discontinued since it was discovered to be poisonous.

- The diverting agent must be able to be cleaned quickly to put the well into production. This can be seen when hydroxyethyl cellulose (HEC) was used instead of guar gum to raise the diverting agent suspension viscosity since it had better clean up characteristics.
- The chemical and physical properties of the diverter must be sustainable during the treatment. This can be seen when paraformaldehyde, which is suitable for reservoir temperatures up to 350°F, was developed as a diverting agent in 1965-1970. Its use was sought out for high-temperature applications since many other diverters quickly melt or sublime if the reservoir temperatures were above 250°F.

Finally, Table 2-1 also shows that although PLA had been used in biomedical and pharmaceutical applications for many years, e.g., it is used in drug delivery systems and tissue engineering (Alsaheb et al., 2015), it has only been used as a diverting agent in matrix acidizing applications over the last decade.

2.2 Characterization of Polylactic Acid as a Diverting Agent

In the publication that introduced PLA as a diverting agent (Glasbergen et al., 2006), the authors describe laboratory tests that were performed to investigate the polyester's degradation rate and particle attrition. The degradation tests showed that PLA (molecular weight 50,000 g/g-mol) was able to fully degrade within 12hrs at a temperature of 250ºF and that its degradation rate was independent of pressure. To test particle attrition, a flow loop was set up that included a centrifugal pump, a high-pressure triplex pump, a

storage tank, and a choke. When 3000psi was applied across the choke, particles with an initial mean size of 150μm were able to maintain a mean size of at least 125μm; this indicates that the particles can retain their size during pumping. The paper also demonstrated a successful field trial that was undertaken on a temporarily abandoned gas well in Louisiana, USA.

Since then, there have been several publications demonstrating successful field trials in the Middle East such as in Saudi Arabia (Malik et al., 2018), Kuwait (Ahmed et al., 2018), Iraq (Gonzalez et al., 2017), Bahrain (Malik et al., 2017) and Qatar (Thabet et al., 2009). Moreover, since the inception of PLA as a diverting agent, several investigators have done work to characterize the pressure drop that can be induced by the degradable diverters.

In 2010, Cohen et al. sought to describe how PLA fibers that accumulate in a perforation could cause diversion. To do this, they carried out several laboratory-based experiments using a slot bridging apparatus. Additionally, they carried out several small-scale computational fluid dynamics (CFD) simulations. Finally, they created a model based on the experimental and simulation results, which was field tested. The model that was presented modified the perforation skin factor by reducing the permeability within the perforations. Implementation of their model in simulations of field treatments showed that the bottom hole pressure increase observed during injection of the diverter should not be used to gauge the effectiveness of the diversion treatment. Instead, the authors propose that pressure measurements along the well and production logging tool (PLT) data matching should be used to test treatment effectiveness.

In 2014, B. Reddy and J. Cortez-Montalvo investigated post-flush fluids that could be used to control the diverter's degradation rate. A part of this investigation was also to determine how the diverter's particle crystallinity affected the degradation rate. To avoid using strong acids or bases that cause corrosion, safety hazards and undesirable effects in the formation, the authors investigated several amine- and amino alcohol-based compounds. Their investigation showed that ethanolamine (EA) could be an effective accelerator regardless of the diverter crystallinity. Ethylenediamine (EDA) and triethylenetetramine (TETA) were effective in degrading PLA unless the PLA particles were semi-crystalline. Tetraethylammonium (TEA) and Polyethylenimine (PEI) were not found to be suitable degradation agents. It was found that amorphous polyesters were the easiest to degrade, followed by low-crystallinity polymers and then semi-crystalline polymers.

In 2015, Sau et al. carried out tests to investigate how the tortuosity of wormholes affect the ability of fibrous PLA to bridge across wormholes and how well the PLA fibers could degrade in a water-depleted environment. To do these investigations, the authors used degradation and bridging tests with slotted sleeves and 3D printed synthetic models of wormhole structures. In the degradation tests, fibers were presoaked with deionized water and then the water was removed by pressing and filtering, the fibers were then placed in various media such as fresh water, diesel, mineral oil, spent acid, and humid air, where they were left to degrade. The degradation tests showed that the hydrolysis reaction rate was dependent on the concentration of water present. Degradation occurred far more

quickly in water-rich environments like the spent acid and fresh water, but the PLA could still be degraded in water-depleted environments.

In the bridging tests, a slurry containing PLA fibers were pumped through sleeves that contained smooth, mechanically created slots (see Figure 2-1). Then the slurry was pumped through a polymeric cylindrical core with a 3-D printed wormhole (see Figure 2-2).

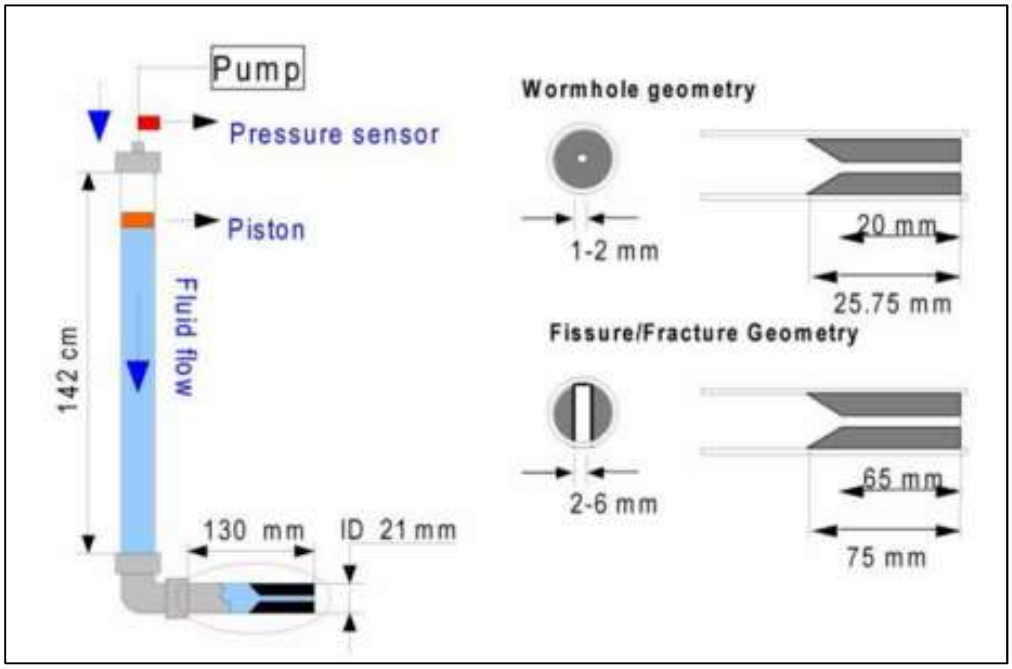

Figure 2-1: Experimental set up used by Sau et al. (2015)

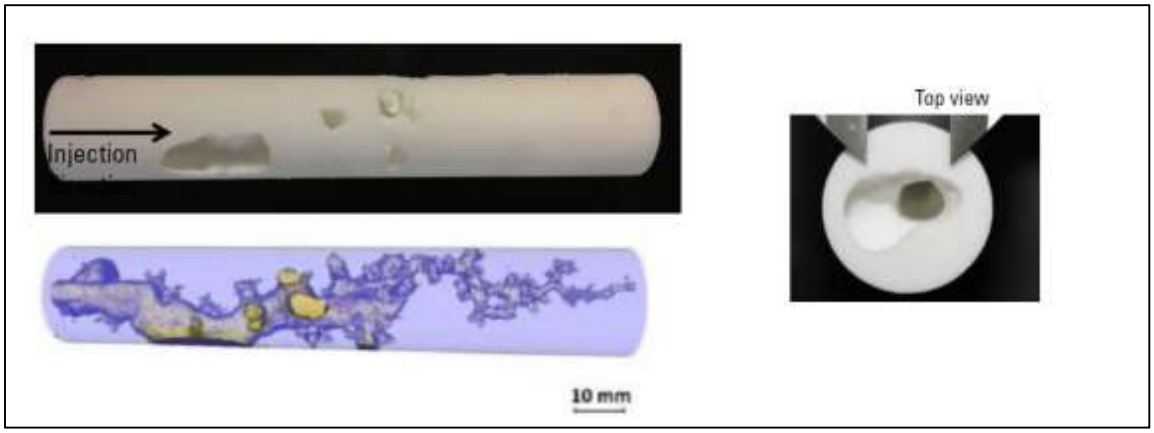

Figure 2-2: 3-D printed wormholes in a polymeric core used by Sau et al. (2015)

The results showed that the tortuosity of the wormholes aided in bridging since the 'spurt loss' (volume of fluid that was able to flow through the slot before a bridge is created) was less for the wormhole path than an equivalent radius smooth slot.

Shahri et al. carried out investigations to determine the mechanism by which bi-modal size diverter particles cause diversion (Shahri et al., 2016, Shahri et al., 2017 and Safari et al., 2017). The authors investigated the diversion mechanism experimentally using bridging tests, coupled computational fluid dynamics (CFD), and discrete element model (DEM) to create wellbore scale simulations (see Figure 2-3).

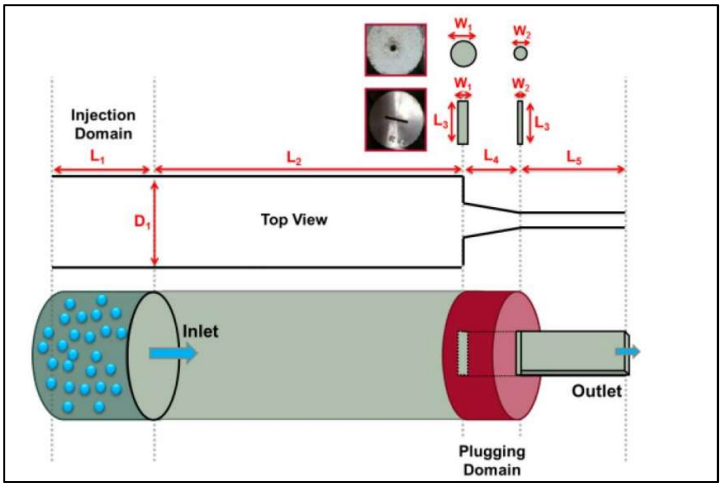

Figure 2-3: Single slot experimental set up (Adapted from Shahri et al., 2016)

The simulation and experimental results were then used to create a model that was field validated. Their investigation revealed that the larger particles firstly bridge the opening of the slot or wormhole (this was described as 'Jamming') and then the smaller particles fill the voids of the larger particles creating a low permeability filter cake (this was described as 'Sealing' or 'Plugging'). Their experiments and simulations also suggest that cylindrical particles are more effective diverters than spherical particles; diverter particles with a higher friction coefficient can more easily bridge wormholes; there is a critical concentration required for particles to bridge the openings; and that the ratio of the large and small particles can impact the magnitude of pressure buildup. Please note that the particle friction coefficient is a parameter used to calculate frictional forces between particles or between a particle and a surface; this parameter plays a role in determining how static particle packs form.

Finally, in 2018, Tan et al. used filter press tests to measure the permeability of the filter cakes developed by degradable diverters. Figure 2-4 shows the experimental set up that was used.

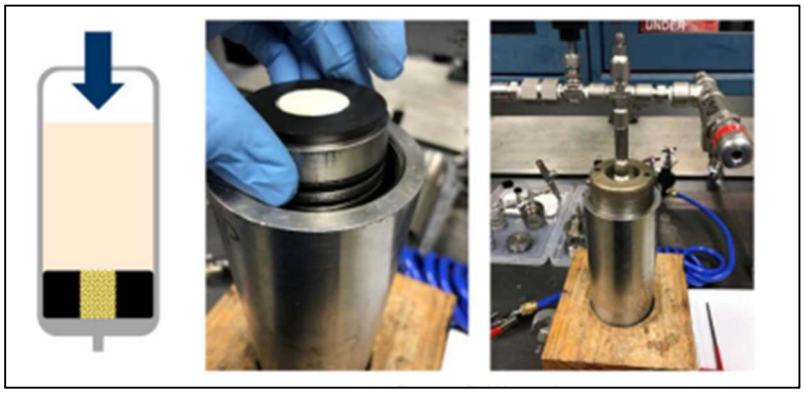

Figure 2-4: Schematic and pictures of the fluid loss cells that were used to determine the permeability of the PLA filter cakes (Adapted from Tan et al., 2018)

Tan et al. (2018) showed that the PLA fibers have a significantly lower permeability than conventional diverting agents. By using the same model that was developed by Cohen et al., 2010, the authors showed that having a lower permeability filter cake can cause reduced local injectivity into the formation where the filter cake is present and, by extension, an improved stimulation distribution.

2.3 Acid Placement and Diversion Models

In 1977, Hong and Millhone developed a computational model to determine the injection profile of stimulation fluids in a vertical well (Hong and Millhone, 1977). Their model accounted for fluid density, fluid viscosity, sequence of injection, wellbore

configuration, reservoir pressure, permeability, and porosity. This model was able to account for gravity segregation of immiscible fluids in the wellbore. They showed that the position of the fluid interface during the treatment could affect which zones were or were not being stimulated. They validated their model using laboratory experiments.

Hill and Galloway (1984) created a fluid placement simulator that could determine the effectiveness of a diverting agent. This model also considered gravity segregation, following Hong and Millone's simulation. The diversion model assumed that the pressure drop resulting from a diverting agent was a linear function of the volume of incompressible filter cake made from the diverter that was deposited in the zone. Their numerical fluid placement simulator and diversion model were validated using experimental results.

In 1986, Taha et al., developed a model that simulated acid placement for sandstone matrix acidizing in vertical wells. This model was able to account for heterogeneity in permeability, formation damage, and particulate diversion (Taha et al., 1986). Hill et al. (1987) added the ability to model the effects of HCl pre-flush to this model.

In 1994, Hill and Rossen used an acid placement simulator to compare four different types of diversion: MAPDIR (maximum pressure differential and injection rates), particulate diverting agents, viscous fluids, and foams (Hill and Rossen, 1994). The diversion types were compared using a reservoir that had two layers, each with a different permeability. The study revealed that the MAPDIR technique would result in the highest injection rate into the low injectivity interval, but that other diversion techniques could increase the efficiency of use of acid.

Following this, Davies and Jones (1998) developed an acid placement simulator for horizontal wells with barefoot completions in sandstone reservoirs. Their simulation allowed modeling of acid placement using coiled tubing, two-phase flow (for foams), and a number of different diverters. Their simulator also modeled the transient fluid flow along the well. A similar model was developed and validated with field cases by Glasbergen and Buijse (2006). Glasbergen and Buijse's model also accounted for ball sealer diversion.

Later, Eckerfield et al. (2000) developed a fluid placement model for horizontal wells that allowed tracking of the fluid interface in the well. The model was used to investigate coiled tubing applications. Their study showed that the movement of the tubing tail has no impact on where fluid enters the formation. Also, their study showed that when using coiled tubing to place the acid, pumping a non-damaging inert fluid in the annulus (i.e., between the coil tubing and the wellbore) could be a useful way of preventing acid from entering high permeability zones near the heel of the well.

In 2007, Mishra et al. developed an acid placement simulator for long horizontal wells in carbonate reservoirs. This model included wellbore interface tracking (Eckerfield et al., 2000), the frictional pressure drop along the well, empirical wormhole models and a variety of completion skin factors (Mishra et al., 2007). Sasongko et al. (2011) added the capability to model acid jetting with drill pipe to the model developed by Mishra et al., 2007.

Mogensen and Hansen (2007) presented an acid placement simulator that could simulate controlled acid jetting in long horizontal wells. The simulator was able to

consider varying wellbore geometries in the completed zones. Their model contained an advanced fluid friction model that accounted for the presence of drag reducing agents.

Finally, Nozaki and Hill (2010) developed an acid placement simulator for long, vertical, gas wells in carbonate reservoirs. The model accounted for gravity segregation in the wellbore, viscosity contrast between the reservoir fluid (gas) and the stimulation fluid (acid), and relative permeability effects.

2.4 Methods Used to Design Diversion Batch Treatments

Glasbergen and Buijse (2006) suggested that while several acid placement simulators have been developed and successfully validated, they are often not used because the models are either not available, or not reliable, or the correct inputs to the models cannot be easily and economically attained. Similarly, Hill and Rossen (1994) showed that the effectiveness of a diversion treatment, and even the best choice of diversion type, depend on knowing the formation permeability of the zones to be treated. However, there are methods that have been used to design diversion treatments when the permeability profile is not known.

In 1967, a technique called Temp-Trol was developed to determine the amount of diverter to be applied during a stimulation treatment (Guinn and Wright, 1968). The method employed temperature surveys at the end of each acid and diversion stage. Depending on the length of the producing interval that was cooled or not, the size of the next diverter stage could be altered. Later, Acock and Sanders (1996) suggested the use of a down hole sensor package run on coiled tubing reel. The down hole sensor package

would measure the formation temperature during the treatment to determine where fluid enters the formation or not, which could be used to determine the amount of diverter needed. More recently, distributed temperature sensing (DTS) has been considered to be used for the same function (Glasbergen, 2009). DTS employs fiber optics to monitor the temperature along the wellbore continuously. Additionally, it has been suggested that induction tools that measure resistivity could be used to delineate wormholed zones post-treatment (Ghommem et al., 2016). These temperature or resistivity based methods are costly and require long periods of planning. These methods are not intended to be carried out in every diversion treatment, but rather to learn how to design future treatments, i.e., they are best used to validate the guidelines, or rules of thumb, in use.

Another method that can be used to design a diverter batch size is to calculate the overall skin factor using the injection rates and pressures. This method can also be used to determine a diverter's effectiveness. McLeod and Coulter (1969) treated each stage of a stimulation treatment as a pressure build-up test. They used the pressure response when acid injection started and stopped to calculate formation permeability and skin factor. Paccaloni (1979) suggested using the injection pressures with a steady state skin factor model to instantaneously and continuously compute the overall skin factor during a treatment. Prouvost and Economides (1987) recognized that the steady state assumption in Paccaloni's method could lead to errors. Prouvost and Economides modified the real-time skin factor calculation developed by Paccaloni (1979); they used a skin factor model based on transient flow into the reservoir, thus, allowing a more accurate real-time skin factor calculation. Paccaloni and Tambini (1993) confirmed that the steady state

assumption leads to an overestimation of skin factor. Behanna (1994) introduced the idea of using the derivative of the skin factor with time in real-time skin modeling to determine the severity of formation damage, or the effectiveness of the diverting agents. Hill and Zhu (1996) used an inverse injectivity versus superimposed time function plot as a diagnostic tool for real-time skin factor monitoring. The real-time skin monitoring models were updated to account for gas wells (Zhu et al., 1998).

However, measuring the skin factor using surface pressure measurements makes two assumptions: the changes in surface pressure caused by changes in the hydraulic head and frictional pressure drop are accurately known and can be used to calculate the bottom hole pressure accurately, and the changes in fluid placement create a change in the pressure differential that is large enough to be measured. The investigations using DTS have shown that neither of these assumptions is true in all cases (Glasbergen 2009). Similarly, Senters et al. (2017) used radioactive tracers in proppants to determine the effectiveness of diversion during hydraulic fracturing treatments. Their study also revealed that surface pumping pressures could be misleading for determining diverter effectiveness or determining how much diverter to use.

Currently, the most common ways of determining the total amount of diverter to be used in stimulation treatments are rules of thumb that have been developed over time from case histories. However, no rules of thumb have been published for PLA (Van Domelen, 2017). Diverter rules of thumb have been summarized by many authors, such as: King and Hollinsworth (1979), McLeod (1984) and Van Domelen (2017). An example of some rules of thumb can be seen in Table 2-2.

Table 2-2: Example of diverting agent rules of thumb (Adapted from Van Domelen, 2017)

Type	Applications	On Perforations	In Perforations (lbs/perforation)	Open Hole Formations (lbs per ft^2)
Rock Salt	HCl and Non-HF Acid Treatments	16lbs @ 1lb/gal	0.5 to 2	5
Benzoic Acid	Gas, Oil, Injection Wells	9lbs @ 0.5lb/gal	0.25 to 1	2.5
Naphtalene	Oil Wells Only	8lbs @0.5lb/gal	0.25 to 1	2.5
Wax Beads	Oil Wells Only	n/a*	0.25 to 0.5	1 to 2
Oil Soluble Resin	Oil Wells Only	n/a*	0.25 to 0.5	1 to 3
Foam	Preferably in higher permeability gas wells	n/a*	60 to 80 Quality	60 to 80 Quality
Ball Sealers	Sinkers - Vertical Wells	200% excess	n/a	n/a
	Neutral Density or floaters - Vertical Wells	50% excess	n/a	n/a
	Mixed Density - Horizontal Wells	no excess	n/a	n/a

* Insufficient strength to hold pressure on perforations

It should be noted, however, that these guidelines do not take into account the permeability and local skin factor of the well to be treated.

3. METHODOLOGY *

3.1 Laboratory Characterization of Polylactic Acid

A new procedure was developed to investigate the effect of PLA in matrix acidizing treatments using core flood apparatus. The purpose of these experiments was to understand how PLA affects multistage matrix acidizing treatments and to provide data for a model that can be used to simulate diversion. The main objectives of these experiments were to investigate:

1. If PLA can enter and fill a wormhole.
2. How wormholes propagate when a previously developed wormhole is filled with PLA.
3. How PLA affects pressure drop when it is in a wormhole versus when it is in a filter cake.

3.1.1 General Procedure for Diversion Experiments

In the experiments, a wormhole was initiated in an outcrop core by injecting hydrochloric acid (HCl). The wormhole was not allowed to break through the core (i.e., the wormhole did not reach the other end of the core). PLA was then injected into the core, and finally, more HCl acid was injected until a wormhole broke through the core. A detailed description of the equipment used and the procedures for measuring permeability

* Parts of this chapter are reprinted with permission from "General Guidelines for Batch Treatments of Polylactic Acid for Diversion in Multistage Matrix Acidizing Treatments" by Shirley and Hill, 2019, Copyright 2019 Society of Petroleum Engineers and from "Experimental Investigation of Particulate Polylactic Acid Diversion in Matrix Acidizing" by Shirley and Hill, 2019, Copyright 2019 Society of Petroleum Engineers.

and injecting acid into the core can be found in Grabski (2012). The experiments were carried out according to the following procedure:

1. Measure the core porosity using its dry and wet weight.
    - The core was dried using a convection oven.
    - The core was saturated in fresh water using a vacuum pump.
2. Measure the permeability of the core using a Hassler Type Core Holder to carry out core flooding with fresh water.
3. Perform an X-Ray Computer Tomography (CT) scan on the core.
4. Create a wormhole in the core that does not fully penetrate the core.
    - To do this, a limited volume of 15% HCl acid was injected. The injected volume was calculated based on the expected pore volume to breakthrough, PV_{bt}. The expected PV_{bt} was determined based on previous matrix acidizing experiments carried out on similar Indiana Limestone cores.
5. Measure the pressure drop across the core and perform a CT scan on the core.
6. Add a spacer between the injection plug and the core to allow the build-up of a filter cake (see Figure 3-1).
7. Inject the PLA suspension.
8. Measure the pressure drop across the core.
9. Remove the spacer and any filter cake that was formed.
10. Measure the pressure drop across the core and perform a CT scan on the core.
11. Inject acid into the core until a wormhole breaks through the core.
12. Perform a CT scan on the core.

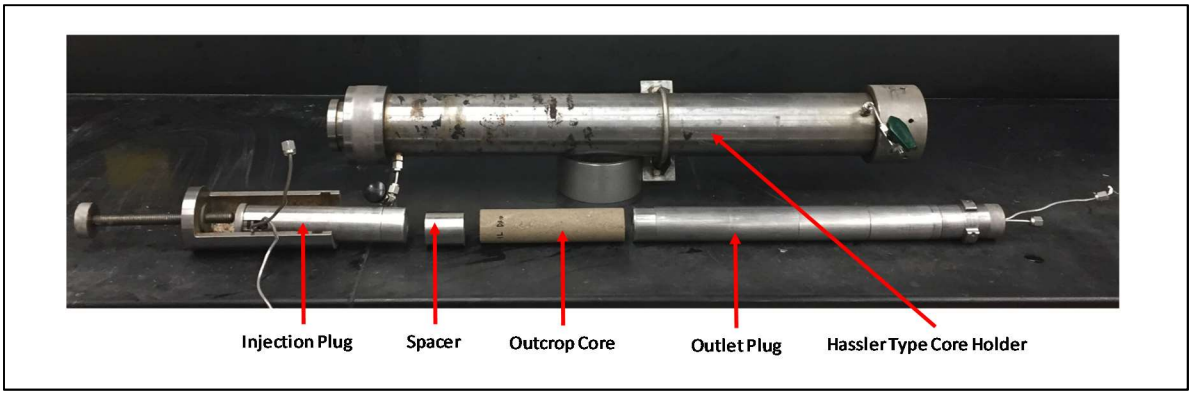

Figure 3-1: Equipment assembly for experiments.
Reprinted with permission from (Shirley and Hill, 2019)

3.1.2 Method to Keep PLA in Suspension

In both the field and the lab, it can be challenging to keep PLA in suspension while pumping. Some of the challenges that needed to be overcome in the laboratory evaluation of PLA were:

- The PLA must be maintained in suspension throughout the injection phase.
- The suspending fluid used must be benign to both PLA and the acid (HCl).
- The suspending fluid must be able to be removed entirely from the core or not cause diversion due to its viscosity.

Various methods were attempted, but the technique that was found to be most successful was suspending the PLA in a heavy $CaCl_2$ brine. According to Stokes' law, if the density of a fluid and a particle in suspension are equal, then the particle has zero settling velocity (i.e., the particle does not settle or rise). The length of time that the PLA particles can remain in suspension, thus, depends on how accurately the density of the brine can be made to match the density of the PLA particles (PLA specific gravity is 1.24

as per product supplier). A laboratory bench scale and a measuring cylinder were used to make up the $CaCl_2$ brine. The suspension that was created showed little signs of the particles settling to the bottom or rising to the surface after 1 hour (typical pump time for the experiment was 20 minutes).

One issue with using $CaCl_2$ brine as the suspending agent was that brine had been shown to increase the rate of hydrolysis of PLA by other investigators (Van Domelen, 2017). The rate of hydrolysis was not directly measured; however, when submerged in fresh water or brine at room temperature, it took several days for a sample of PLA in a test tube to fully hydrolyze (to the point that the white particles could no longer be seen, and the brine solution was clear) in both fresh water and brine. Hence, within 20 minutes any change in the amount of PLA present due to its hydrolysis was insignificant.

Tests were carried out to show that the $CaCl_2$ brine could be sufficiently removed from the core. A $CaCl_2$ brine with a specific gravity of 1.24 has a viscosity of nearly three times that of fresh water. Hence, when it was pumped into a fresh water saturated core (without any PLA particles in suspension), there was a rise in the pressure drop across the core. When fresh water was injected after the brine, the original pressure drop across the core was attained (see Figure 3-2), thus demonstrating that the brine was removed from the core.

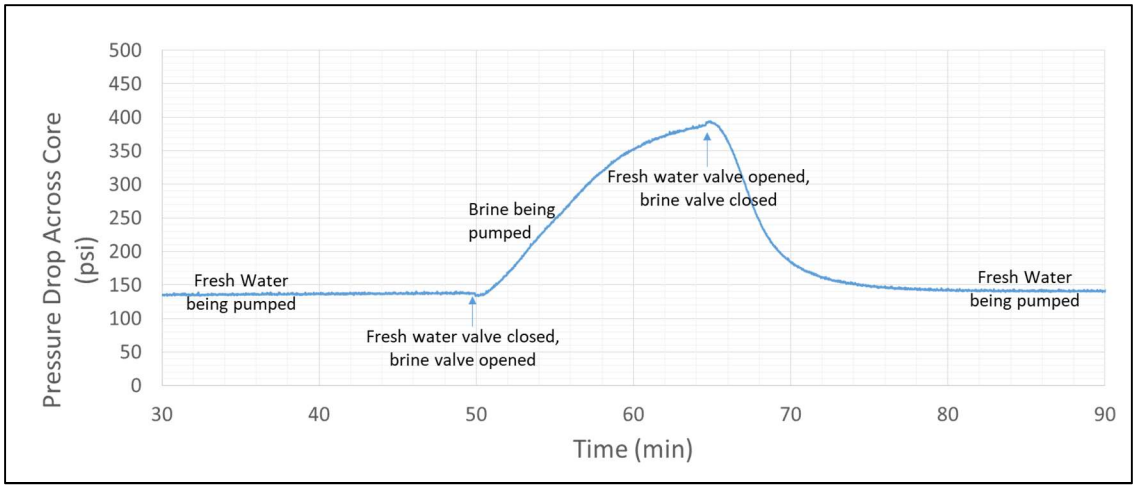

Figure 3-2: Test to show that $CaCl_2$ can be flushed out of a core. Reprinted with permission from (Shirley and Hill, 2019)

The procedure that was used to suspend PLA in a $CaCl_2$ brine solution is as follows:

- Mix ACS reagent grade $CaCl_2 \cdot 2H_2O$ salt with fresh water in a mixing flask (41g of $CaCl_2 \cdot 2H_2O$ /100ml solution). Keep the mixing flask in a water bath during the mixing of the brine because $CaCl_2$ dissolving in water has a positive heat of solution. The heat of solution could cause a temperature rise and, subsequently, evaporation of water and a change in the solution's specific gravity.
- Add a small amount (0.5ml surfactant/100ml solution) of a surfactant (dish soap) to the solution. The surfactant is used to prevent PLA from adhering to the walls of the flask or forming any bubbles in the solution.
- Add PLA to the solution based on the desired concentration.
- Place the PLA and brine suspension into a sonicator to remove any bubbles (air bubbles can cause errors in determining the pressure drop across the core). Note: bubbles tend to form in the solution because $CaCl_2$ releases heat when it dissolves.

Figure 3-3 shows a sample of the PLA suspended in the $CaCl_2$ brine when the procedure described above was followed.

Figure 3-3: PLA in $CaCl_2$ brine suspension.
Reprinted with permission from (Shirley and Hill, 2019)

3.2 Implementation of the Diversion Model into a Near Wellbore Simulator

A model that describes how PLA causes diversion when it is deposited in or on the formation was created and incorporated in a near wellbore simulator. The near wellbore simulator used in this study was Horizontal Well Acidizing Simulator (HWAS). A full description of the model can be found in Mishra et al. (2007). HWAS couples several models including:

- Wellbore Flow
- Fluid Interface Tracking
- Transient Reservoir Flow
- Well Completion Skin Factor

- Empirical Wormhole Model

HWAS was altered to use the PLA skin factor models. In order to incorporate the PLA skin factors, the mass of PLA, location of PLA, and volume of the wormholes needed to be known. In HWAS, the wellbore is discretized into grids, and the treatment is discretized into small time steps. Since making the modifications to HWAS, the program now records the total amount of acid and the total amount of the diverting agent, at each grid and for each time step. The total volume of wormhole that is created at a particular grid is calculated using the volume of acid injected into the formation, at that grid, and the dissolving power of the acid. If the mass of the particulate diverting agent is not enough to fill the wormhole, then it enters the wormhole. However, if the mass of PLA that enters that grid can fill the wormhole, then the excess PLA builds a filter cake. Alternatively, the model can be manipulated so that all of the PLA that is deposited in a given grid makes up a filter cake on the sand face (this occurs if the PLA is sized to bridge or be unable to enter the wormhole). This procedure allows the simulation program to calculate the mass of PLA in the filter cake and mass of PLA in the wormhole at each grid for any given time.

Once the PLA skin factor model was implemented into the simulator, it was validated using published field data. To do this, inputs that describe field stimulation treatments using PLA diversion were taken from publications, and appropriate assumptions were made where necessary. To determine if the developed model was valid, the simulated skin factor profiles were compared with the published field skin factor profiles.

Finally, after the model was validated, the model was then used to create general guidelines for diversion. The model was used to carry out sensitivity analysis on the design parameters of published field treatments. The efficiency of the diversion treatment was measured based on the total skin factor of the resulting treatment as well as the uniformity of the skin profile.

The main output used to compare various treatments of a particular well was the final skin profile along the well. The final skin factor is the skin factor of the well after all the PLA has hydrolyzed, so there is no filter cake or PLA inside the wormholes. This profile can clearly show if the treatment was well distributed and how low a skin factor could be obtained. However, if there were many treatments to be compared, it was not always feasible to compare their results by plotting the skin profiles along the well. Whenever we wanted to compare more than two simulated treatments, we compared the simulation results based on two values: the standard deviation of the skin profile and the total skin factor.

The standard deviation of the skin profile was found by calculating the standard deviation of the skin factors for each grid block. This value was useful in determining how uniformly the treatment was distributed across the well. If the standard deviation was low, it meant that each of the grid blocks had a similar final skin factor. The total skin factor was calculated based on a well inflow performance equation.

Using the inflow performance equation for a horizontal well as developed by Furui et al. (2002) in field units:

$$q = \frac{\bar{k}L\Delta P}{141.2\mu B_0 \left(\ln\left[\frac{hI_{ani}}{r_w(I_{ani}+1)}\right] + \frac{\pi y_b}{hI_{ani}} - 1.224 + s_{total}\right)} \quad (3\text{-}1)$$

Where q is the total volumetric production rate in STB/d,

$\bar{k}$ is the average permeability of the well in mD,

L is the total length of the producing interval in ft,

ΔP is the drawdown pressure in psi,

μ is the viscosity in cP,

B_0 is the formation factor in reservoir bbl/ STB,

h is the pay zone thickness in ft,

I_{ani} is the anisotropy ratio,

r_w is the wellbore radius in ft,

y_b is the well spacing in ft (or distance to the drainage boundary in the y-direction) and

s_{total} is the total skin factor of the well.

The average permeability is based on the permeability at each grid, i.e.

$$\bar{k}L = \sum k_i L_i \quad (3\text{-}2)$$

Where k_i permeability of the ith grid in mD and

L_i is the length of the ith grid in ft.

The total production rate can also be described as a summation of the flow rates into each grid from the formation:

$$q = \sum \frac{k_i L_i \Delta P}{141.2 \mu B_0 \left(\ln \left[\frac{hI_{ani}}{r_w (I_{ani} + 1)} \right] + \frac{\pi y_b}{hI_{ani}} - 1.224 + s_i \right)} \tag{3-3}$$

Where s_i is the skin factor of the ith grid.

Substituting Eq. 3-3 into Eq. 3-1

$$s_{total} = \frac{\sum k_i L_i}{\sum \left(\frac{k_i L_i}{ln \left[\frac{hI_{ani}}{r_w (I_{ani} + 1)} \right] + \frac{\pi y_b}{hI_{ani}} - 1.224 + s_i} \right) - \left\{ ln \left[\frac{hI_{ani}}{r_w (I_{ani} + 1)} \right] + \frac{\pi y_b}{hI_{ani}} - 1.224 \right\}} \tag{3-4}$$

3.3 Method to Design Diversion Batch Treatments

If the near wellbore permeability profile is known for a given well, the stimulation treatment can be modeled and optimized using skin factor expressions and reservoir simulations. Unfortunately, determining the permeability profile before the stimulation requires core data to be obtained, production logs to be run before the treatment of the well, or fiber optics to be installed in the well. This can often be costly and is not available before every treatment. A method was developed for cases where the permeability profile of the well is unknown that utilizes known permeability profiles from neighboring wells and sequential indicator simulation (SIS) to determine the most likely optimal diverter batch size. The proposed method is summarized in Figure 3-4.

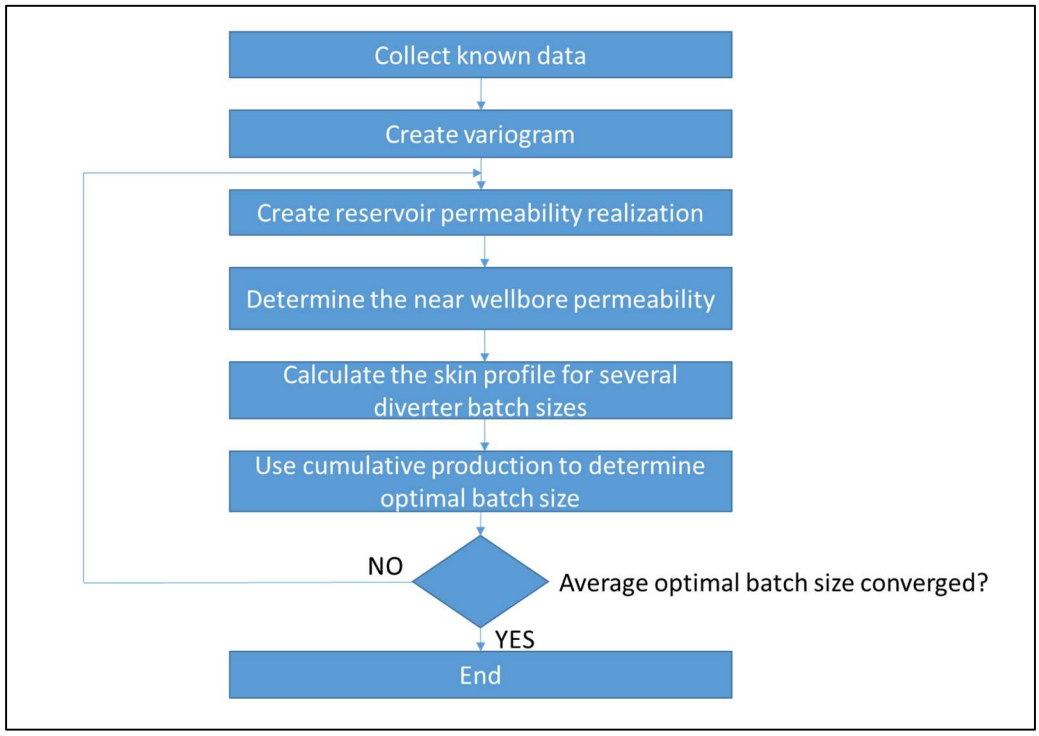

Figure 3-4: Method to determine optimal diverter batch size for a well with an unknown permeability distribution

3.3.1 Collect known data

In order to carry out geostatistical interpolation of the permeability in a reservoir, one needs to have some known permeability data in that reservoir. This data typically comes from core data or well logs. It is also important to know the location of the known measurements or at least to know the relative distance between the known data points since kriging is a spatial interpolation method. Having more data available and more densely populated data, creates realizations that have lower estimation variances and by extension that are more consistent with each other. For the examples that were carried out, permeability profiles were obtained from published field data.

It is also important to note that one can also take advantage of having data sources other than permeability, especially if this secondary data is more widely available. This secondary data source (often called soft data) may include porosity data, seismic data or any log or geological data that has some correlation with permeability. This data can be incorporated using collocated kriging (co-kriging) and can substantially improve the quality of the reservoir permeability realizations.

3.3.2 Create Variogram(s)

Once the data and their locations were collected, they were used to create a variogram. A variogram is a plot of semi-variance versus lag distance. The variogram mathematically describes how similarity between property measurements (in this case, permeability) varies with separation distance between points (see section 1.3). An experimental variogram was created by plotting the calculated semi-variance versus lag

distance from the known data; then the variogram was modeled by identifying the nugget, sill, range and variogram model type (see Figure 1-3). If soft data is being used, then separate variograms must be created for that data also (no soft data was available for the examples carried out). Variograms were created in a variety of directions to find the directions of maximum, medium and minimum variogram range; doing this allowed the anisotropy of the reservoir to be included in the interpolation. A geostatistical software called Stanford Geostatistical Modeling Software (SGeMS) was used to create the indicator variograms.

Note, the kriging method that was used in the examples, Indicator Kriging, does not have any underlying assumptions about the distribution of the property values. This means that the data does not need normal score transformation before creating the variogram. However, if a different kriging method that has an underlying assumption of the distribution of the property is used, the data may need to be transformed before the variogram is created. For example, Ordinary Kriging and Simple Kriging assume that the property being estimated has a Gaussian distribution and typically require the available data to undergo a normal score transform before the variogram is used. If the data was transformed before kriging, the result should be back-transformed after kriging.

3.3.3 Create Reservoir Permeability Realizations

A permeability realization was then created using the modeled variograms along with the available data. As discussed in section 1.4, sequential indicator simulation was used since it preserves the connectivity between extreme values, which is important in the

characterization of permeability. The permeability realization was created in a cartesian grid. In order to take advantage of the variogram data, the size of the grids must be smaller than the variogram ranges. However, in later stages of this procedure, when we needed to predict the production of a well in that reservoir using a reservoir simulator, we needed the grid size to be large enough to account for the equivalent wellbore radius of a well with negative skin. As such, it was necessary to upscale the grid size after the initial realization was created. Stanford Geostatistical Modeling Software (SGeMS) was used to carry out sequential indicator simulations and to upscale the gridded permeability realizations.

3.3.4 Determine Near Wellbore Permeability

It should be noted that the permeability of the grid blocks that the well is located in is not necessarily equal to the near wellbore permeability. As shown in Figure 3-5 below, the grid that the well passes through may be surrounded by other grids with very different permeabilities. This will impact the flow rate that enters wellbore through this grid. On the other hand, the inflow performance relationship that was used treats the reservoir as having a constant permeability along the flow path to the wellbore for a given well grid.

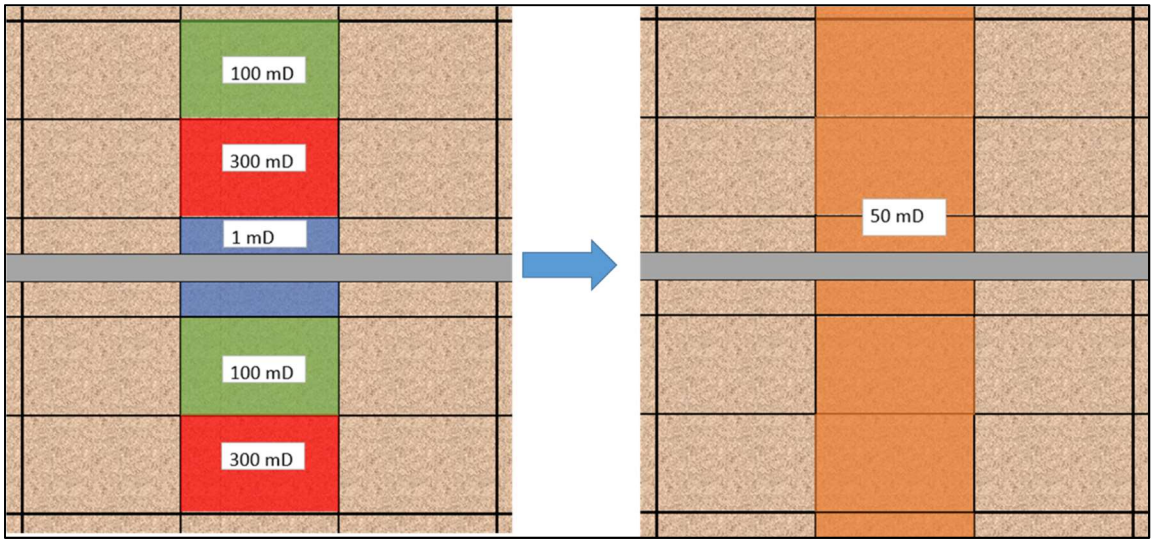

Figure 3-5: Cartoon showing the difference between the grid permeability and near wellbore permeability

The near-wellbore permeability was found by simulating the production of the well in a given permeability realization for a fixed time. The simulated flow rate and pressure profile along the well were then used with an appropriate inflow performance relationship to calculate a permeability profile. The simulation was carried out using a reservoir simulator (Schlumberger ECLIPSE E100).

3.3.5 Calculate Skin Profiles

The near-wellbore permeability, reservoir properties, treatment fluid properties, and pump schedule were then inputted into the near wellbore simulator (HWAS) to calculate the skin profile for a given treatment. This calculated skin profile took into account the effects of the PLA diverter based on the expressions developed by the

experimental results of this study. A variety of skin profiles were generated for different diverter batch sizes.

3.3.6 Calculate Long Term Production Rate

We then predicted the long-term cumulative oil and gas production by including the skin factor profiles that were generated for each diverter batch size into the completion data for the well in the reservoir simulation. The well production was simulated for a fixed period of time with a fixed bottom hole pressure. The optimal diverter batch size was then selected to maximize the long-term cumulative production of the well. The simulation was carried out using a reservoir simulator (Schlumberger ECLIPSE E100).

3.3.7 Repeat Until Average Optimal Batch Size Converges

This procedure was then repeated for multiple permeability realizations to find an average optimal batch size. The iterations were stopped when the average optimal batch size converged within an acceptable tolerance range.

4. EXPERIMENTAL RESULTS *

4.1 Does PLA Enter the Wormhole?

It is possible for the PLA to bridge across the wormhole entrance on the face of the core and prevent any particles from propagating further. PLA can be used in various shapes and sizes, and its behavior varies with both molecular weight and temperature. In this study, PLA was used in a granular or particulate form. The particle size was kept under 45 microns (325 mesh) and was separated using sieves and an RO-TAP® Sieve Shaker. The average wormhole diameter was 1-2mm. Experiments were carried out at room temperature. The author attempted to run some of the tests at temperatures above the glass transition temperature of the PLA (140ºF). However, at these temperatures, the PLA kept plugging the 1/8" tubing and the injection plug.

It was hoped to determine if PLA invaded the wormholes using the CT scans. However, the density of the PLA particles (S.G.:1.24) was too similar to that of fresh water (S.G.:1.0) in comparison to the Indiana Limestone Cores (S.G.:2.71), and thus the CT scans were unable to distinguish the PLA from the fresh water in the wormholes. To deduce if PLA was invading the wormhole, a core with a partially penetrating wormhole was injected with the PLA suspension via core flood and then sliced into thin sections (approximately 4 mm slices). Figure 4-1 shows two of these slices.

Figure 4-1: Two 4mm slices of a core after PLA injection
Left: 2nd slice
Right: 13th slice
Reprinted with permission from (Shirley and Hill, 2019)

As can be seen in the two slices shown in Figure 4-1, wherever there was a wormhole, the void was thoroughly invaded by the white PLA particles. These results indicate that for the conditions being tested (i.e., the temperature, particle size, and particle shape), PLA was able to enter and fill the wormhole.

4.2 How Does PLA Affect Wormhole Propagation?

It is important to understand how wormholes propagate after having been filled with PLA to know how to simulate a multi-stage treatment. Matrix acidizing in carbonate reservoirs stimulates a well by creating a zone around the well (equivalent to the radius of the wormholed region) where there is very little pressure drop for fluid flowing into the

well. The wormholes have significantly higher permeability than the reservoir matrix. The fluid that is within this wormholed zone can travel through the wormholes to go directly to the well. The goal of the stimulation is, thus, to create the longest possible wormholes.

In a multi-stage treatment, adding PLA into the wormholes adds resistance to flow during subsequent treatment stages, but it does not completely prohibit flow from entering the formation at that location. If the acid flow during subsequent stages propagates in competing wormhole branches, as opposed to the dominant wormholes, then the only way to further stimulate that zone is when the competing branches become longer than the original dominant wormholes. However, if the acid flow during subsequent stages continues to propagate the dominant PLA filled wormholes, making them longer, then that acid continues to stimulate the formation once it reaches the tip of the existing wormhole.

The CT scans were used to determine how the wormholes propagate when further acid enters a wormhole that has been filled with PLA. Figure 4-2 and Figure 4-3 show the CT scans of two separate experiments at various stages of the experimental procedure described earlier.

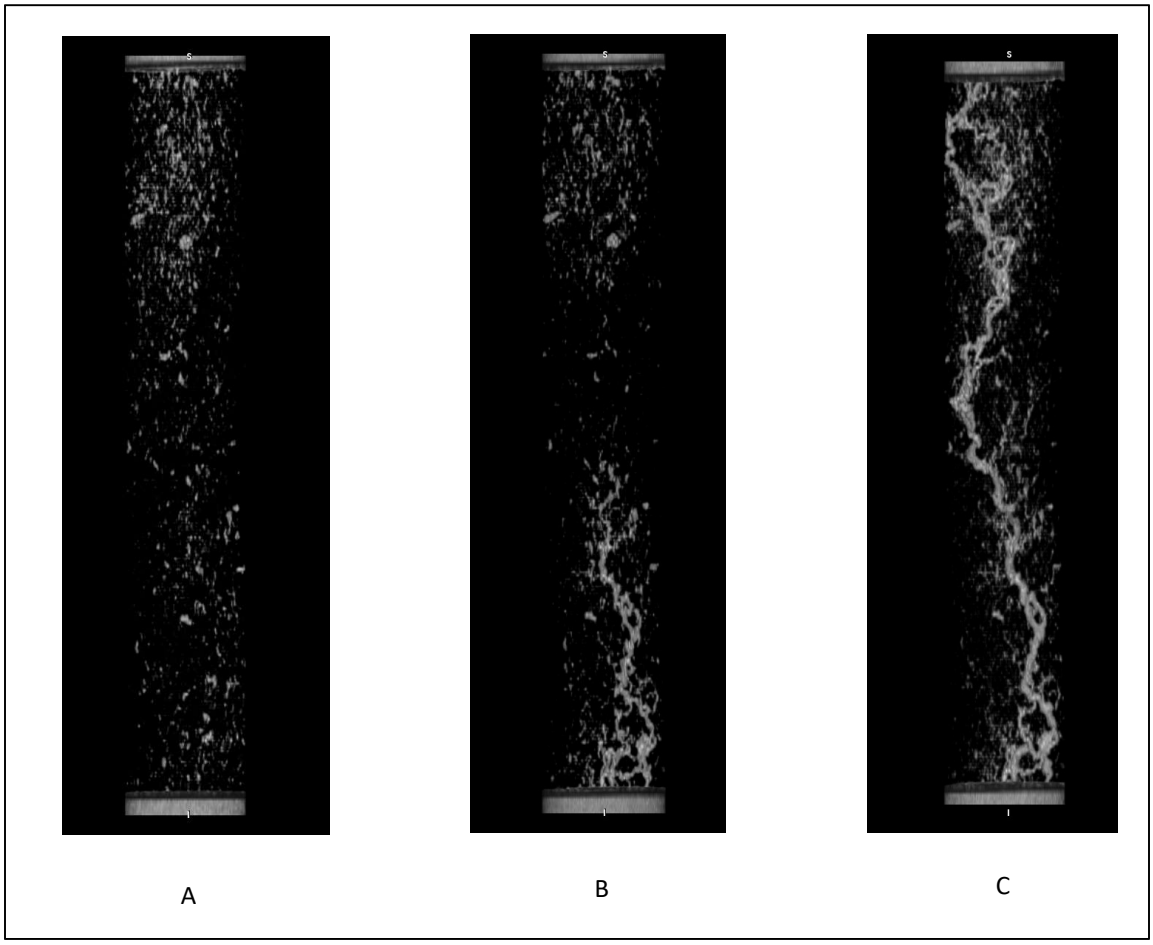

Figure 4-2: CT scans at the various stages of the first experiment
A: Fresh water-saturated core before any acid or PLA was injected
B: Core after 1st stage of acid in injected and PLA was injected
C: Core after 2nd stage of acid was injected
Reprinted with permission from (Shirley and Hill, 2019)

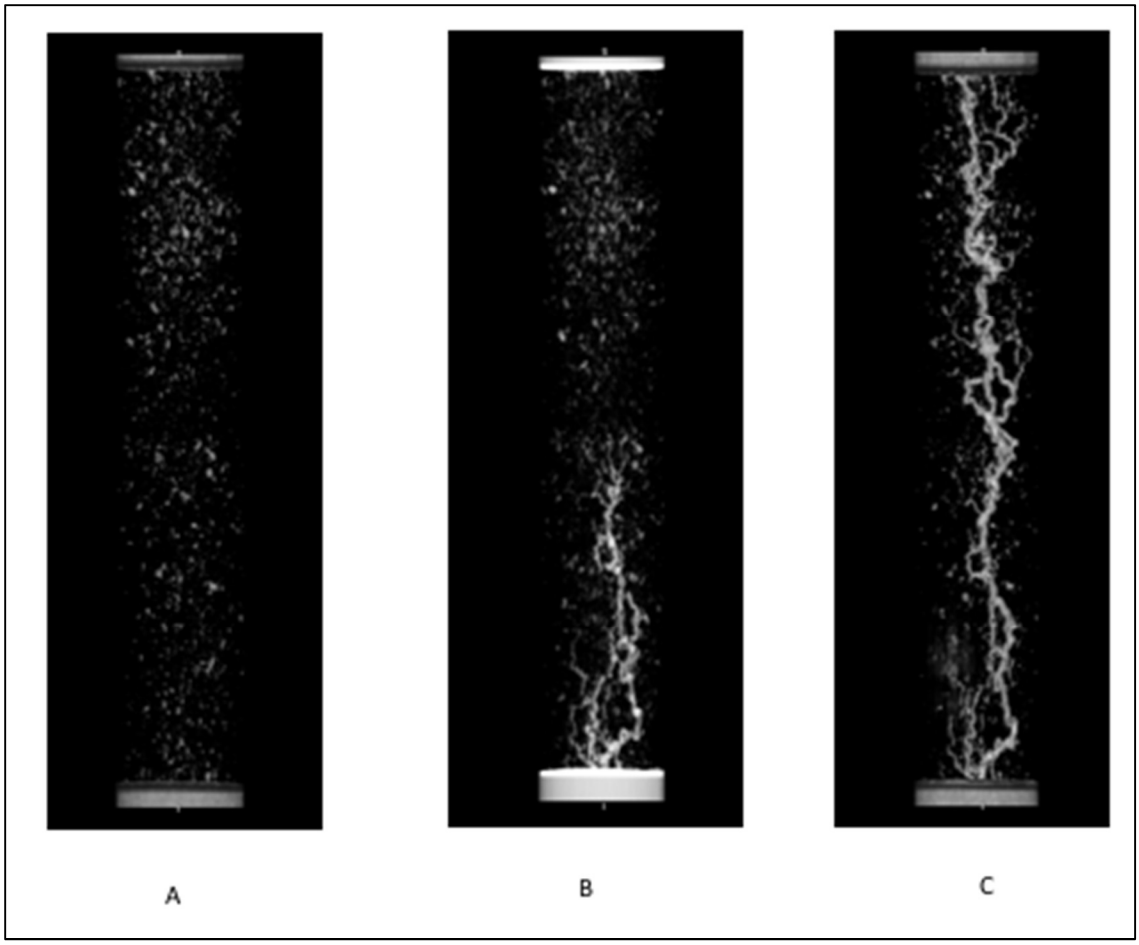

Figure 4-3: CT scans at the various stages of the second experiment
A: Fresh water-saturated core before any acid or PLA was injected
B: Core after 1st stage of acid in injected and PLA was injected
C: Core after 2nd stage of acid was injected
Reprinted with permission from (Shirley and Hill, 2019)

Both Figure 4-2 and Figure 4-3 show that the acid added in the 2nd stage of acidizing continued to propagate the dominant wormholes.

4.3 How Does PLA Affect Pressure Drop?

The experiments that were carried out allowed us to investigate the pressure drop caused by PLA both when it is in a filter cake (on the surface of the core), as well as when it is in the wormhole. The pressure drop across the core was measured at four different stages during each experiment. During each measurement, fresh water was flowing through the core at 5 ml/min. The first measurement was taken after the core was saturated with fresh water, and before any acid or PLA was injected into the core (Figure 4-4 - ΔP_0). The next measurement was made after the 1st stage of acidizing. No PLA had been added at this stage; the fresh water-saturated core contained a wormhole that did not fully penetrate the core (Figure 4-4 - ΔP_1). The pressure drop was then measured after the PLA was injected, and fresh water was pumped into the core to remove the $CaCl_2$ brine (Figure 4-4 - ΔP_2). At this time, there was PLA in the filter cake (on the surface of the core in the spacer) and the wormhole. The core was then removed from the core holder. The filter cake on the surface of the core and the spacer were then removed. The core was then put back in the core holder, and the final pressure drop was measured (Figure 4-4 - ΔP_3). At that time, PLA was only in the wormhole. Figure 4-4 illustrates the stages that the four pressure drop measurements were taken.

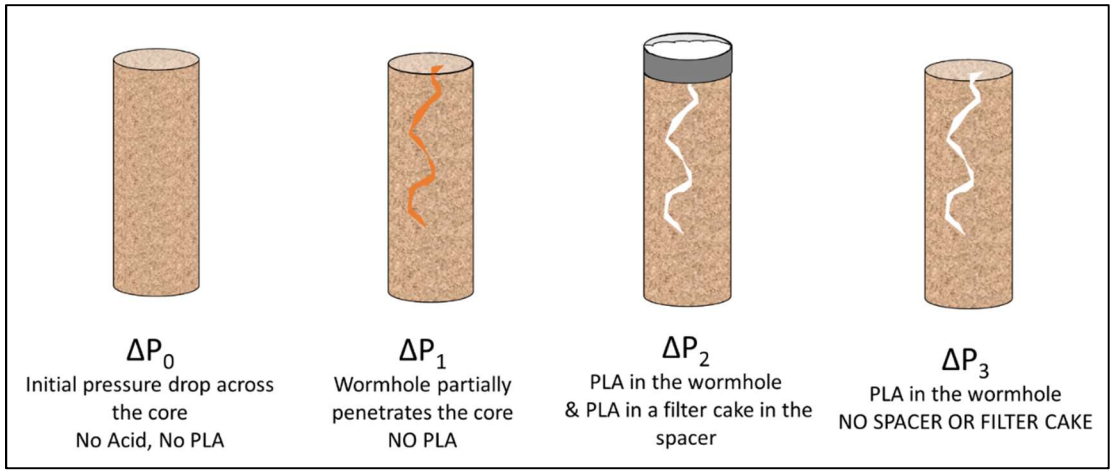

Figure 4-4: An illustration of the core during the four differential pressure drop measurements that were taken in each experiment.
Reprinted with permission from (Shirley and Hill, 2019)

Figure 4-5 illustrates how the measurements were used to calculate the pressure drop caused by the PLA inside the wormhole.

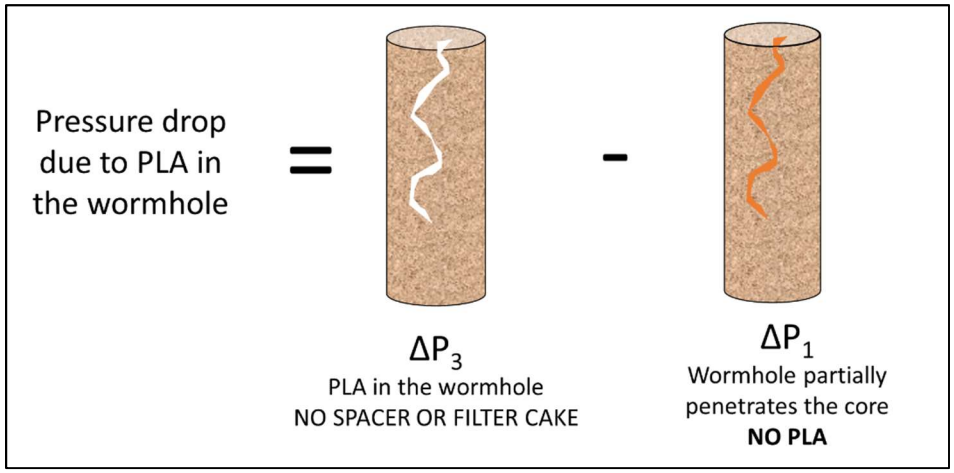

Figure 4-5: Calculation of pressure drop due to PLA in the wormhole
Reprinted with permission from (Shirley and Hill, 2019)

Figure 4-6 illustrates how the measurements were used to calculate the pressure drop caused by PLA in the filter cake.

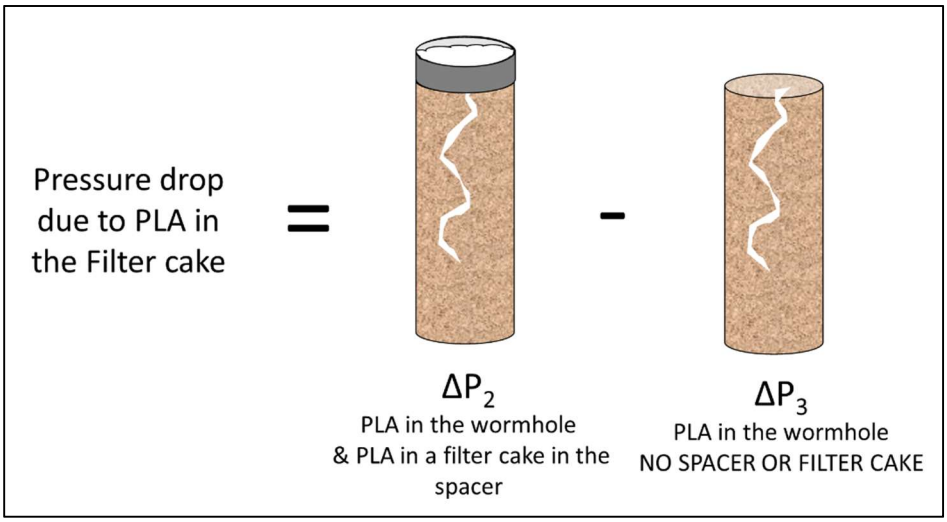

Figure 4-6: Calculation of pressure drop due to PLA in the filter cake. Reprinted with permission from (Shirley and Hill, 2019)

Additionally, we calculated the mass of PLA in the wormhole and the mass of PLA in the filter cake. A CT scan image processing software (Horos Project ©) was used to calculate the volume of the wormholes. Since we have previously shown that PLA fully invaded the wormholes, the mass of PLA in the wormholes was calculated based on the volume of the wormhole, the density of PLA particles and the porosity of the PLA filter cake. Note, the permeability and porosity of the filter cake were calculated from experiments where a filter cake is built on a core without any wormholes; this is discussed in more detail in the next section. Since we also knew the total mass of PLA that was

pumped, the mass of PLA in the filter cake was calculated by the difference between the total mass of PLA injected and the mass of PLA in the wormhole.

A total of five experiments were carried out as described above. An additional two experiments were carried out where the PLA suspension was pumped onto a core with no wormhole developed. When there was no wormhole in the core, the pressure drop due to PLA in the filter cake was calculated as the difference between the pressure drop across the core before and after pumping the PLA suspension. Also, the mass of PLA in the filter cake was simply the mass of PLA that was pumped. Figure 4-7 shows a plot of pressure drop in a PLA filter cake versus the mass of PLA in the filter cake. Each point represents a separate experiment. Note that though five experiments were carried out using cores with partially penetrating wormholes, insufficient data was measured to find the pressure drop in the filter cake for two of those tests.

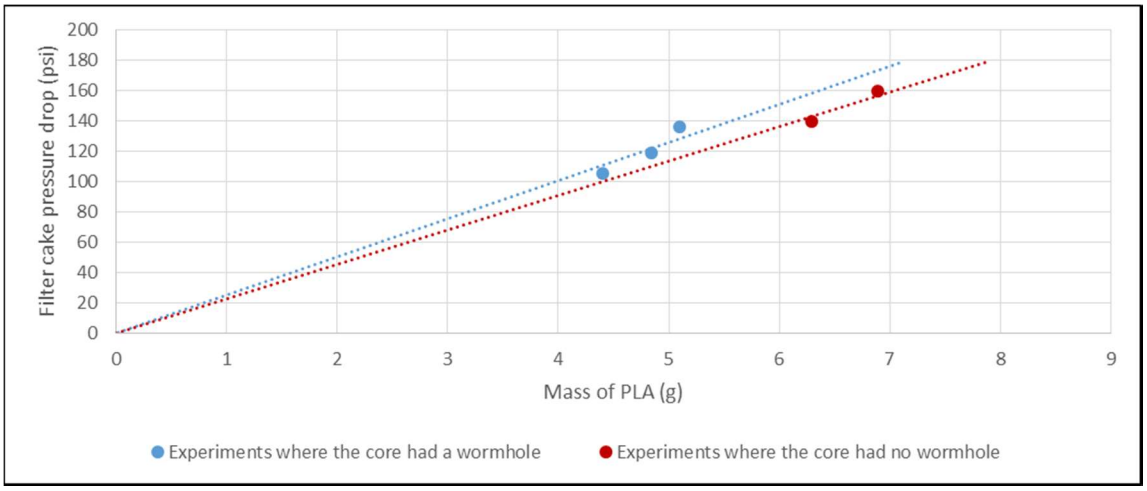

Figure 4-7: Linear relationship between pressure drop due to a filter cake and mass of PLA in the filter cake on the surface of the core.
Reprinted with permission from (Shirley and Hill, 2019)

The pressure drop due to PLA in the filter cake is directly proportional to the mass of PLA in the filter cake. This relationship is precisely as expected for an incompressible filter cake. This relationship was also shown experimentally by Hill and Galloway (1984) (provided that the diverting agent covers the face of the core). The two trend lines almost overlap each other, which suggests that the constant of proportionality between pressure drop and mass is the same whether or not there was a wormhole.

Figure 4-8 shows the relationship between pressure drop and mass for the PLA in the wormhole.

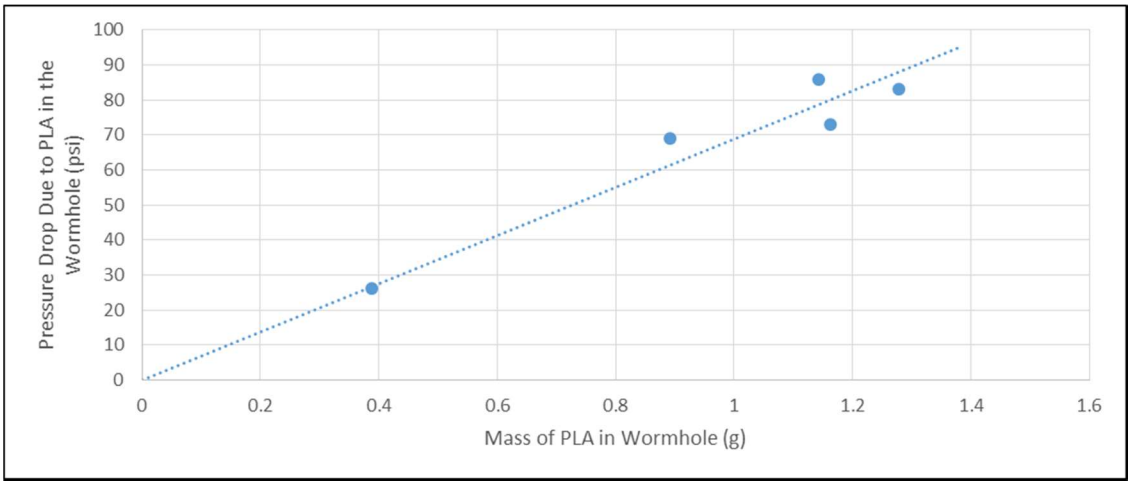

Figure 4-8: Linear relationship between pressure drop due to PLA in the wormhole and mass of PLA in the wormhole.
Reprinted with permission from (Shirley and Hill, 2019)

Figure 4-8 shows that even in the tortuous and narrow wormholes, the pressure drop is proportional to the mass of PLA. If we combine the plots from Figure 4-7 and Figure 4-8 as in Figure 4-9, we find that while pressure drop is proportional to the mass

of PLA in or out of a wormhole, and the constant of proportionality is higher when PLA is in the wormhole.

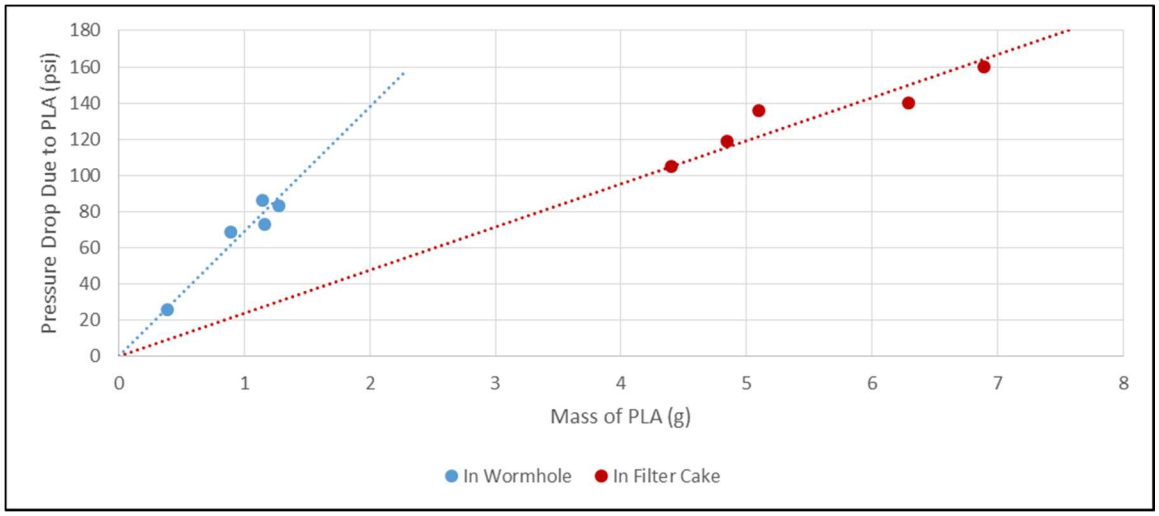

Figure 4-9: Comparison of the relationship between pressure drop and mass of PLA when the PLA is on the core surface and in the wormhole. Reprinted with permission from (Shirley and Hill, 2019)

It is the author's view that this is caused by the PLA in the wormhole forcing flow to have to go through the rock matrix around the wormhole, rather than through the wormhole. This is discussed in more detail in the following sections.

4.4 Skin Factor Due to PLA in a Filter Cake on the Surface of the Core

From Darcy's Law, the pressure drop across a porous medium of length, l, is:

$$\Delta P = \frac{\mu q l}{A k} \tag{4-1}$$

Thus for a filter cake of thickness, $l_{cake,}$ and permeability, k_{cake}:

$$\Delta P_{cake} = \frac{\mu q l_{cake}}{A k_{cake}} \tag{4-2}$$

Using Eq. 4-2, we estimated the permeability of the PLA filter cake from our experiments. We measured the pressure drop across the filter cake (Figure 4-7). The cross-sectional area was calculated based on the inner diameter of the spacer. The flow rate was known because it was fixed throughout the experiment, and we measured the thickness of the filter cake at the end of the experiment. This resulted in k_{cake} of 0.5mD. This was significantly smaller than the permeability of the Indiana Limestone cores being used (10-20mD). Note though, that the thickness of the filter cake, and by extension its permeability, was a rough estimate because it was difficult to depressure and disassemble the core holder without disturbing the filter cake.

The expression in Eq. 4-2 was modified to obtain a skin factor in terms of the mass of PLA in a filter cake. To do so, we first replaced the thickness of the filter cake with the mass of PLA accumulated, m_{cake}:

$$l_{cake} = \frac{V_{cake}}{A} \tag{4-3}$$

Where V_{cake} is the volume of the filter cake.

$$l_{cake} = \frac{V_{pc}}{A \times (1 - \varphi_{cake})} \tag{4-4}$$

Where V_{pc} is the volume of the particles deposited in the filter cake.

$$l_{cake} = \frac{m_{cake}}{A \times (1 - \varphi_{cake}) \times \rho_{da}} \tag{4-5}$$

Substituting Eq. 4-5 into Eq. 4-2:

$$\Delta P_{cake} = \frac{\mu q m_{cake}}{A^2 \rho_{da} k_{cake} (1 - \varphi_{cake})} \tag{4-6}$$

We adopted the approach to group the properties that are intrinsically related to the filter cake into a term called specific cake resistance, α (Ruth 1933, Grace 1953):

$$\alpha = \frac{1}{\rho_{da} k_{cake} (1 - \varphi_{cake})} \tag{4-7}$$

Substituting this expression into Eq. 4-6:

$$\Delta P_{cake} = \frac{\mu q \alpha m_{cake}}{A^2} \tag{4-8}$$

Using Eq. 4-8 and the plot shown in Figure 4-7, the specific cake resistance for the PLA used was calculated to be: α = 3.65 x 10^{12} ft/lb. This value is specifically based on the PLA size and shape used and the conditions tested in the experiments. Since we knew the permeability of the filter cake and the specific cake resistance, we also calculated the porosity of the filter cake using Eq. 4-7 (φ_{cake} = 0.36). Eq. 4-8 is very useful because it can be converted to a skin factor via van Everdingen's expression for skin factor (van Everdingen 1953, Doerler and Prouvost 1987, Economides et al., 2013):

$$s_{cake} = \frac{2\pi kL}{q\mu} \Delta P_{cake} \tag{4-9}$$

Substituting Eq. 4-8 into Eq. 4-9:

$$s_{cake} = \frac{2\pi kL}{A^2} (\alpha\, m_{cake}) \tag{4-10}$$

4.5 Skin Factor Due to PLA in the Wormhole

As can be seen from Figure 4-8, there was a pressure drop that was induced by having PLA inside of the wormholes. We have shown earlier that the PLA filter cake had a permeability that was much lower than the rock matrix. When there are multiple paths for fluid to flow into, some fluid may travel through each of the available paths, but the majority of the fluid will flow through the paths of least resistance. From Figure 4-2 and Figure 4-3, we know that the majority of the acid flowed in an annulus around the PLA filled wormhole since the dominant wormhole continued to propagate during the second stage of acidizing.

We can prove this by considering the pressure drop across the cores when there was PLA inside the wormhole but no spacer or filter cake on the surface (ΔP_3 in Figure 4-4), compared to the initial pressure drop across the cores, i.e., before any acid or PLA was injected (ΔP_0 in Figure 4-4) – see Figure 4-10. The flow rate was 5ml/min when either pressure drop measurement was taken for each core.

This plot shows that the pressure drop across the core when there was PLA in the wormhole was approximately equal to the initial pressure drop across the core. This suggests that fluid was flowing through the matrix of the rock and not through the PLA filled wormhole. Note that the pressure drop when the PLA filled the wormhole was generally slightly less than the original pressure drop across the core, at the same flow rate. This may be because the PLA did not entirely invaded the pore space created by the acid even though the PLA fully invaded the dominant wormholes.

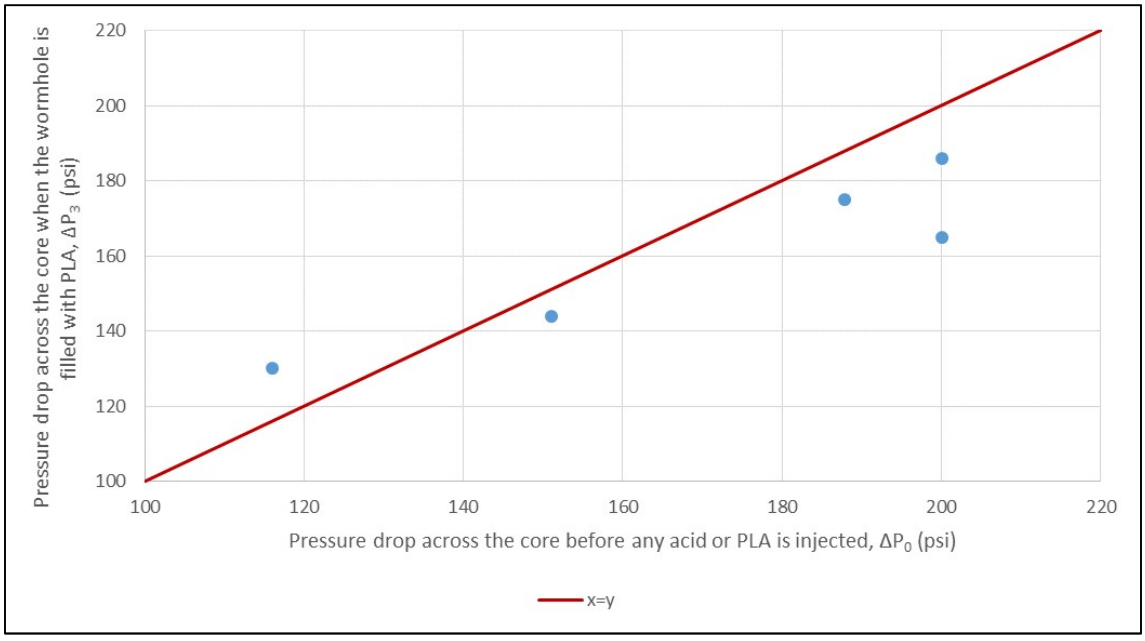

Figure 4-10: Comparison of the pressure drop across the core when the cores have PLA filled wormholes and when the cores have no PLA or wormholes. Reprinted with permission from (Shirley and Hill, 2019)

In conclusion, when PLA enters a wormhole, providing that its filter cake has a lower permeability than the surrounding rock, it affects pressure drop by preventing flow to go through the wormhole. Based on this, we created a general expression for skin factor due to PLA in field acidizing treatments as follows.

If PLA does not enter the wormholes:

$$s_{PLA} = \frac{2\pi kL}{A^2}(\alpha\, m_{cake}) - \ln\frac{r_{wh}}{r_w} \tag{4-11}$$

Where r_{wh} is the radius of the wormholed region = length of the wormholes

r_w is the radius of the wellbore

L is the length of the producing interval

k is the formation permeability

A is the area perpendicular to flow leaving the wellbore:

$$A = 2\pi r_w L \tag{4-12}$$

s_{PLA} is the skin factor due to the PLA and the wormhole after injection of PLA.

Once the PLA hydrolyzes, the first term becomes zero since the mass of filter cake becomes zero.

If PLA enters the wormhole:

$$s_{PLA} = \frac{2\pi kL}{A^2}(\alpha\, m_{cake}) - \ln\frac{r_{wh} - l_{PLA}}{r_w} \tag{4-13}$$

Where l_{PLA} is the length of the wormholed region that is filled with PLA.

Figure 4-11 shows the various dimensions being described.

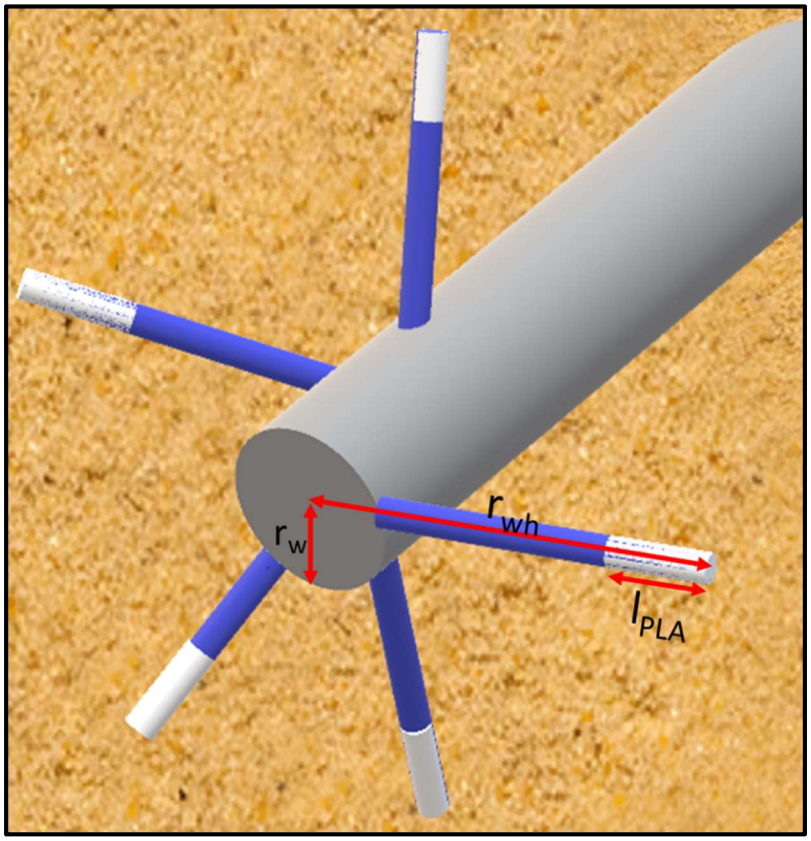

Figure 4-11: An illustration of PLA inside of wormholes during a field treatment. Reprinted with permission from (Shirley and Hill, 2019)

The length of the wormholed region that is filled with PLA, l_{PLA} can be calculated based on the volume of acid that is used and the mass of PLA that enters the wormhole. The total volume of the wormholes (V_w) is the total volume of rock dissolved by the acid injected:

$$V_w = V_{acid} \times \chi \tag{4-14}$$

Where V_{acid} is the total volume of acid injected and

χ is the acid dissolving power.

The length of the wormholes filled with PLA is simply the ratio of the volume of PLA cake in the wormhole (V_{pw}) to the total volume of wormholes created (V_w) multiplied by the length of the wormhole (r_{wh}):

$$l_{PLA} = \left(\frac{V_{pw}}{V_w}\right) \times r_{wh} \tag{4-15}$$

We can substitute expressions for the volume occupied by PLA in the wormholes and total volume of the wormholes created as follows:

$$l_{PLA} = \frac{m_{PW} r_{wh}}{\rho_{da}(1 - \varphi_{cake}) V_{acid} \chi} \tag{4-16}$$

Where m_{PW} is the mass of PLA in the wormholes.

In terms of specific cake resistance:

$$l_{PLA} = \frac{\alpha k_{cake} m_{PW} r_{wh}}{V_{acid} \chi} \tag{4-17}$$

Once the PLA hydrolyzes, the mass of filter cake, m_{cake}, and the length of the wormholed region that is filled with PLA, l_{PLA}, become zero.

4.6 Comparison with Other Experimental Investigations

In this study, experiments were only done with one particle size of PLA. The PLA that was used in the experiments described earlier were a fairly uniform size distribution (0-45 microns). However, it has been shown that using a mix of PLA sizes is preferential to ensure that PLA plugs the wormholes, or perforations, and builds as a filter cake instead of filling the wormholes (Shahri et al., 2017). Fortunately, we can use the results of another investigator (Huang et al., 2018) who has experimented with various sizes and even carried out experiments with bi-modal PLA size distributions. Their results were used to validate the equations that were developed to describe the pressure drop effects when PLA builds a filter cake on the surface.

The data that was presented by Huang et al. (2018) was derived from their "single slot" (or particle plugging) experiments and models. Figure 4-12 shows the setup of the experiments where a slurry containing the diverter was injected into a sleeve that contained a single machined slot on the outlet. Figure 4-13 shows permeability, porosity, average particle size, and pressure build-up data for a bi-modal size distribution (7 and 100 mesh). In Figure 4-13, 'small particle ratio' refers to the percentage of the mixture that is made up of 100 mesh particles. In the first two plots, the green band shows the mixture of particles that the investigators found to appropriately plug the slotted sleeve and build a filter cake in the 'plugging domain' as shown in Figure 4-12.

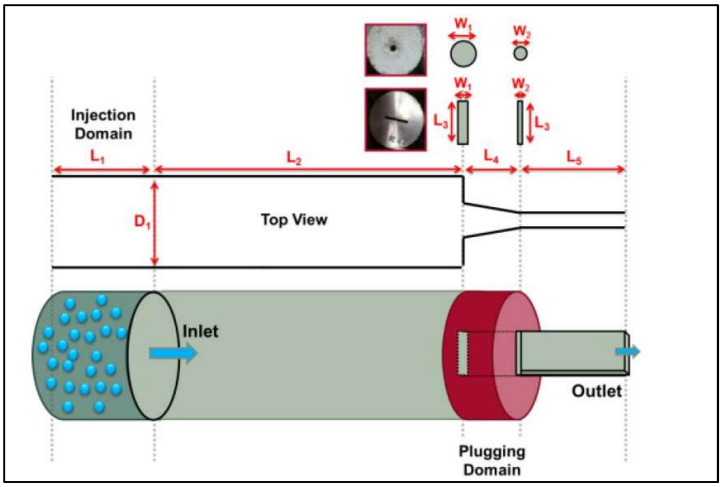

Figure 4-12: Experimental set up used by Huang et al. (Adapted from Huang et al., 2018)

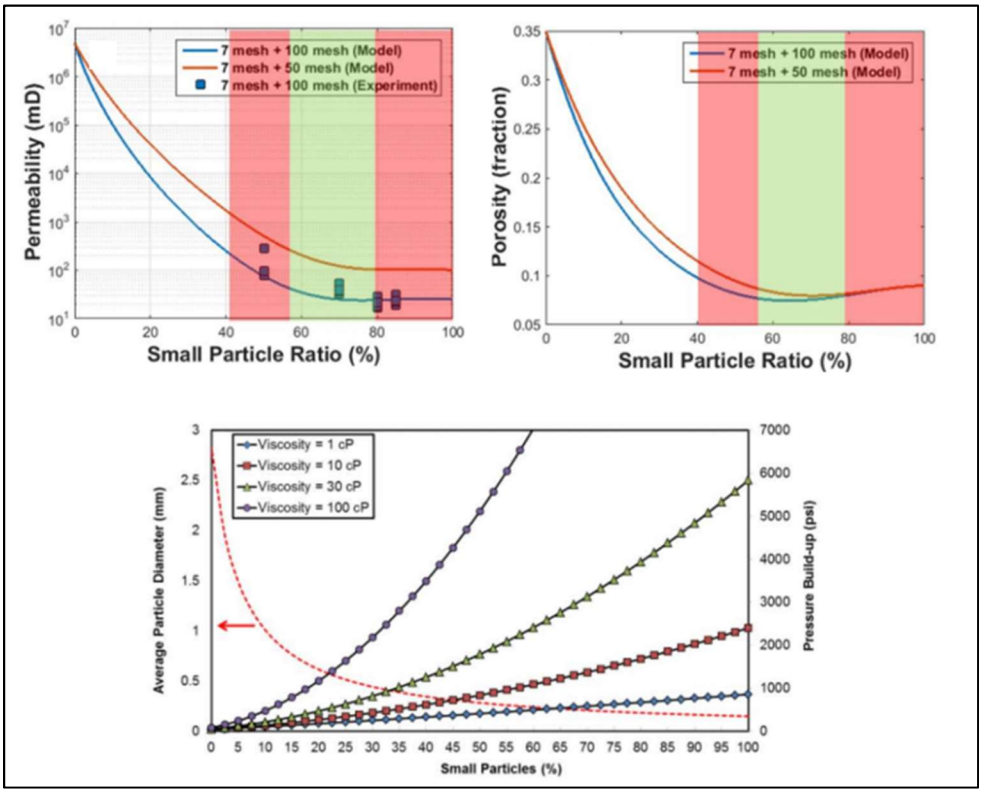

Figure 4-13: Permeability, porosity and pressure drop data for varying PLA particle sizes (Adapted from Huang et al., 2018 and Shahri et al., 2017)

We used the given permeability and porosity data to calculate the specific cake resistance via Eq. 4-7. Please note that we did not calculate the specific cake resistance using the pressure drop data, as was done using our core flood results. If the expression in Eq. 4-8 is true for the PLA cake that was built up in their experiments, then a plot of their given pressure drop values versus specific cake resistance should be linear for the particle sizes that result in a stable plug. This is shown in Figure 4-14.

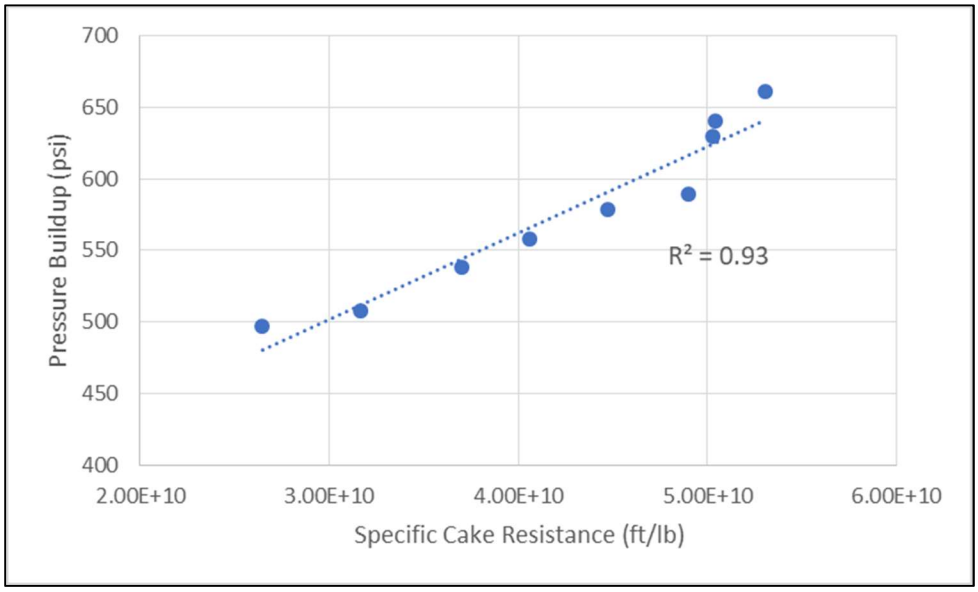

Figure 4-14: Confirmation that pressure drop across a PLA filter cake is proportional to specific cake resistance for a variety of particle sizes

It is also worth noting that the permeability of the PLA filter cakes that were developed in the experiments carried out for this dissertation followed the same trend of the filter cakes that were developed by Huang et al. (2018) based on average particle size. This can be seen in Figure 4-15.

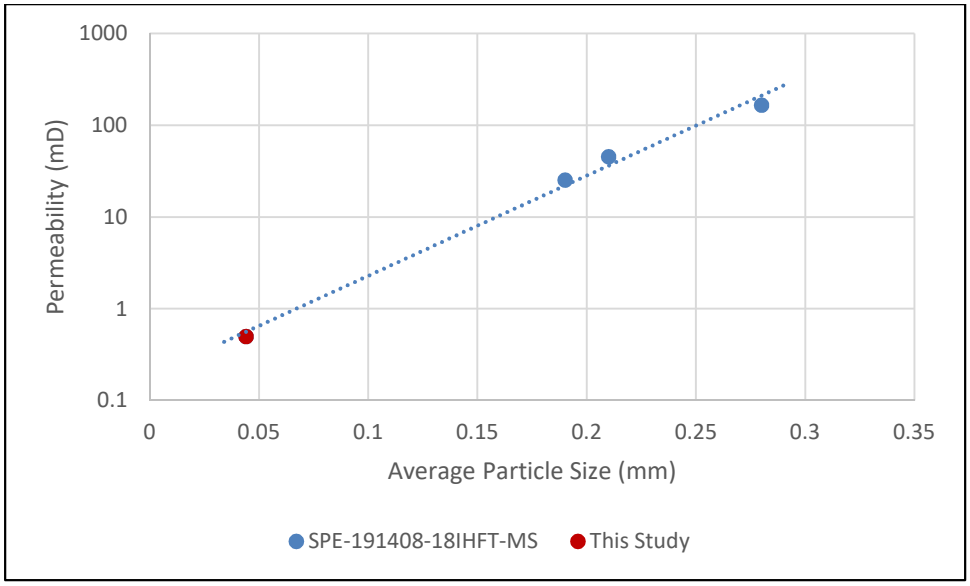

Figure 4-15: A plot of PLA filter cake permeability versus particle size combining our result with those from Huang et al. (2018)

Additionally, in order to use PLA as a diverting agent in field applications, PLA must meet many other criteria, aside from its ability to add local resistance to flow wherever it is deposited. The PLA particles must be stable under surface and pumping conditions, able to quickly form a filter cake and able to degrade quickly and completely after the stimulation treatment. While many of these criteria were not tested in this study, others have investigated these key criteria; their results will be presented in the subsequent sub-sections.

4.6.1 Effect of Particle Concentration on Plugging

In the same study that was used to compare our PLA filter cake pressure drop relationship and permeability, Huang et al. (2018) used the same apparatus to justify the presence of a critical PLA concentration. The authors suggest that there exists a concentration below which a stable plug does not form. They used their experimental results (see Figure 4-16) to show that this concentration is not a fixed value but depends on the ratio of the size of the particles to the size of the opening to be plugged.

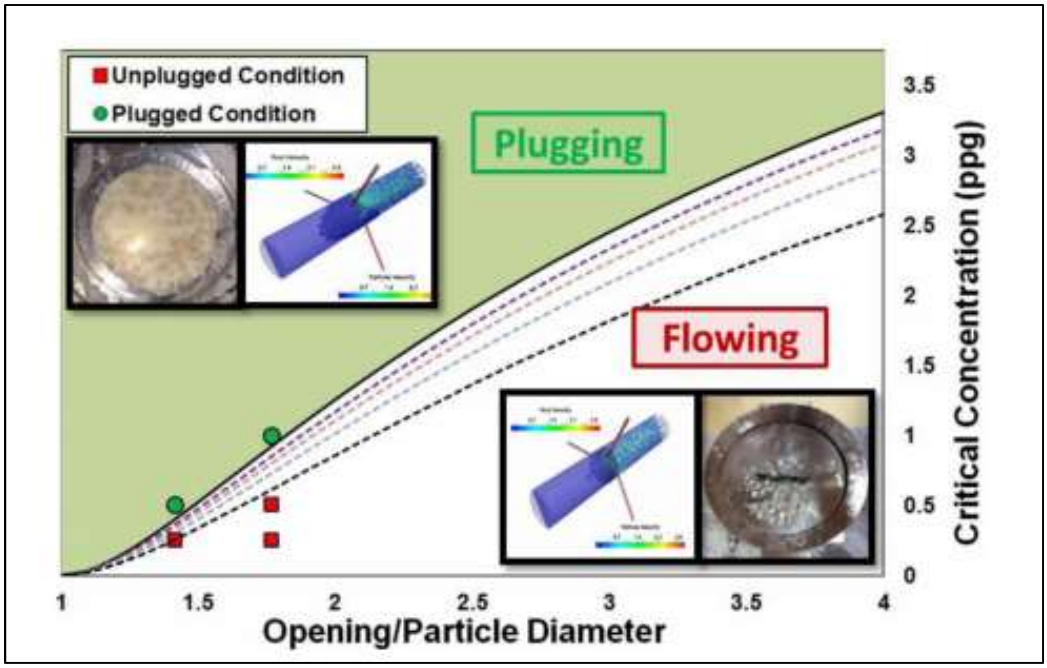

Figure 4-16: Critical concentration of PLA that is required to plug a slot based on the opening to particle size ratio (Adapted from Huang et al., 2018)

4.6.2 Particle Attrition

Given how important the particle size is to both developing a plug, as well as the permeability of the filter cake that is developed, it is important that the PLA that is injected can remain the same size throughout the treatment. This is important because the filter cake that is developed can create resistances of several hundred pounds per square in (psi) pressure. A study carried out by Glasbergen et al. (2006) tested particle attrition using a flow loop that included a centrifugal pump, a high-pressure triplex pump, a storage tank and a choke. As can be seen in Table 4-1, even when exposed to pressure differentials of up to 3000psi, the PLA particles that were originally on average 150μm were able to maintain an average size of at least 125μm. This suggests that PLA particles can maintain their size during the treatment.

Table 4-1: Results of a study carried out to test particle attrition of PLA (Adapted from Glasbergen et al., 2006)

Tool	Particle Size Mean Diameter (D50) μm
Centrifugal Pump	150
Centrifugal Pump + Choke + HT400 (1000psi)	131
Centrifugal Pump + Choke + HT400 (2000psi)	135
Centrifugal Pump + Choke + HT400 (3000psi)	125

4.6.3 Hydrolytic Degradation Rate

One of the most important features of PLA as a diverting agent is its ability to degrade at the end of the treatment. If it does not fully degrade, it can cause severe formation damage. Shahri et al. (2018) have shown that both pH extremes can accelerate the hydrolytic degradation reaction (see Figure 4-17).

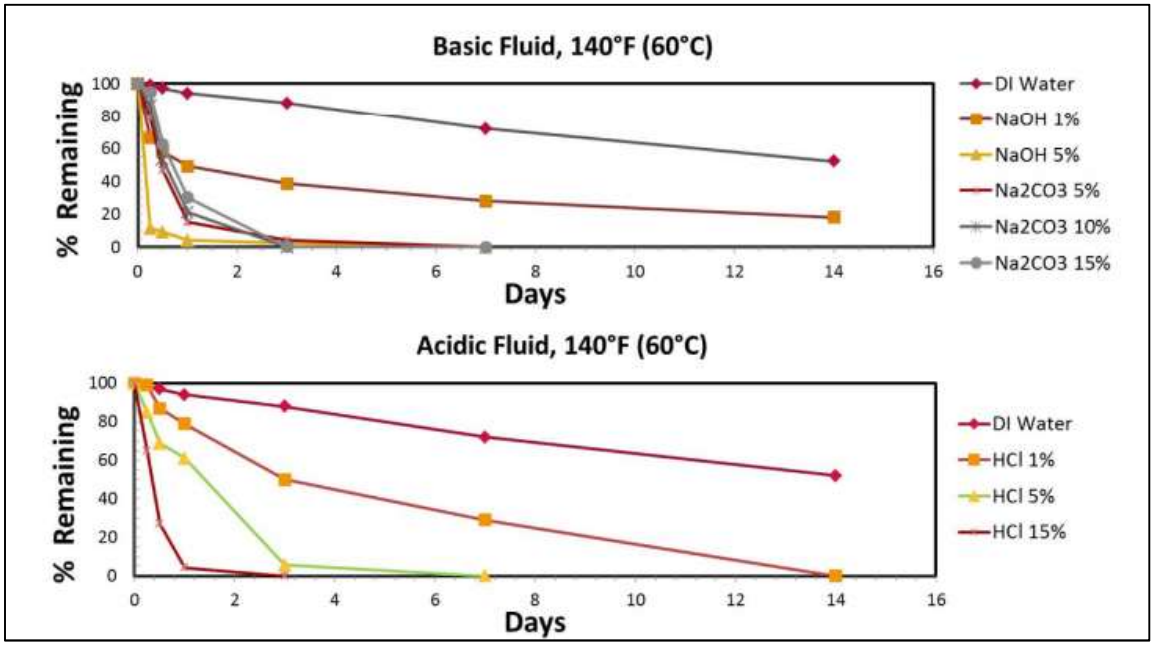

Figure 4-17: Impact of pH on rate of PLA degradation (Adapted from Shahri et al., 2017)

As an alternative, if highly acidic or basic fluids are not preferred, Reddy and Cortez (2014) investigated some fluids such as ethanolamine (EA), ethylenediamine (EDA) and triethylenetetramine (TETA) that were found to be suitable degradation accelerators. In their study, Reddy and Cortez also suggest that the crystallinity of the PLA

that is used can have a significant impact on the degradation rate. The more amorphous (less crystalline) the PLA is, the faster its degradation rate tends to be.

Like many other reactions, the degradation reaction rate is accelerated by higher temperatures (see Figure 4-18). This indicates that low-temperature reservoirs may not be suitable candidates for the use of PLA diversion.

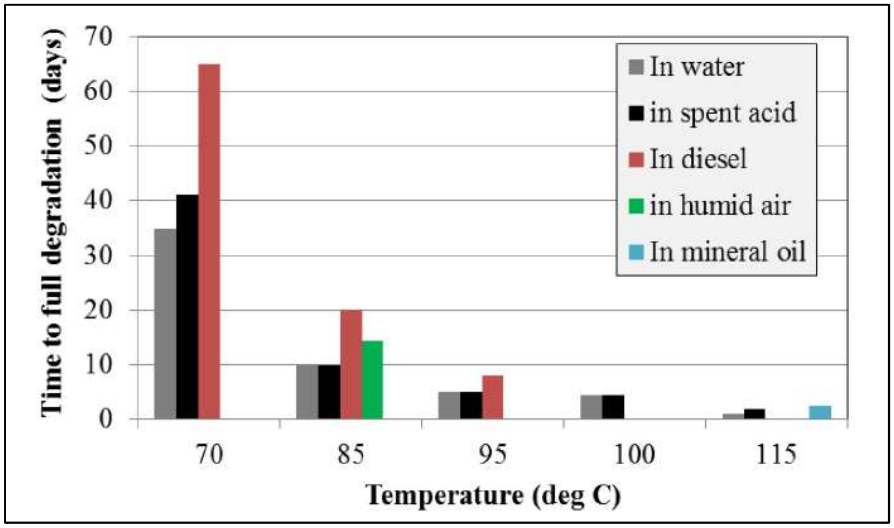

Figure 4-18: The impact of water content and temperature on PLA degradation rate (Adapted from Sau et al., 2015)

In the study carried out by Sau et al. (2015), the impact of water content on the degradation rate was investigated. If the water that is used to deliver the stimulation and diversion treatment quickly dissipates into the reservoir, the PLA relies on the connate water to degrade. This raises the question of how quickly PLA can degrade in water-depleted environments. To test this, PLA fibers were soaked in water, the water was then pressed out of the fibers, and finally, the fibers were stored in various environments such

as diesel, mineral oil, spent acid and humid air (see Figure 4-18). Even in the water-depleted environments like the diesel, PLA degrades, but it takes considerably longer than in water-rich environments.

In the same study, Sau et al. also studied the impact of water concentration on the degradation rate by directly varying the water content in another type of experiments. In these experiments, 2g of fibers were added to a bottle with 4ml of kerosene and between 0.25-1g of water. Each of these bottles were kept at a constant temperature, and the degradation rate was measured. Note that degradation was measured by removing the bottle after a set time, cooling the contents, filtering the solids out and weighing the solids.

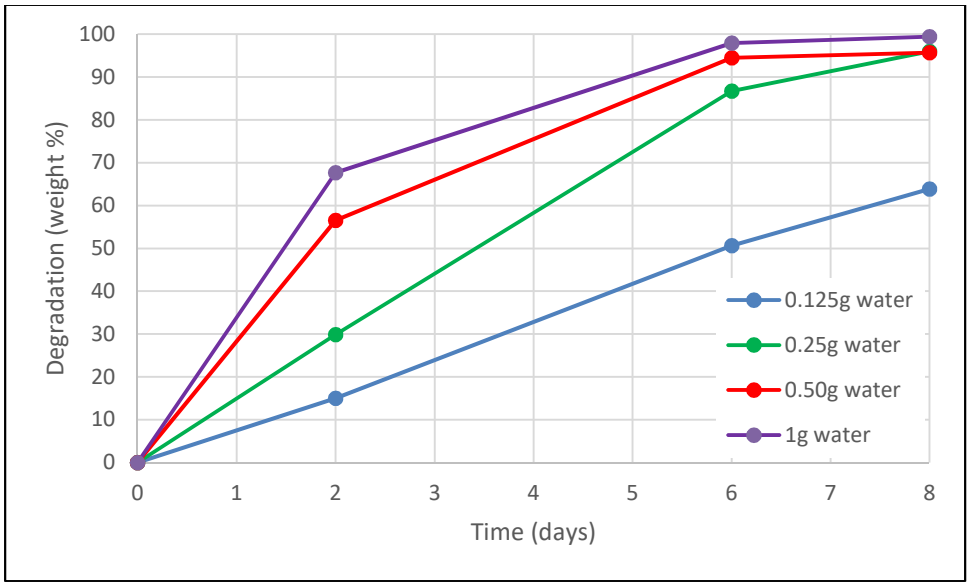

Figure 4-19: Degradation rate of PLA based on water content (Adapted from Sau et al., 2015)

The results, as seen in Figure 4-19, clearly show that between 0.25-1g of water, higher water content corresponded with a higher rate of PLA degradation.

4.7 Model Validation

The expressions shown in Eq. 4-11 and Eq. 4-13 were implemented in a comprehensive near wellbore matrix acidizing simulator called Horizontal Well Acidizing Simulator (HWAS). A full description of the model can be found in Mishra et al. (2007). The skin factor model was validated using the simulator and field data for two wells provided by Thabet et al. (2009). The deviated, cased and perforated wells were drilled in thick carbonate gas reservoirs in North Field, offshore Qatar in the Middle East. Due to the high level of heterogeneity in these reservoirs (a few milli-darcy to several Darcy), the presence of naturally occurring fractures and other factors, it was decided to use a multi-stage treatment including a degradable diverting agent to obtain a uniform acid placement along the well.

The treatment fluid consisted of alternating stages of 28% HCl acid and diverting solutions. The diverting solutions included degradable fibers in a 15% HCl acid solution and a viscoelastic surfactant (VES) in a 15% HCl acid solution. In their paper, Thabet et al. (2009) claim that though VES self-diverting acids have been successful for several carbonate reservoirs, they were unable to effectively create an even acid distribution in the presence of large permeability contrast, such as in formations where there are natural fractures and fissures, vuggy formations and "super-k" high permeability intervals. Because of this, we have not modeled the effects of the VES in our model. No details were given about the size of the degradable diverter that was used. However, the paper states that the diverter was sized to fill and plug perforations during the experimental

investigation, thus, we assume that the PLA did not enter the wormhole but quickly bridged and built a filter cake.

In each case, the permeability distribution along the well, the pump schedule, and fluid composition were given. In the paper, Thabet et al. (2009) show the field skin profile of the pumped treatment. The given skin profile for the pumped treatment was validated using production logging tool (PLT) data and the bottom-hole pressure (BHP) history. To verify our proposed model, we simulated and matched the skin profiles using the same input data. The specific cake resistance of PLA in the filter cake was modified to allow our simulated skin profile to match the published skin factor.

Case 1

Figure 4-20 shows the permeability profile for the first well that was simulated.

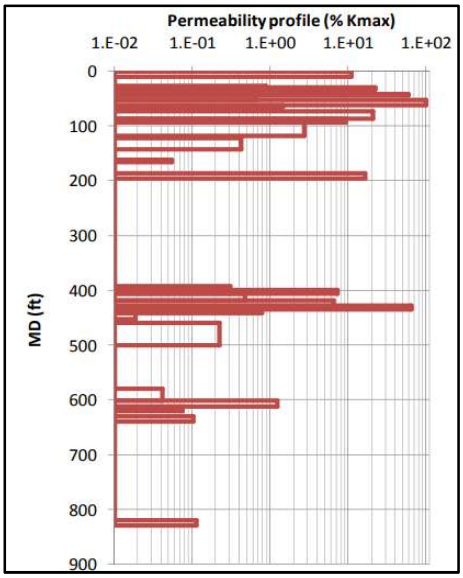

Figure 4-20 Permeability profile of the well that was used in the 1st validation case (Adapted from Thabet et al., 2009)

Figure 4-21 shows the pump profile that was used for the actual field treatment. The duration and pump rate for each of the five acid stages and the four diversion stages are given in this figure.

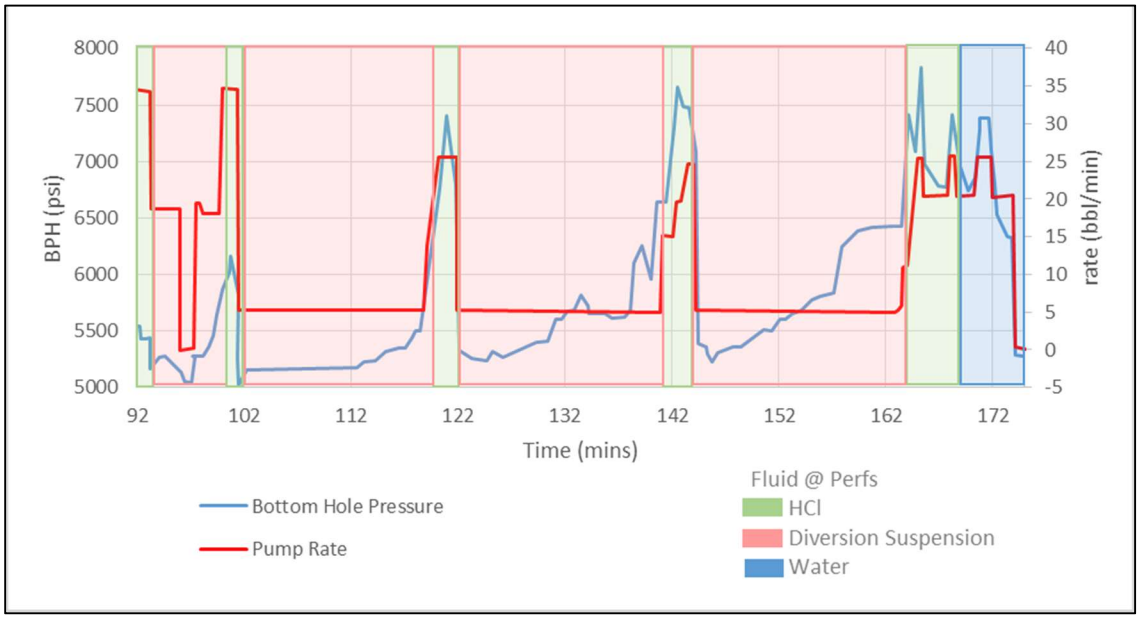

Figure 4-21: Pump schedule and BHP Profile for well used in the 1st validation case (Adapted from Thabet et al., 2009)

Figure 4-22 shows the published pre and post production logging data for this well. Thabet et al. (2009) explain that the logging data was used to calculate the permeability profile for the well. They also show that their simulations were able to recreate the production logging data. This suggests that the skin profiles that they obtained from their simulations were verified with field data. For this study, we will attempt to match our simulated skin profile with their published skin profile.

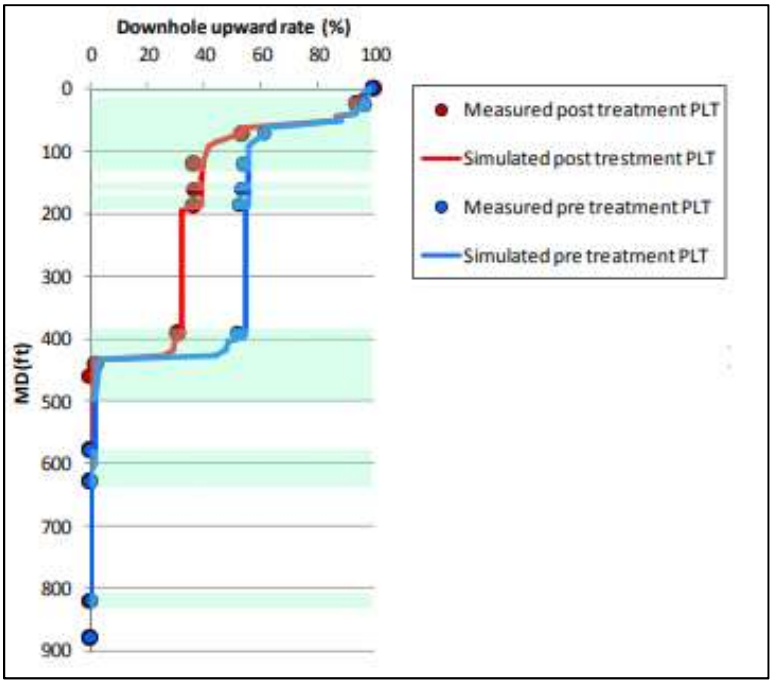

Figure 4-22: Pre and post production logging data for 1st case (Adapted from Thabet et al., 2009)

Table 4-2 shows all of the parameters that were used for simulating this treatment.

Table 4-2: Parameters used to simulate case 1

Parameters	Units	Value	Comments
Well Completion		Cased and Perforated	
Placement Method		Bullheading	
Reservoir Type		Gas	
Reservoir Fluid Viscosity	cP	0.015	assumed
Wellbore radius	ft	0.51	assumed
Porosity		15%	assumed
Max Permeability	mD	2000	
Perforation length	in	15	assumed
Perforation Diameter	in	0.39	assumed
Perforation Phasing	deg	120	
Shot density	spf	3	
PLA concentration	lb/1000 gal	75	
Damage Penetration	ft	1.25	assumed
Permeability Impairment Ratio		0.1	assumed
Specific Gravity of Diverting Agent		1.24	
Acid Concentration in Pure Acid Stages		28%	
Acid Concentration in Diversion Suspension Stages		15%	
Specific Cake Resistance	ft/lb	9.0e13	

The specific cake resistances used were higher than those observed in the experiments. This could be due to differences in the temperature (PLA behaves very differently above its glass transition temperature; recall that during the attempted high-temperature experiments PLA could not even be pumped through the 1/8" tubing), as well as differences in the PLA particle size and shape.

The optimal pore volume to breakthrough and interstitial velocity points were obtained from several experiments done on 1.5" diameter and 8" length outcrop limestone cores. The Furui et al. (2012) empirical wormhole model was used to calculate the wormhole propagation. Table 4-3 shows the optimal conditions that were used as inputs for the simulation.

Table 4-3: Optimal points used for wormhole propagation calculations

Optimal Pore Volume to Break Through	Optimal Interstitial Velocity	Min Perm that this optimal point refers to	Max Perm that this optimal point refers to
PV_{bt-opt}	V_{i-opt}	k_{min}	k_{max}
	cm/min	mD	mD
0.94	1.80	0	10
0.98	2.04	11	100
1.18	1.88	101	200
1.40	1.33	201	2000

Figure 4-23 shows the skin profile that was generated by our model and the field skin profile as per Thabet et al. (2009). There is a close match between our simulated results and the published results; this validates our model.

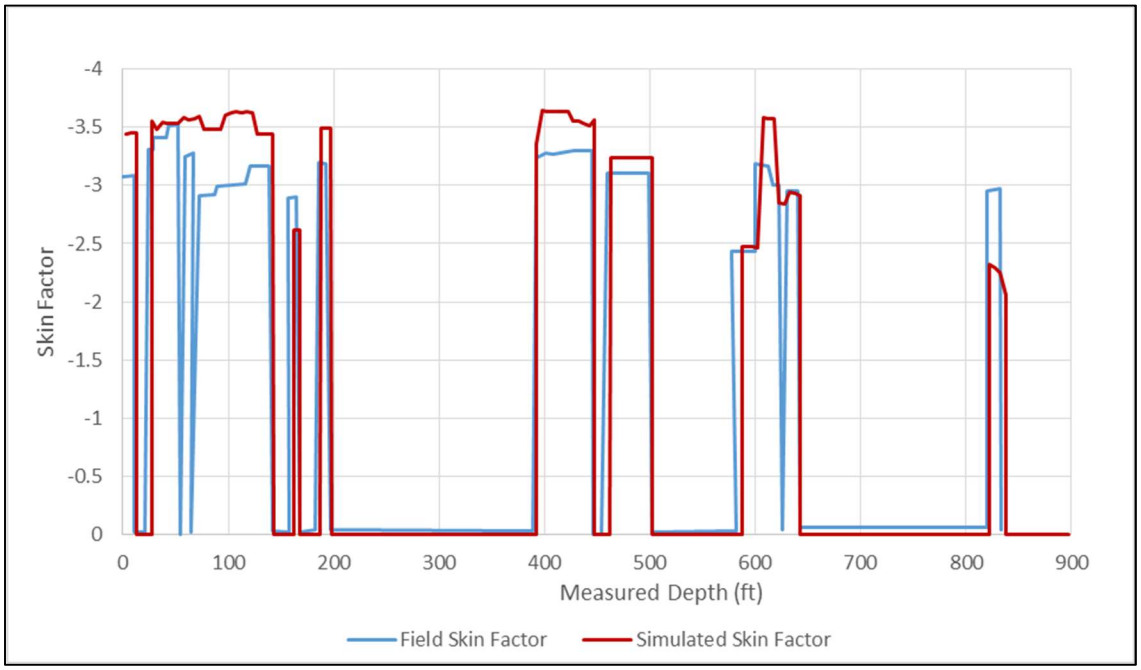

Figure 4-23: Comparison of the simulated and field skin factors for case 1

Figure 4-24 shows the skin profile of the well if all of the pure acid and diversion stages were replaced with 15% HCl acid. The permeability profile is also shown on the secondary y-axis. The figure clearly shows that, without the use of diverter, the high permeability zones were stimulated (skin factors of -3 to -4) but the lower permeability zones, (500-900 ft away from the heel) were not stimulated well (skin factors > -1).

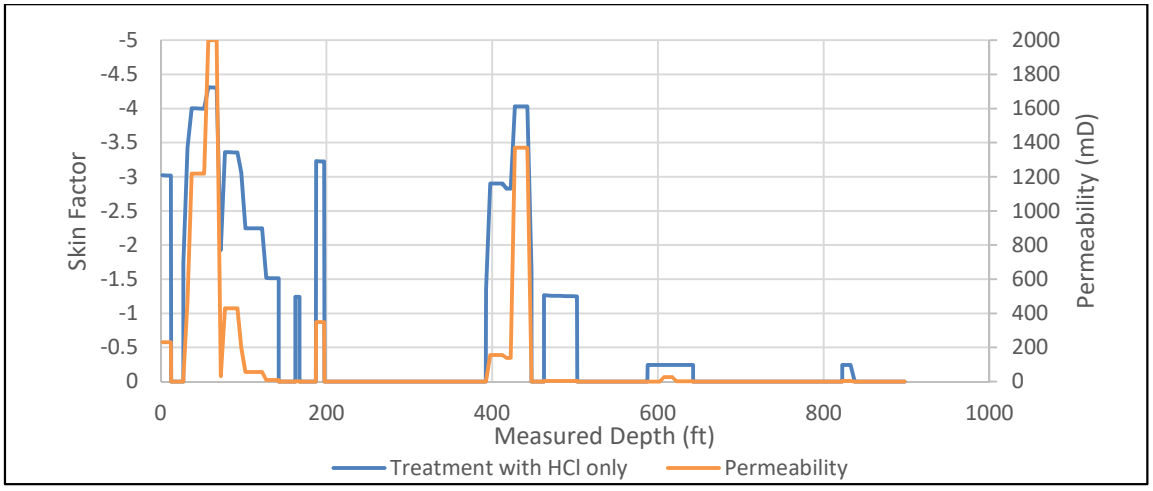

Figure 4-24: Skin factor profile for case 1 when no diverting agent is used

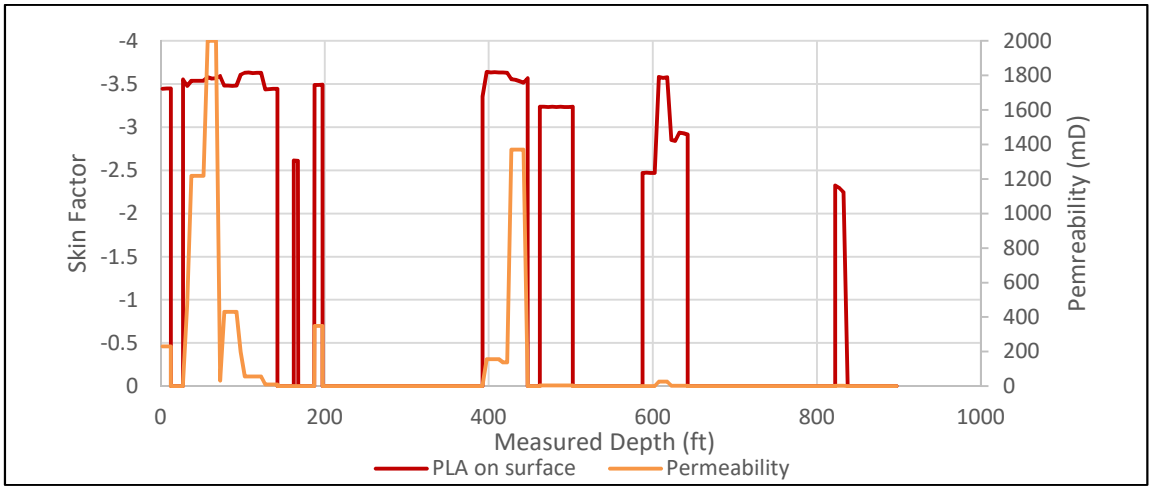

Figure 4-25: Skin factor profile for Case 1 when diverting agent is used

On the other hand, Figure 4-25 shows the skin profile if PLA diversion is used (PLA was assumed to build a filter cake on the sand face). This figure shows that all of the perforated zones were stimulated. Even when the permeability was 100-1000 times smaller than the maximum permeability in the well, skin factors as low as -2.5 were obtained through the use of the diversion. It should be noted that even though the low

permeability zones close to the toe were stimulated, they still did not have a large contribution to the production of the well since the permeability is so low – see the post stimulation production log in Figure 4-22.

Finally, Figure 4-26 shows a comparison of the skin factor for the pumped treatment and a treatment where all of the acid and diverter stages were replaced by 15% HCl. The graph clearly demonstrates that diversion allowed a more uniform treatment of all of the completed zones when PLA diversion was used. The use of PLA created restrictions to subsequent acid flow in the high permeability zones and allowed a uniform treatment of the well.

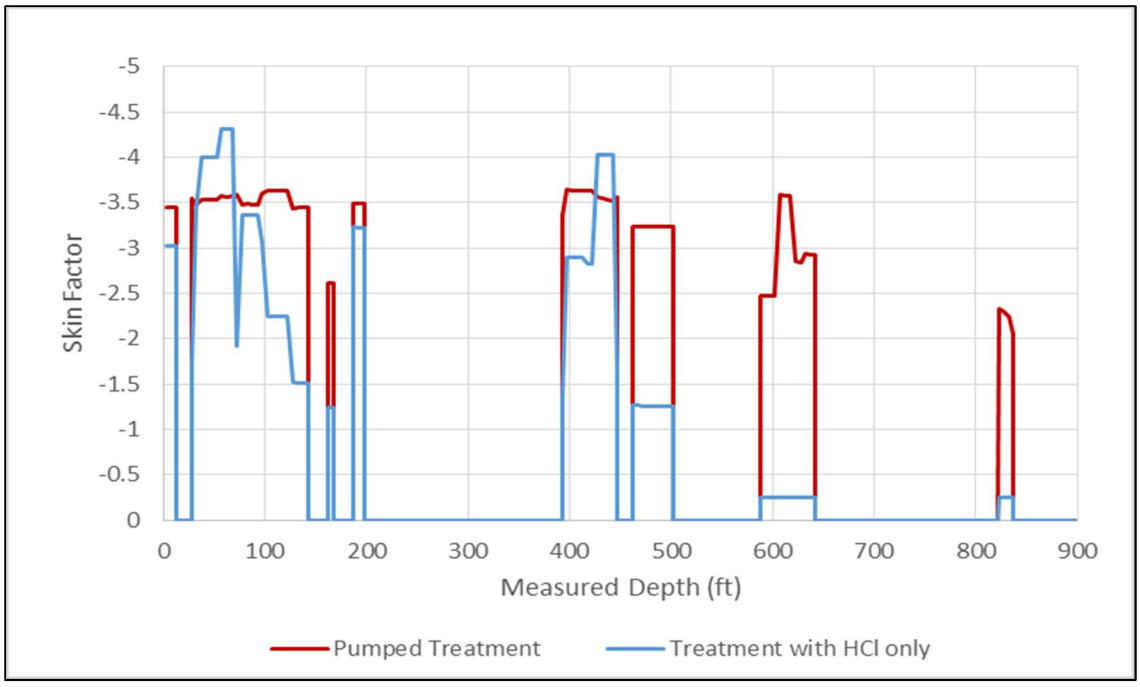

Figure 4-26: Comparison of the simulated treatment with and without diverter for case 1

Case 2

In this case, all of the assumed values, including the specific cake resistance, were kept the same as the first case, i.e., Table 4-2 and Table 4-3 apply to this case also. Figure 4-27 shows the given permeability profile for the well that was simulated in this case.

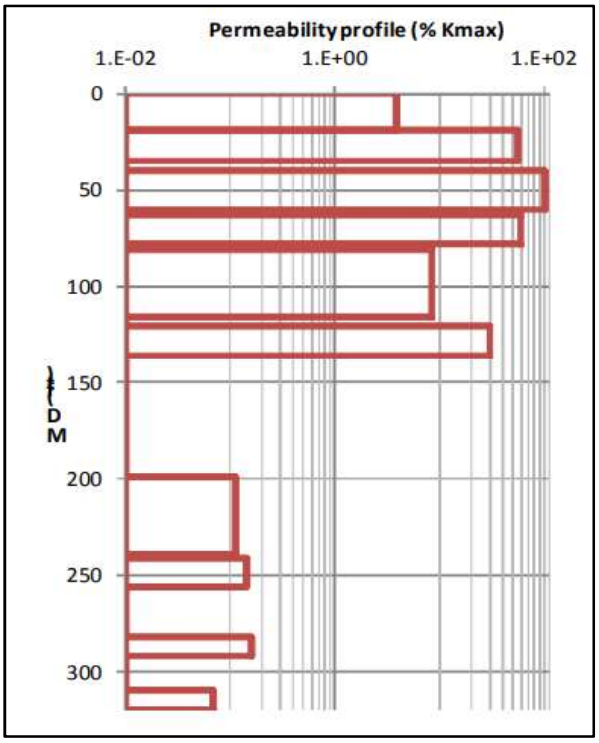

Figure 4-27: Permeability profile of the well used in the 2nd validation case. (Adapted from Thabet et al., 2009)

Figure 4-28 shows the pump schedule for this case. The duration and pump rate for each of the four acid stages and the three diversion stages are given in this figure. Thabet et al. (2009) explain that production log data was also available for this well and was also used to develop the permeability profile and verify their simulated skin factor profile, however, the log data was redacted from the paper for this well.

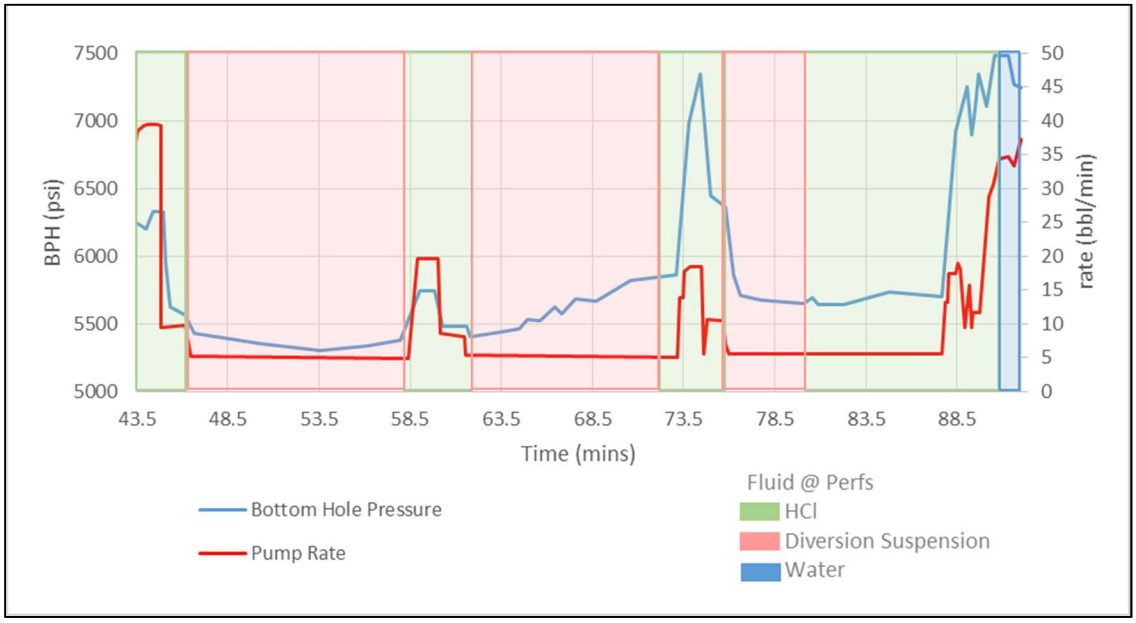

Figure 4-28: Pump schedule and BHP profile for well used in the 2nd validation case (Adapted from Thabet et al., 2009)

The simulation results compared to the field skin factor profile is shown in Figure 4-29. Just as with the first case, the simulated treatment is very similar to that published by Thabet et al. (2009). This results also validate the skin factor model that is proposed in this paper. Recall that specific cake resistance was kept constant so no parameters were tuned.

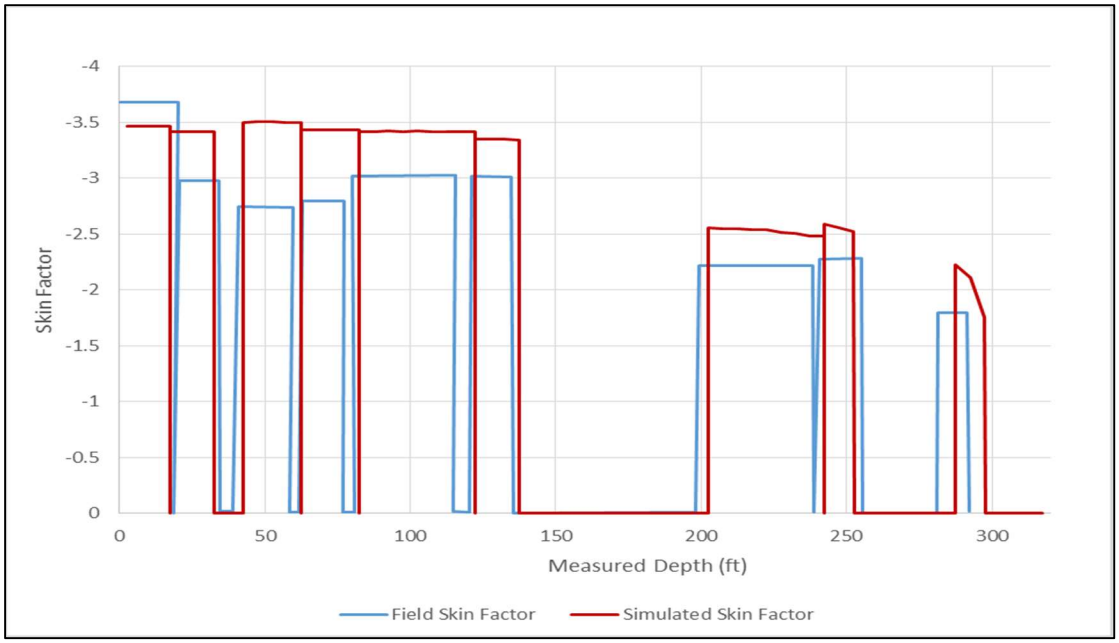

Figure 4-29: Comparison of simulated and field skin factors for case 2

Figure 4-30 shows the skin profile that would be obtained if all of the acid and diverter stages were replaced by 15% HCl. The permeability profile is also shown on this plot. Just like case 1, the highest permeability zones clearly accepted most of acid flow when there is no diversion. This resulted in the high permeability zones being well stimulated and the low permeability zones (100ft closest to the toe) having little stimulation. Figure 4-31 shows the simulated skin profile when the field treatment was pumped. This plot clearly shows that when diversion is applied there was significant wormholing and low skin factors in all completed zones, even the 100ft closest to the toe of the well, where the permeability was very low.

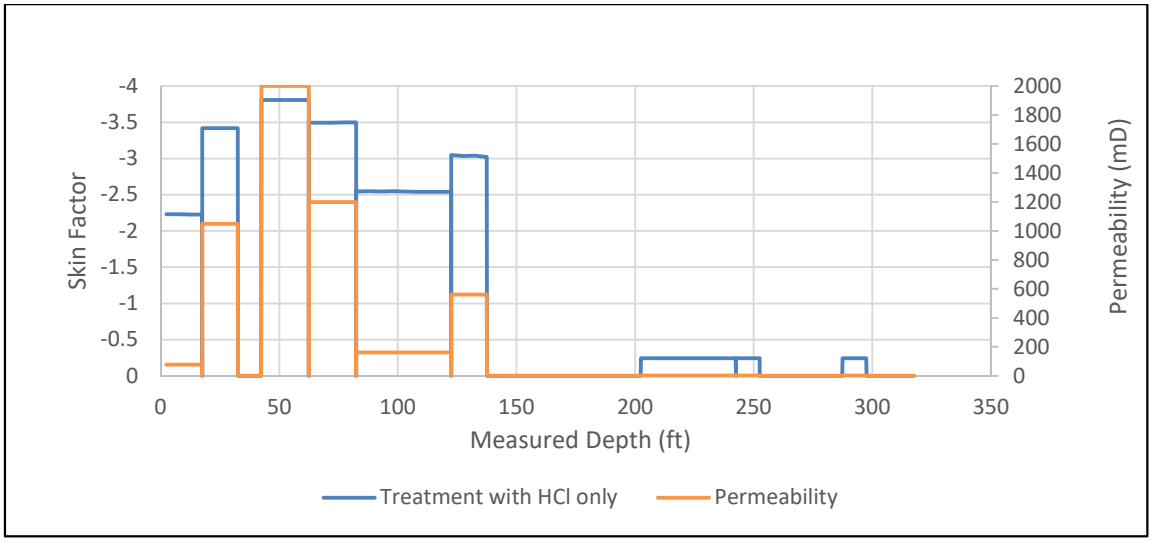

Figure 4-30: Skin factor profile for case 2 when no diverting agent is used

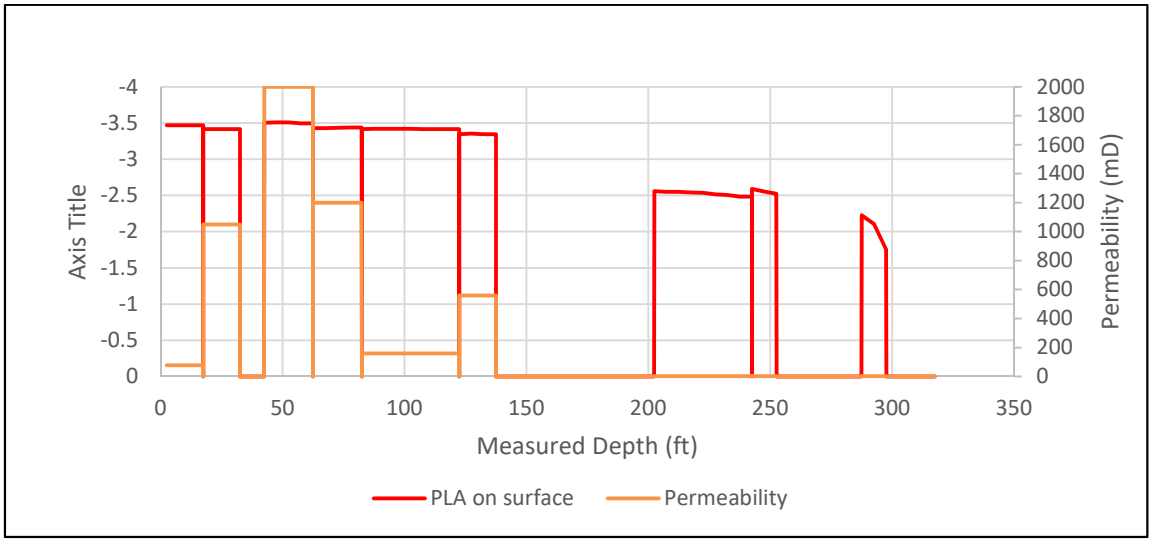

Figure 4-31: Skin factor profile for case 2 when diverting agent is used

Figure 4-32 compares the skin profiles when diversion was used or not. The plot shows that a more uniform profile was obtained when diversion was used. It is worth noting that for the highest permeability zone (50ft from the heel) using no diversion

resulted in a lower skin factor. By using PLA diversion, some of the acid that would have been used in stimulating this high permeability zone was redistributed to other zones.

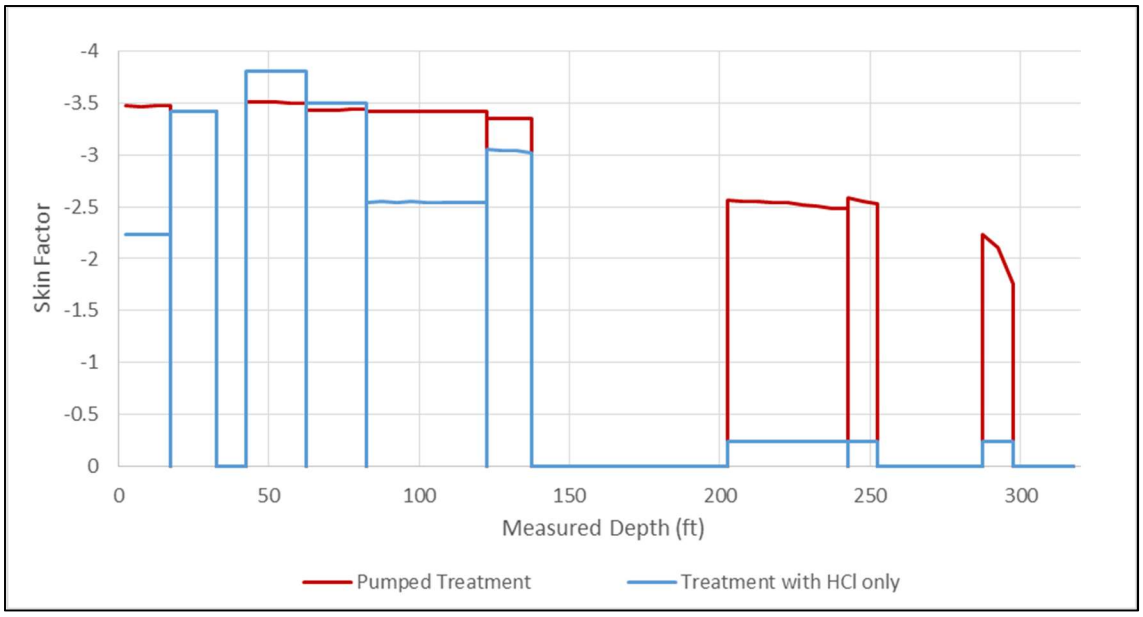

Figure 4-32: Comparison of the simulated treatment with and without diverter for case 2

4.8 Conclusions

In this study, an experimental procedure was developed to investigate the effects of particulates in a wormhole. Using the results from these experiments, a new skin factor for particulate diversion in matrix acidizing was developed. This model was then validated using published results of two wells in Qatar that used a multi-stage approach with a degradable diverter. The conclusions are as follows:

- $CaCl_2$ brine is a suitable suspending agent for PLA laboratory experiments.
- Particles if sized correctly fill wormholes despite the wormholes' tortuosity.

- Based on experimental conditions used (room temperature, limestone outcrop cores, and granular PLA sized smaller than 325 mesh) pumping additional acid still propagates the dominant wormhole even when a wormhole is filled with PLA.
- When PLA enters a wormhole, it creates pressure drop by forcing the fluid to flow in the rock matrix instead of through the wormhole.

5. SENSITIVITY ANALYSIS *

This section presents a sensitivity study that was carried out to investigate the impact of the design parameters of a diversion treatment on the treatment's effectiveness. The study used the PLA skin factor models that were discussed in section 4 and that were incorporated into the near wellbore simulator, Horizontal Well Acidizing Simulator (HWAS). The following parameters are investigated:

- Where the diverter is deposited – on the sand face or in the wormhole,
- Diverter concentration,
- Diverter specific cake resistance,
- Number of diverter slugs, and
- Volume of acid used.

5.1 Description of Wells for Sensitivity Analysis

In this study, we analyzed three different wells. Each well was taken from published field cases where PLA was used as the primary form of diversion. In each case, we know the permeability distribution along the well and some key details about the applied treatments. The first two cases are the same as those used in section 4.7. The third case is described below.

* Parts of this chapter are reprinted with permission from "General Guidelines for Batch Treatments of Polylactic Acid for Diversion in Multistage Matrix Acidizing Treatments" by Shirley and Hill, 2019, Copyright 2019 Society of Petroleum Engineers.

Case 3

Case 3 was a horizontal well described by Huang et al. (2018). Huang et al. (2018) did not reveal where the well is located, but we are told in the publication that the wellbore was initially filled with oil. We are given all of the data about the well and the pumped treatment that is needed to simulate the treatment. The permeability and porosity profiles are shown in Figure 5-1 and Figure 5-2. It should be noted that the completed interval in Case 3 is longer than the first two cases, but the range in permeability is much smaller (0-50mD as compared to 0-2000mD).

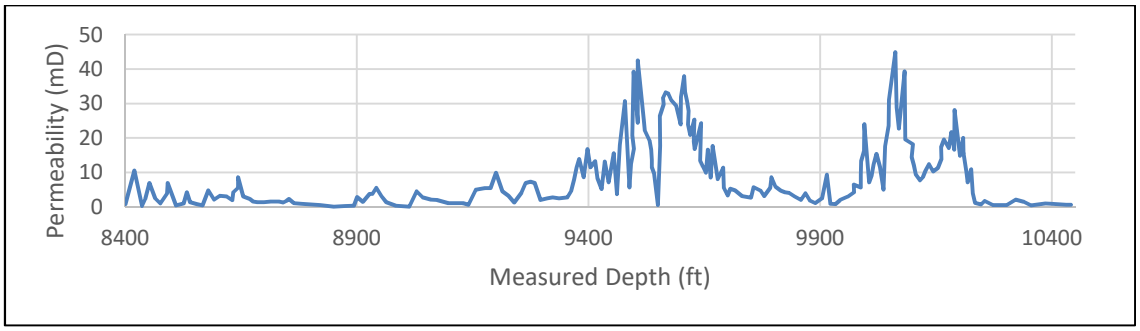

Figure 5-1: Permeability Profile for Case 3 (Adapted from Huang et al., 2018)

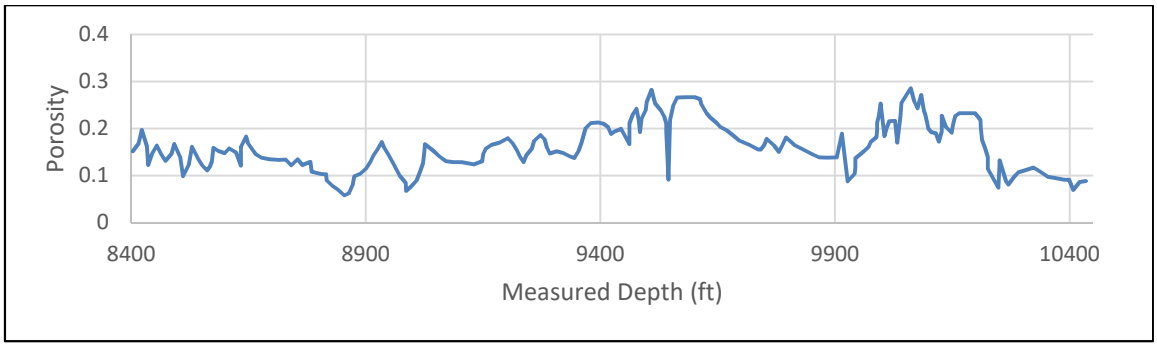

Figure 5-2: Porosity Profile for Case 3 (Adapted from Huang et al., 2018)

According to Huang et al. (2018) a bi-modal mixture of PLA sizes was used in the diversion stages (7 and 100 mesh). The mixture used was designed to be able to plug the opening of perforation tunnels or wormholes, so it was assumed that the PLA formed a filter cake at the sand face instead of entering the wormholes. The pump schedule that was used is shown in Figure 5-3. Table 5-1 shows the parameters that were used to simulate the treatment

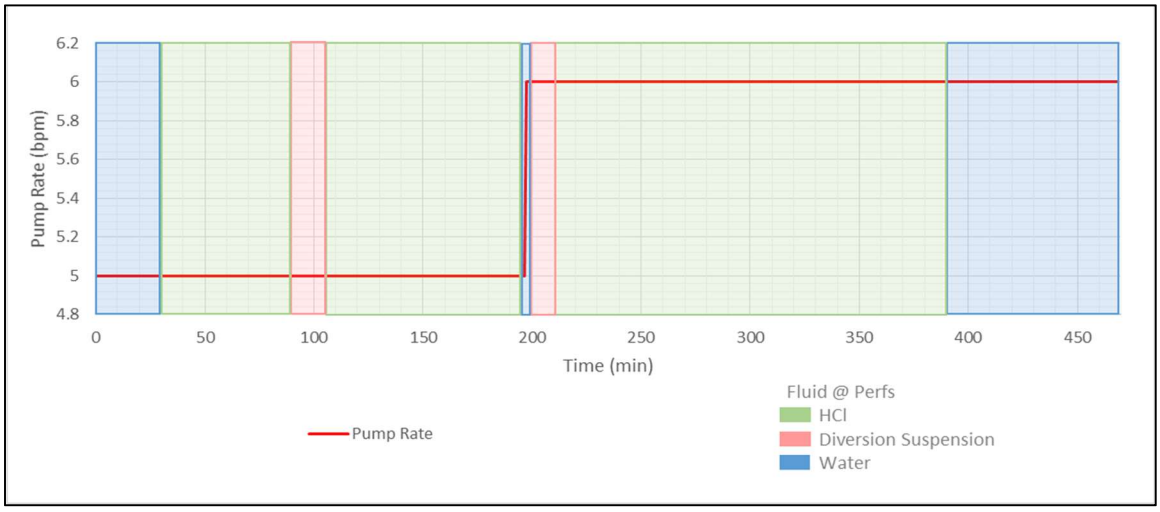

Figure 5-3: Pump schedule for Case 3 (Adapted from Huang et al., 2018)

Table 5-1: Parameters used to simulate case 3

Parameters	Units	Value	Comments
Well Completion		Cased and Perforated	
Placement Method		Bullheading	
Reservoir Type		Oil	
Total Reservoir Compressibility	psi^{-1}	1×10^{-6}	
Reservoir Fluid Viscosity	cP	1.2	
Wellbore radius	in	8.75	
Damaged Zone Radius	in	18	
Permeability Impairment Ratio in Damaged Zone		20	
Perforation length	in	18	
Perforation Diameter	in	0.35	
Perforation Phasing	deg	0	
Shot density	spf	0.5	
PLA concentration	lb/gal	2.0	Assumed
Specific Gravity of Diverting Agent		1.24	
Acid Concentration in Pure Acid Stages		15%	
Acid Concentration in Diversion Suspension Stages		0%	
Specific Cake Resistance	ft/lb	4.0E13	

Note, the diverter concentration was not given by Huang et al. (2018). However, another paper (Gonzalez et al., 2017) states the same bi-modal sized particulate diverter is

typically used in a concentration of 1-3 lb/gal for matrix acidizing treatments. The same optimal acid efficiency parameters were used for case 3 as were used for cases 1 and 2. These optimal acid efficiency parameters are given by Table 5-2 below.

Table 5-2: Optimal Points Used for Wormhole Propagation Calculations

Optimal Pore Volume to Break Through	Optimal Interstitial Velocity	Min Perm that this optimal point refers to	Max Perm that this optimal point refers to
PV_{bt-opt}	V_{i-opt}	k_{min}	k_{max}
	cm/min	mD	mD
0.94	1.80	0	10
0.98	2.04	11	100
1.18	1.88	101	200
1.40	1.33	201	2000

Figure 5-4 shows the skin profile of the well if no diversion was used i.e. all of the pure acid and diversion stages were replaced by 15% HCl. The permeability profile is also shown on the secondary axis of this plot. Clearly, without diversion, the acid was primarily distributed based on the permeability. The zones with higher permeability receive higher acid flow, resulting in lower skin factors. The zones with lower permeability (for example 500ft closest to the heel) did not receive much acid and were not stimulated well.

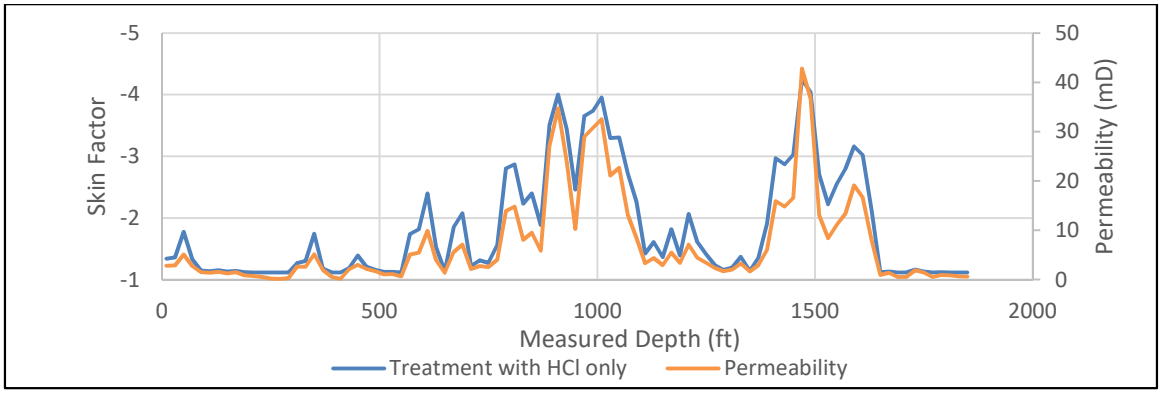

Figure 5-4: Skin factor profile when no diversion is used – Case 3

On the contrary, Figure 5-5 shows the skin profile when PLA diversion was used i.e., the treatment that was pumped in the field. In this simulation, it was assumed that PLA forms a filter cake on the sand face. When diversion was used, the figure demonstrates that there is a more uniform skin profile that does not directly follow the permeability profile. The high permeability zones still had the lowest skin factors but the differences in skin factors between high and low permeability zones were much lower than when no diversion was used. Also, the figure shows that there were still some parts of the well that had very little wormholing.

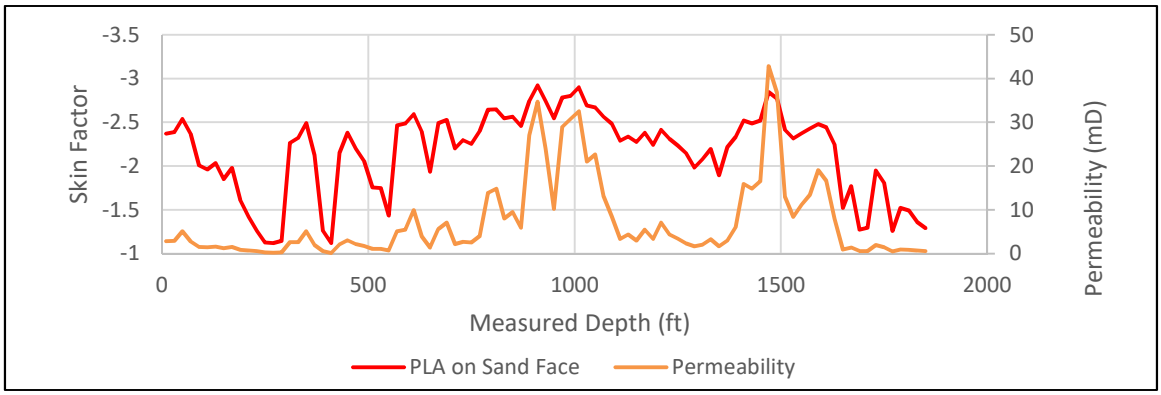

Figure 5-5: Skin factor profile when diversion is used – Case 3

Figure 5-6 shows a comparison of the simulated results of the treatment that was pumped in the field versus a treatment if all of the pure acid and diversion stages were replaced by 15% HCl. This figure shows that the pumped treatment was successful in treating several zones that would not have been treated without diverter. However, it also shows that attaining a more uniform treatment came at the cost of worsening the skin factor at the two highest permeability peaks. The following sensitivity studies demonstrate ways that the treatments could have been altered and improved.

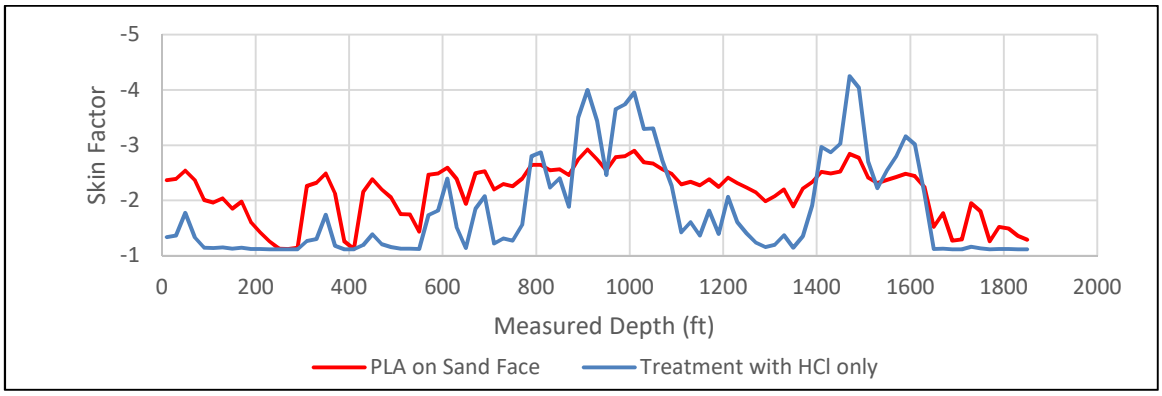

Figure 5-6: Comparison of the pumped treatment and the treatment with no diverter – Case 3.
Reprinted with permission from (Shirley and Hill, 2019)

5.2 Diverting Agent Inside of the Wormholes or on the Sand Face

The first parameter that was investigated is whether it is better to design PLA to fill the wormholes, or to bridge the opening of the wormholes and build a filter cake at the sand face. As shown in Eq. 4-11 and Eq. 4-12, PLA induces pressure drop very differently if it forms a filter cake on the sand face versus if it enters the wormhole. Figure 5-7 shows a comparison of the final skin factor profiles for each case when the PLA enters the wormhole and when it does not. Figure 5-7 clearly shows that an equal mass of PLA can create a more uniform distribution of the skin factor across the well if it forms a filter cake, compared to if the PLA fills the wormholes.

When PLA forms a filter cake at the sand face, fluid has to flow through the filter cake to get into the formation, which can create a large pressure drop depending on the filter cake properties. The amount of diverter used in each of these cases was small relative to the volume of wormhole that was generated, and as such, there was little diversion effect when PLA enters the wormholes. Even in case 3, where the concentration of the diverter is much larger than that in cases 1 and 2 (2lb/gal compared to 75lb/1000gal), the skin profiles when the PLA enters the wormhole is very similar to that when no diverter was used.

Even if enough PLA is added to fill the created wormholes, the pressure drop required to enter the formation can only be as high as the initial pressure drop at that location, i.e., before any acid was injected. This is because the fluid can simply flow in the rock matrix around the PLA filled wormholes (provided the permeability of the PLA cake is less than the permeability of the rock matrix). This suggests that the diverter should

generally be designed to bridge the wormhole opening as quickly as possible to avoid PLA entering the wormholes.

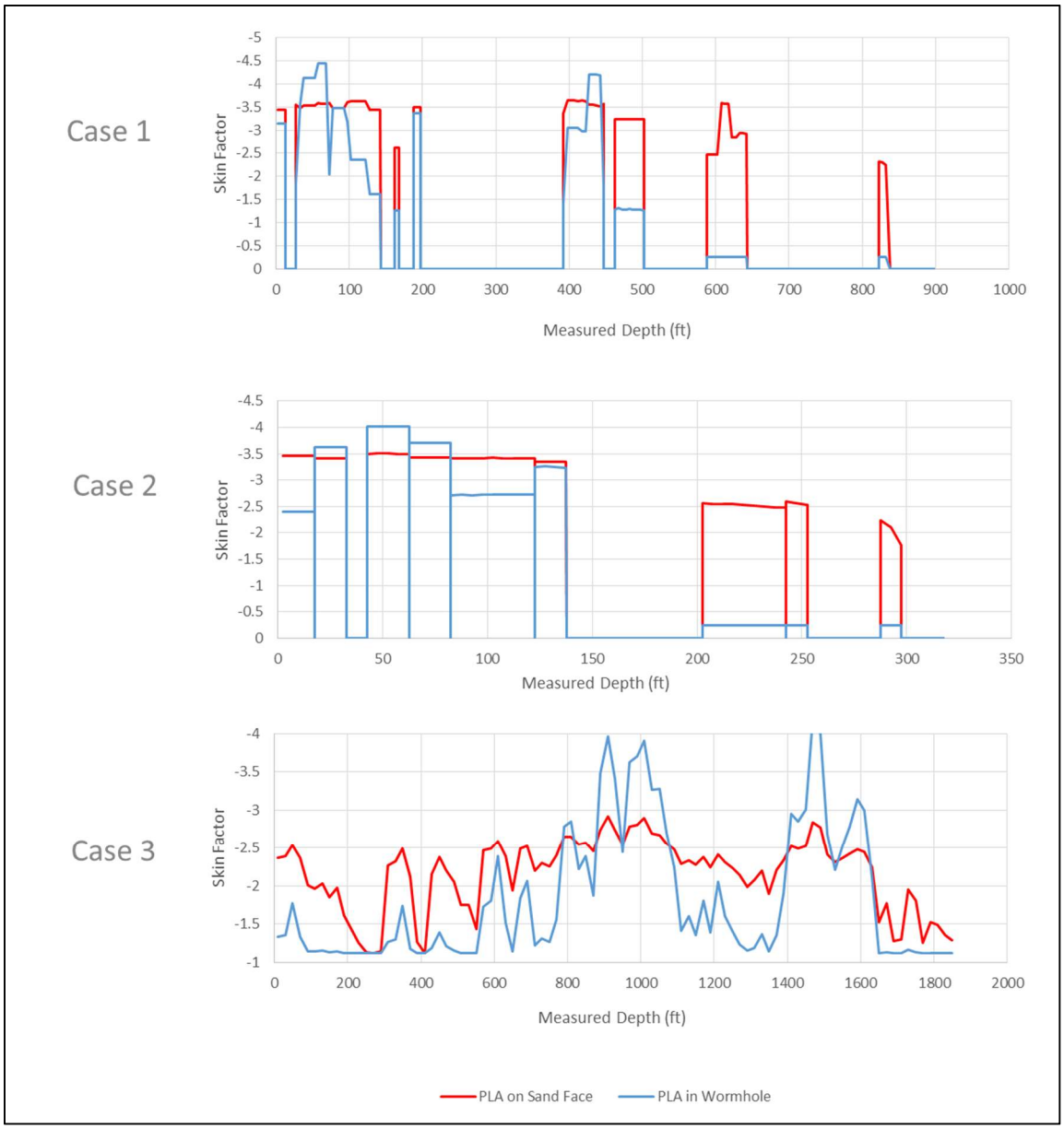

Figure 5-7: Skin factor profiles for each case when PLA is sized to enter the wormhole or not

Table 5-3: Total skin factors and standard deviation of the grid skin factors when PLA enters the wormhole or not for each well

	Case 1		Case 2		Case 3	
	PLA on Sand Face	PLA in wormhole	PLA on Sand Face	PLA in wormhole	PLA on Sand Face	PLA in wormhole
Total Skin Factor	-3.54	-3.82	-3.44	-3.58	-2.58	-2.80
Grid Skin Factor Standard Deviation	0.42	1.43	0.5	1.51	0.48	0.87

Table 5-3 shows the total skin factor and the standard deviation of the skin profile for each case when PLA is on the sand face or in the wormhole. It is useful to compare Figure 5-7 with Table 5-3. It should be noted that a difference in a skin factor standard deviation of 1 is a significant difference in the shape of the skin profile along the well. It is also important to note that even though PLA in the wormhole did not cause a significant diversion, the total skin factor is lower than that when PLA is on the sand face. This is because when there is poor diversion, the highest permeability zones continue to be stimulated. As can be seen from Eq. 3-4, the effect of each grid on the total skin factor is weighted by the grid's permeability, so a small improvement in the skin factor of a high permeability zone can be more effective in lowering the total skin factor than a large improvement in skin factor of a low permeability zone.

5.3 Concentration of Diverter

In this sensitivity analysis, the total amount of PLA pumped into the wells was varied by altering the concentration of the diverter, i.e., the same field pump schedules were used, but the concentration of the PLA in the slurry was changed. Figure 5-8 shows the results of this study.

The first observation from Figure 5-8 is that increasing the amount of diverter tends to lower the standard deviation, i.e., create a more uniform skin profile, but it also increased (worsened) the total skin factor. By using a higher concentration of diverter, the mass of diverter in the filter cake, m_{cake}, increased, adding more resistance to flow wherever the filter cake is built (see Eq. 4-11). Adding resistance to the zones of high permeability allowed more flow to enter the lower permeability zones. Hence, more uniform skin profiles were attained. It also caused less acid to enter the high permeability zones and caused lower skin factors at these grids that have the highest contribution to the total skin factor. Hence, lower total skin factors were attained.

If the main goal of the treatment is to maximize the production rate, then in many cases even when there a highly heterogeneous permeability profiles, it may be best not to use any fluid diversion technique and allow the highest permeability zones to be stimulated, as this could result in the lowest total skin factor. In the next two chapters, we investigate scenarios where attaining a more uniform skin profile can lead to higher cumulative long-term well production, even if the diversion treatment worsens the total skin factor.

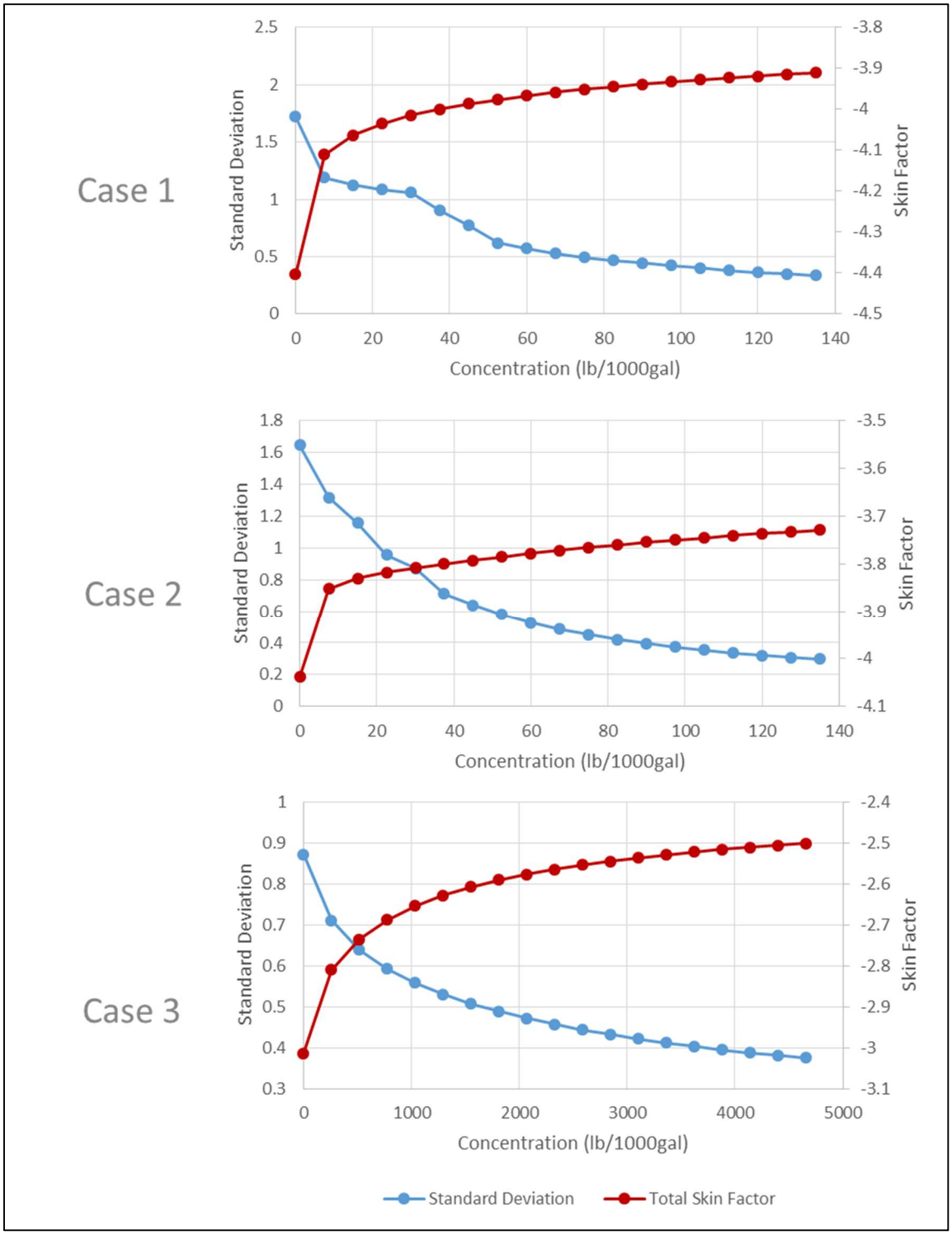

Figure 5-8: Sensitivity analysis of diverter concentration on the 3 cases

Another observation from Figure 5-8 is that increasing the diverter concentration can have a diminishing effect, on both standard deviation and overall skin factor, above some concentration. This is particularly evident in cases 1 and 2. This suggests that at some point adding more diverter no longer changes the distribution of flow into the formation along the wellbore. Furthermore, using large amounts of diverter could also cause the injection pressures needed to maintain the same pumping rates to increase to the point of fracturing the formation and necessitate a reduction of the pumping rates. Case 3 does not clearly show the same effect. This is because a more uniform profile can still be attained for case 3, even if the concentration of diverter that was used in the field treatment (2lb/gal) is doubled.

Increasing the concentration of particles in suspension can, however, become operationally difficult to pump and keep the particles in suspension. If a more uniform skin profile is desired, other parameters may also need to be changed such as the total volume of slurry pumped or the specific cake resistance (see next section). It should also be noted that it has been shown that higher diverter concentrations can lead to faster bridging effects (Gonzalez et al. 2017). Given that the same mass of PLA can cause a significantly higher pressure drop in a filter cake on the sand face versus being in the wormhole, the concentration of the diverter should be high enough to allow fast bridging of the wormhole entrances.

5.4 Specific Cake Resistance

In this analysis, we varied the specific cake resistance, α. Recall from Eq. 4-11, specific cake resistance is a component in the constant of proportionality between the mass of the diverter to the amount of pressure drop induced by its filter cake. In a practical sense, α can be increased by using diverter particles of different shapes and sizes that result in filter cakes of lower permeabilities.

As expected, the trends observed in Figure 5-9 are similar to those observed in Figure 5-8. This is because, by increasing α, we increase the amount of pressure drop that is induced by the same mass of diverter (see Eq. 4-11). This study shows that the relationship between both the standard deviation of the skin profile and the total skin factor are not linear with the specific cake resistance. This suggests that if the specific cake resistance is too low, the same mass of diverter could be very ineffective. It is more conservative to err on the side of having a higher specific cake resistance than necessary to obtain a more uniform skin profile. However, it should be noted that increasing the specific cake resistance also increases the bottom hole pressure.

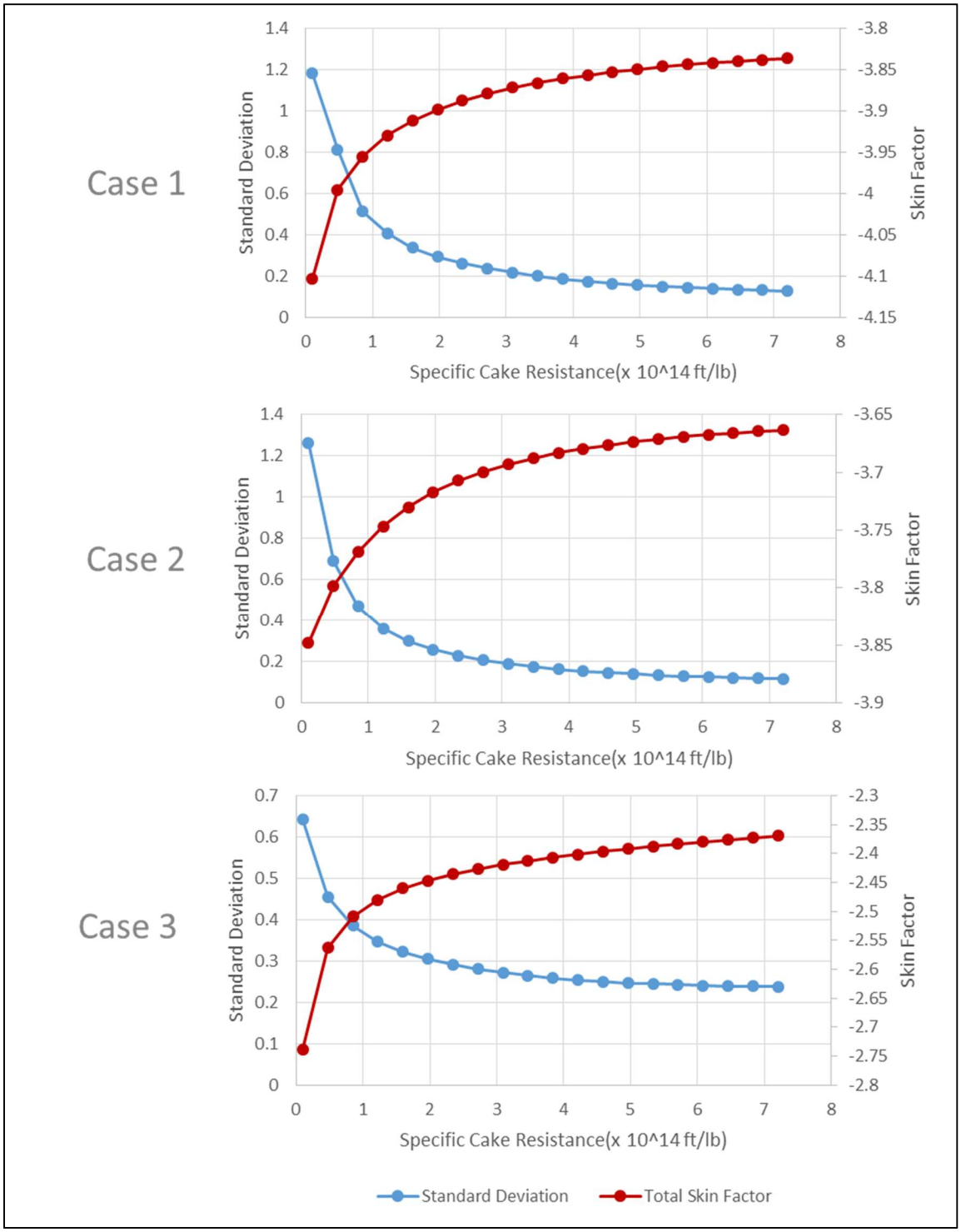

Figure 5-9: Sensitivity analysis of specific cake resistance on the 3 cases

5.5 Number of Diverter Slugs

This study investigated the effect of the number of slugs of the diverter on the treatment efficiency. The total amount of diverting agent and acid was kept the same, but the number of diverter stages was varied. To do this, we deviated from the pump schedule given by Figure 4-23, Figure 4-30 and Figure 5-3. Instead, we used alternating stages of acid and diverter suspension. One water stage was used at the end of the treatment. All of the acid and water stages were assumed to be injected at 10bpm while the diverter stages were assumed to be injected at 5bpm. An example of the new pump schedule for two diverter stages is shown in Table 5-4 below, where X is the total volume of acid in bbl and Y is the total volume of diverting agent suspension in bbl.

Table 5-4: An example of the pump schedule used for two diverter stages

Total Volume of Acid: X bbl Total Volume of Diverter Suspension: Y bbl Number of Diverter Stages: 2			
Stage No.	Fluid	Total Volume Injected	Rate
		bbl	bpm
1	Acid	$\frac{X}{3}$	10
2	Diverter	$\frac{Y}{2}$	5
3	Acid	$\frac{X}{3}$	10
4	Diverter	$\frac{Y}{2}$	5
5	Acid	$\frac{X}{3}$	10
6	Water	60	10

Please note that in the field treatment for cases 1 and 2, the diverter suspension included 15% HCl. An equivalent amount of acid that was used in the diversion stages was pumped during the acid stages instead. Also, for cases 1 and 2 the specific cake resistance used was 3.6E14 ft/lb. Figure 5-10 shows the results of this study for each case.

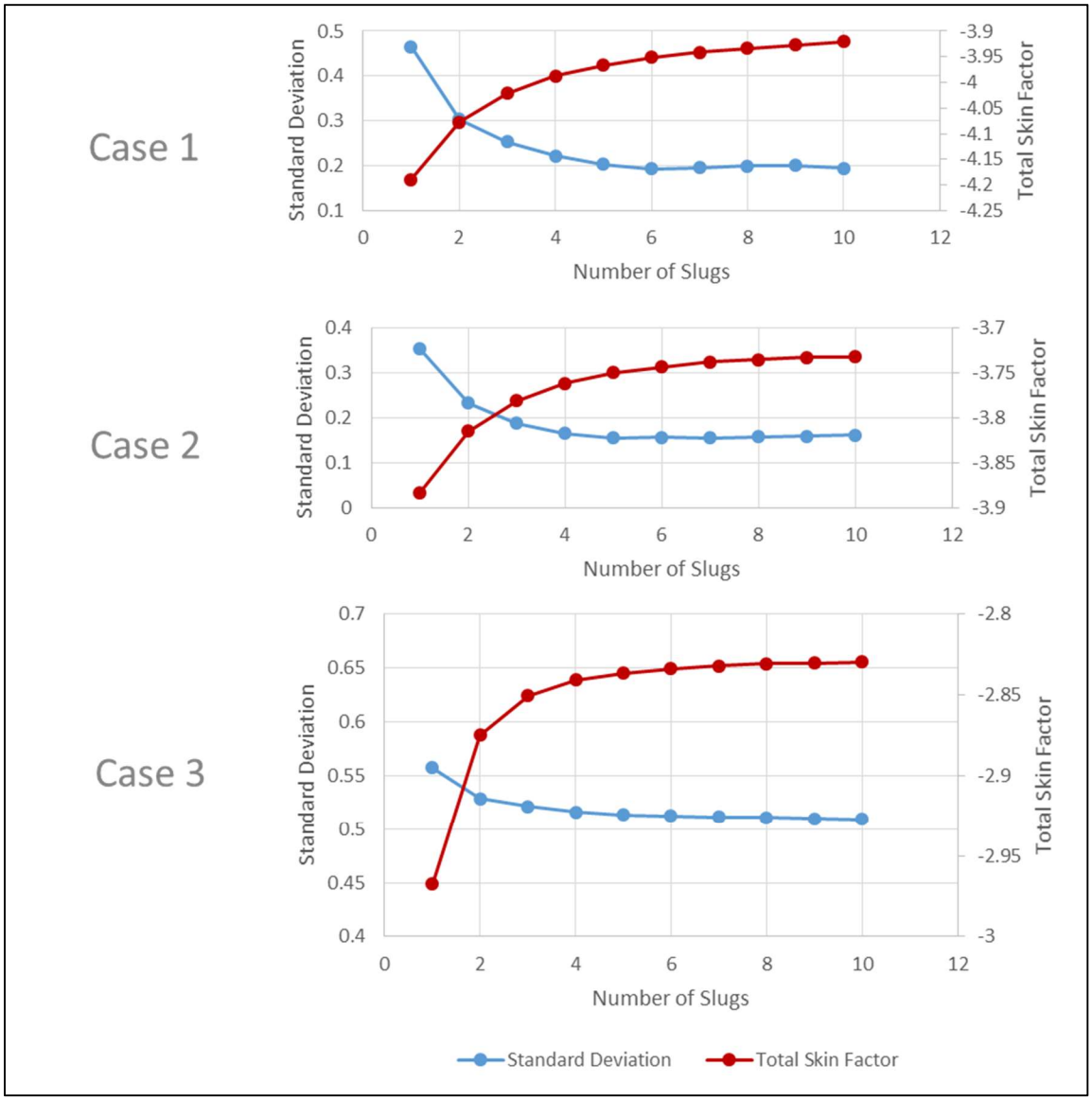

Figure 5-10: Sensitivity analysis of the number of diverter stages on the 3 cases

Cases 1 and 2 suggest that it is better to have four to six diverter stages rather than to apply all of the diverter in a single stage. After each diverter stage, the flow distribution into the formation along the well is changed. By injecting acid in between these stages, the acid has a better chance of contacting and creating wormholes in each zone along the well. Using more than six diversion stages does not add any more benefit to the treatment.

In case 3, there was little variation in the standard deviation regardless of the number of diverter stages used. In this case, there was little benefit to using several diversion stages. One possible reason for this could be that insufficient acid and diverting agent were used. If the total amount of diverting agent or specific cake resistance is not large enough, then using multiple stages of diversion may not help in distributing acid where it is needed regardless of how many stages are used. Also if insufficient acid is used, then even when the acid is being distributed more evenly along the well, there may not be sufficient stimulation in lower permeability zones. Figure 5-11 below shows the same sensitivity analysis for case 3 but the total volume of acid used was increased from 1 bbl/ft 15% HCl to 2 bbl/ft 28% HCl, and the specific cake resistance was changed from $4x10^{13}$ ft/lb to $2x10^{14}$ ft/lb. In this case, multiple diversion stages lead to a more uniform distribution compared to having a single diverter slug. With these new treatment parameters using as many as six diverter stages can continue to improve the treatment uniformity; beyond six stages there is minimal improvement.

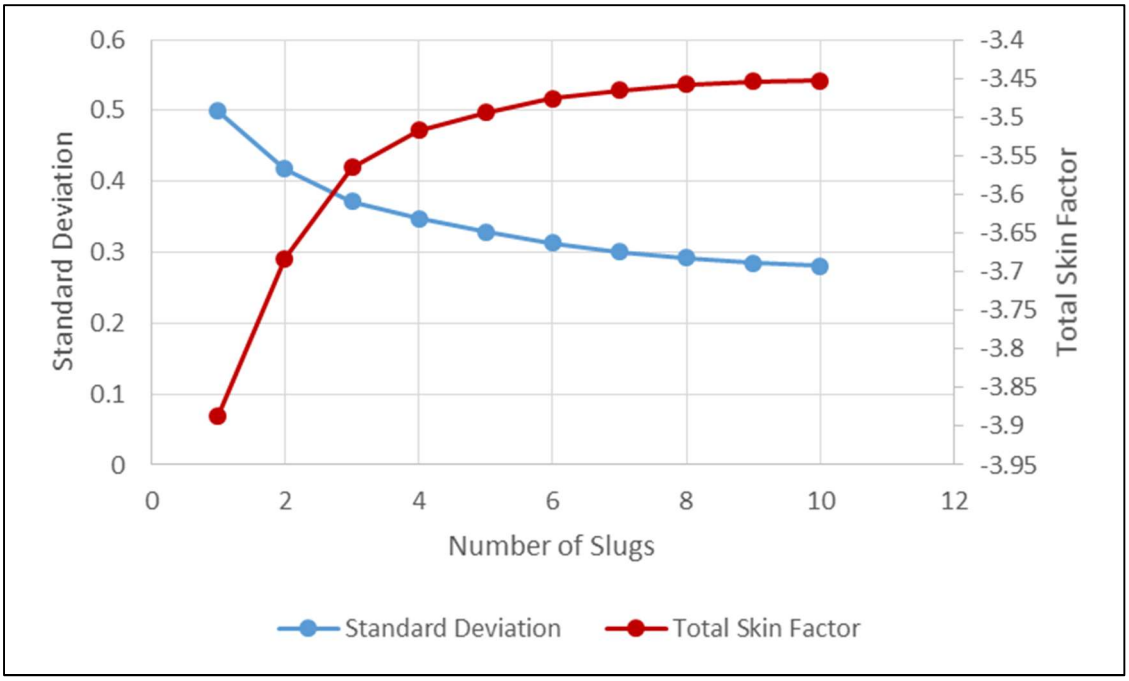

Figure 5-11: Sensitivity analysis of the number of diverter stages on case 3 with 2bbl/ft 28% HCl and $\alpha = 4x10^{14}$ft/lb

5.6 Total Volume of Acid

In the previous sensitivity analyses, varying the parameters concerning the diverting agent had a significant impact on how uniform a treatment could be obtained. However, a more uniform skin profile can come at the cost of a worsened total skin factor. The effects on the total skin factor were relatively small (in the range of 0.2-0.5). Moreover, several of the total skin factors obtained were between -2 and -3. It has been shown that matrix acidizing in carbonate reservoirs can obtain skin factors of -4 to -5 (Burton et al., 2018). In this sensitivity study, the total amount of acid used was varied, but the same volume of diverter suspension was used as the field cases. For each well, there were four equally sized acid stages pumped at 10bpm and three equally sized diversion stages pumped at 5bpm.

Figure 5-12 shows that each of the cases could have a significantly improved total skin factor and still maintain a uniform skin profile if more acid was pumped. This sensitivity study emphasizes the need for sufficient acid especially when diverting agents are used. Using larger volumes of acid increases the cost of the treatment, but it could offset the increase in the skin factor caused by using diversion to obtain a more uniform profile.

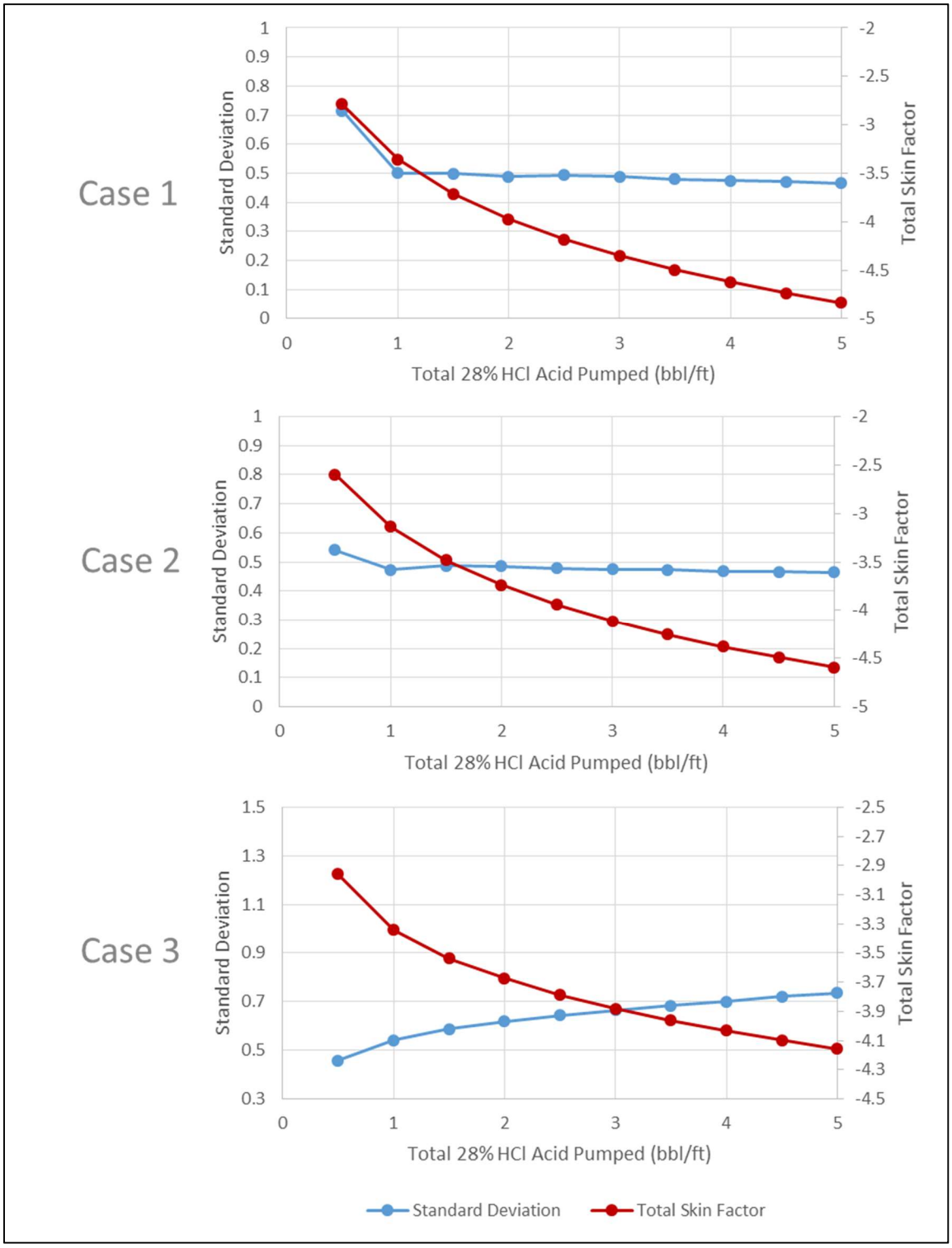

Figure 5-12: Sensitivity analysis of the total volume of acid used on the 3 cases

5.7 Conclusions

In this study, an empirically derived model for skin factor due to PLA was implemented into a near wellbore model. This model was then used to carry out sensitivity analyses of various treatment parameters using three field cases. The sensitivity analysis revealed that:

- The same mass of PLA creates a more uniform skin profile along the well if it forms a filter cake on the sand face compared to if it enters the wormholes.
- Increasing the concentration or the diverter's specific cake resistance can create a more uniform skin profile, but it can come at the cost of worsening the total skin factor for the well.
- Using multiple diverter stages is better than applying all of the diverter in a single stage as this allows an improved acid distribution and could facilitate higher acid injection rates in between diversion stages.

6. DIVERTER BATCH SIZE OPTIMIZATION

In field applications, diversion treatments are considered effective if they cause an increase in the pumping pressure while injecting treatment fluids at a constant rate. It is assumed that this surface pressure increase is caused by an equivalent pressure increase in the bottom hole pressure. An increase in the bottom hole pressure indicates that one of the paths of least resistance in the formation has been blocked, forcing more fluid to enter a different path. This does not indicate that using diversion has benefited the stimulation and production of the well, nor does it indicate that sufficient diversion has occurred to maximize the possible production of the well. The proposed method for optimizing the diverter size is based on maximizing the cumulative production of the well. In this study, the proposed method was demonstrated on a well with an unknown permeability profile.

To do this, we used three main tools: a geostatistical software to develop permeability realizations for a reservoir based on known permeability profiles in that reservoir; the near wellbore acidizing simulator that includes the PLA skin factor model that was previously developed from the experiments; and a reservoir simulator to determine the cumulative production of the well based on the generated skin profiles. The optimal batch size was determined using the maximum cumulative production of the well. The full description of the method is presented in section 3.3 and a brief summary is given below.

6.1 Batch Size Optimization Methodology

In the proposed method, the optimal diverter batch size for a matrix acidizing treatment is determined when the near wellbore permeability is not known but permeability data is available from nearby wells. Essentially, the method involves creating several possible and equally probable permeability realizations and finding the diverter batch size that would optimize the long term cumulative production of the proposed well for each permeability realization. The average optimal batch size is the most likely diverter batch size to optimize cumulative production of the proposed well based on the data available. Figure 6-1 shows a workflow that summarizes the methodology.

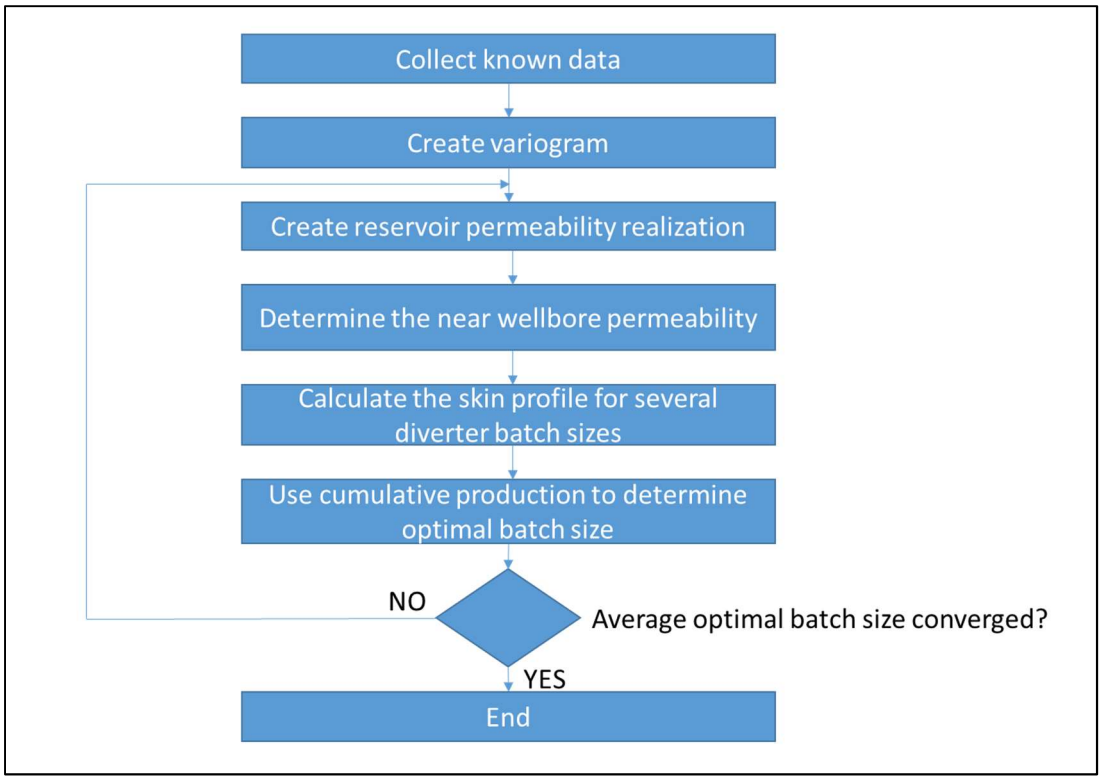

Figure 6-1: Batch Size Optimization Method

The proposed method was carried out for a synthetic data set that contains real well log data sourced from published papers.

6.2 Description of Available Data

The wells that were used for these examples are all contained in the offshore, North Field, Qatar reservoir (see Figure 6-2).

Figure 6-2: North Field, Qatar (Adapted from Clancey et al., 2008)

The field extends over 6000 km^2 and contains about 900 TCF of sour gas. The gas reservoir is a thick (1000-1400ft) carbonate reservoir in the Khuff formation. The wells that are typically drilled into the reservoir have large wellbores (13.375" x 9.675" production casing), are deviated (20-75° from vertical), and typically have cased and perforated completions. These large wellbore wells are designed for nominal production rates as high as 200 MMSCFD (Clancey et al., 2008).

The thickness alone of the reservoir presents a challenge in achieving a uniform treatment over the entire well. In addition, the reservoir is abnormally pressured due to large sealing layers of anhydrite and mudstone. The reservoir is broken into two sections, an upper section, typically referred to as K1-K3 and a lower section, K4 (see Figure 6-3).

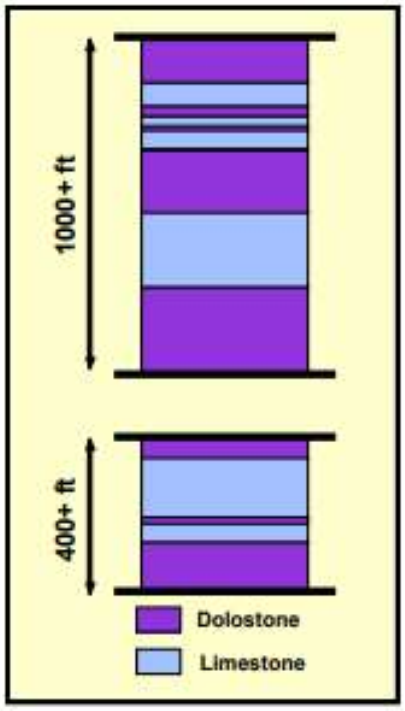

Figure 6-3: A typical lithology distribution in North Field Reservoir (Adapted from Clancey et al., 2009)

A layer of anhydrite separates K3 and K4 (Whitson and Kuntadi 2005). Many wells are drilled into only one of the two zones, but some wells are completed in both zones. Even in layers K1-K3, there are layers of anhydrite that prevent communication between the layers in some parts of the reservoir.

Furthermore, there are often alternating sequences of dolomite and limestone. In addition, there is a large variance in permeability (from a few millidarcys to several darcys), and there are natural fractures or 'super k' zones that act as major thief zones for stimulation fluids. All of these issues make it challenging to attain a uniform treatment in this reservoir, and make this an ideal reservoir to test our optimal batch size selection method.

In order to use our method, we must begin with some known permeability data in the reservoir. Five well permeability profiles were obtained based on data from Thabet et al. (2009), two from Shuchart et al. (2009), and one from Abou-Sayed et al. (2007) (see Figure 6-4, Figure 6-5 and Figure 6-6). In each case, some of the data needed to create these permeability profiles was redacted from the publications, so assumptions were made to obtain permeability profiles.

Data was used from Van Vliet et al. (2011) to determine the depths and well deviation of the five wells described by Thabet et al. (2009). Figure 6-7 and Table 6-1 summarize the depth, length, and deviation data of all eight wells based on data from the publications.

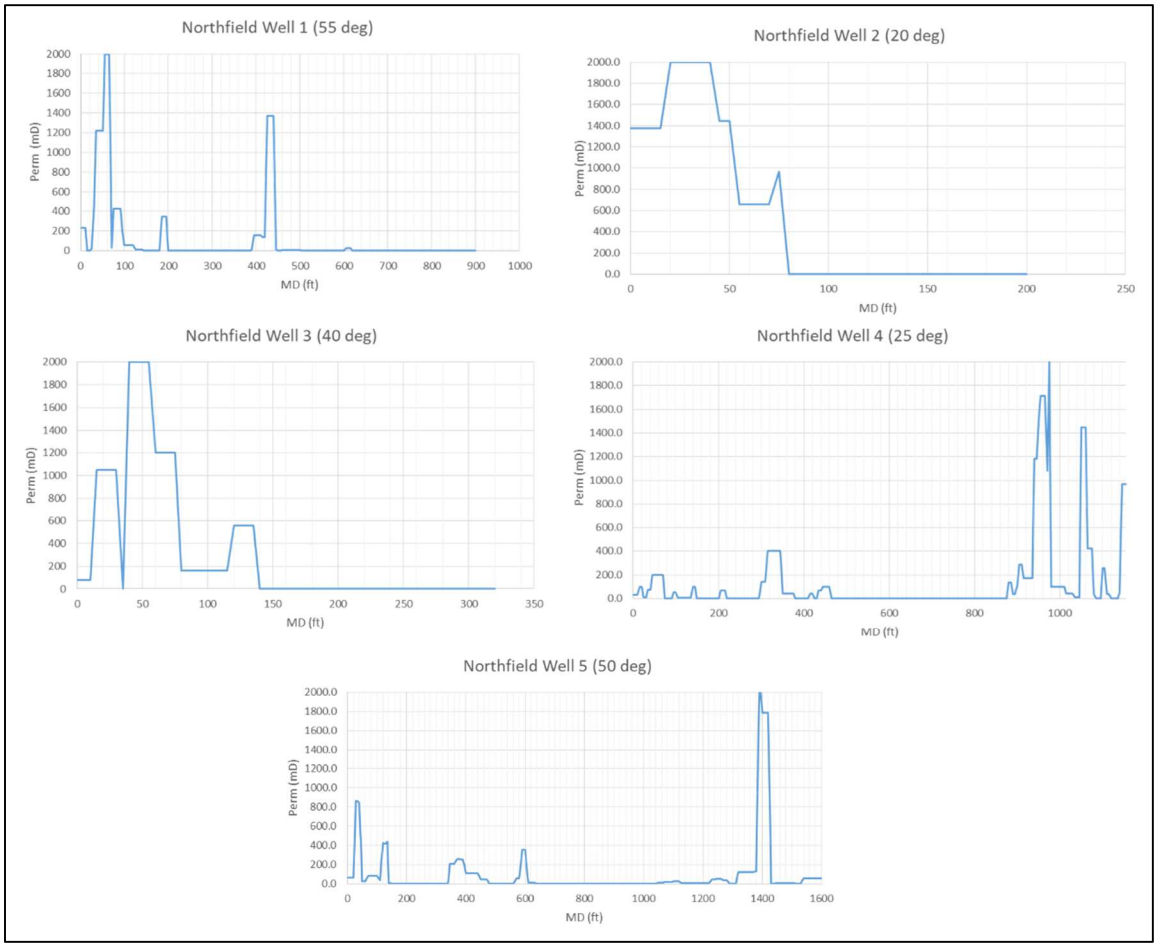

Figure 6-4: Near wellbore permeability profiles based on data published by Thabet et al. (2009)

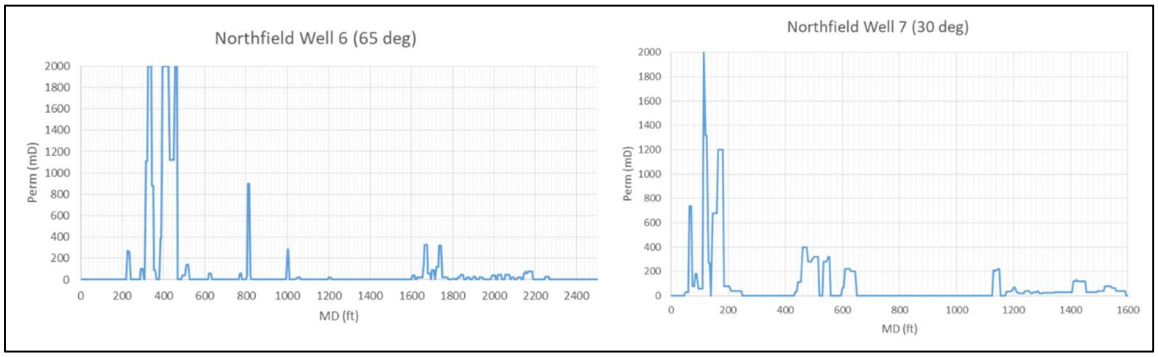

Figure 6-5: Near wellbore permeability profiles based on data published by Shuchart et al. (2009)

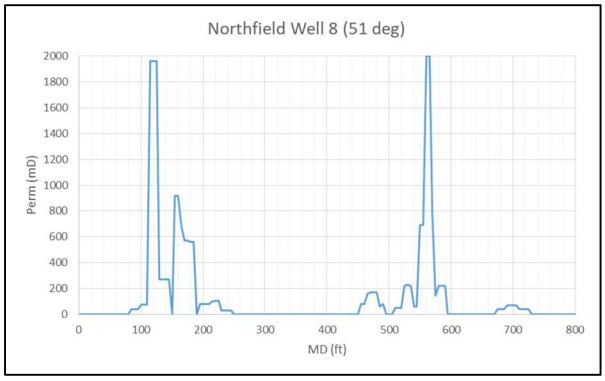

Figure 6-6: Near wellbore permeability profile based on data published by Abou-Sayed et al. (2007)

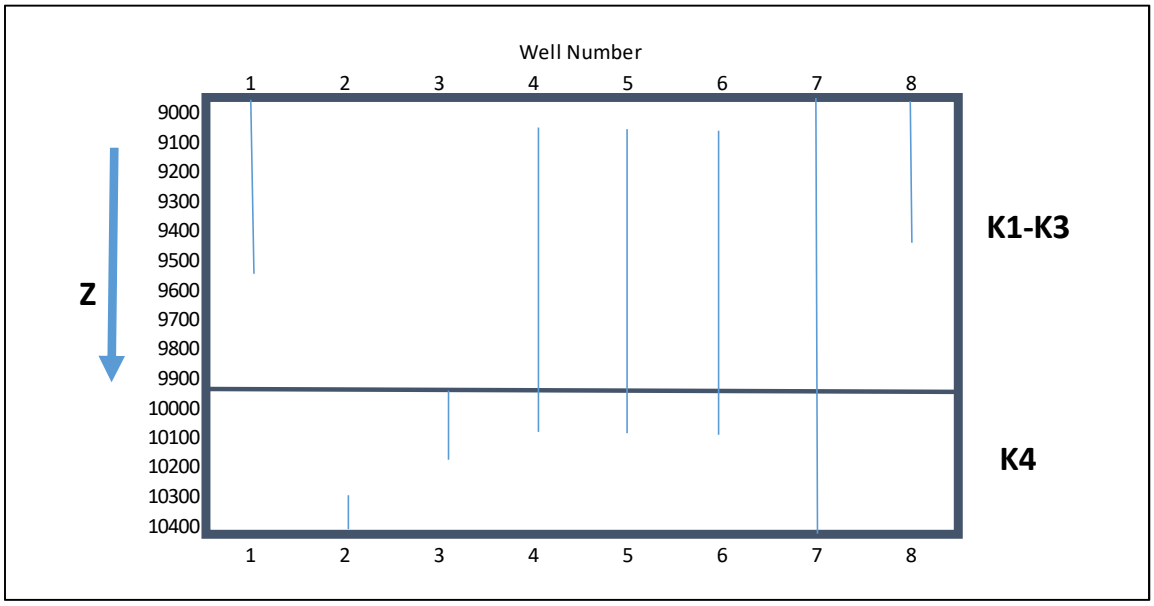

Figure 6-7: Depths of the eight North Field wells

Table 6-1: Depth, deviation, and length of the eight North Field wells

Well	Length	Angle	Zone	Start pt	End Pt
1	900	55	K1-K3	9000	9516
2	200	20	Lower K4	10212	10400
3	320	40	K4	10000	10245
4	1155	25	K1-K4	9100	10146
5	1600	50	K1-K4	9100	10128
6	2500	65	K1-K4	9100	10156
7	1600	30	K1-K4	9000	10385
8	800	51	K1-K3	9000	9503

The specific location of each well is unknown; however, based on data from publications, we know which wells share the same platforms. Based on data from Hajj et al. (2009), we deduced the approximate spacing of the platforms (≈17,000ft). We assumed that the 11 platforms are equally spaced in the 15km x 20.5km block that was allocated to Qatargas3 and Qatargas4 to develop. Furthermore, since each platform has 15 slots for wells and we know the approximate depth of the reservoir (10,000ft TVD) and average deviation of the wells (55° from vertical), we deduced the approximate spacing between wells on a given platform (≈5,000ft). Hence, even though we did not have actual well locations, we created a distribution of wells that is realistic for this reservoir. The geostatistical tools that were used are based on the relative distances between points as opposed to the actual locations, so our synthetic well locations should be sufficient for testing the batch size optimization method. Figure 6-8 shows the assumed well locations in an X-Y plane.

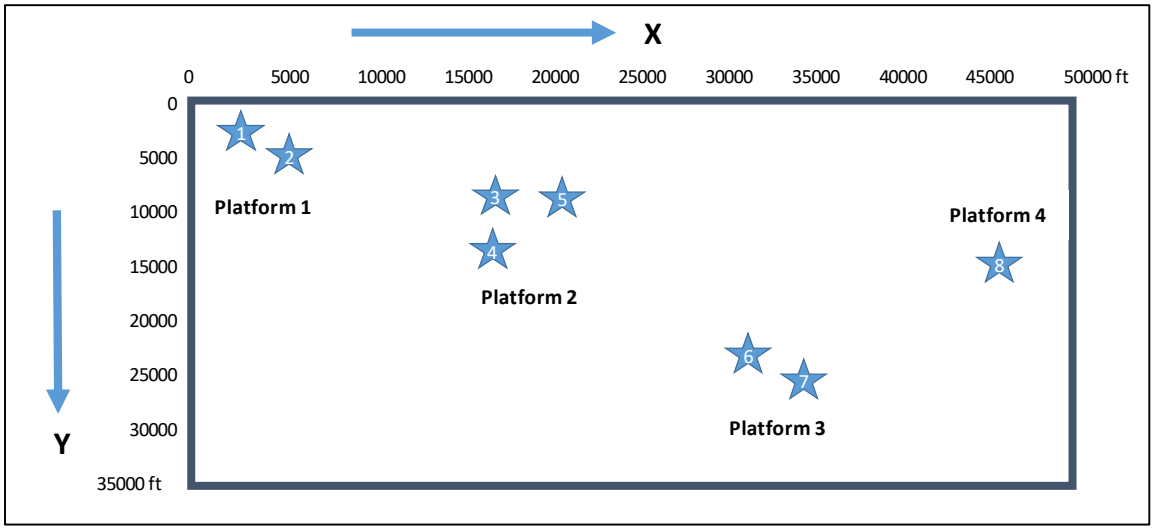

Figure 6-8: Location of the eight North Field wells on an X-Y plane

This data set was used to carry out two examples of the methodology described earlier, in section 4.3 and section 6.1.

6.3 Example 1: Deviated Well

In this example, we simulated a deviated well (55°) that has a completion and stimulation design that is as close as possible to the eight other wells. Figure 6-9 shows the location of this well as a red star.

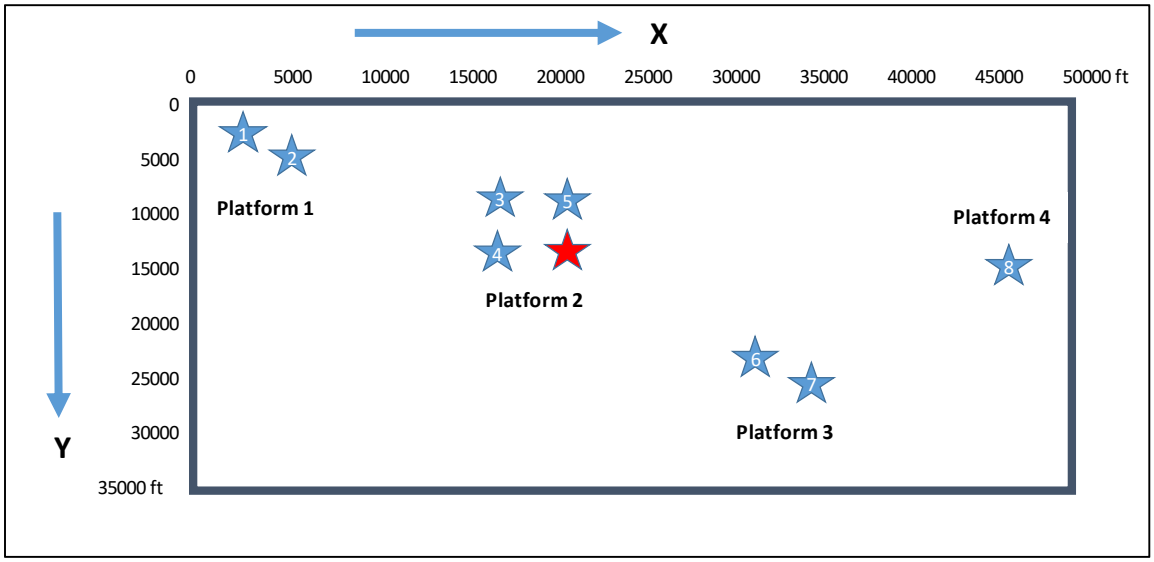

Figure 6-9: Location of the well to be simulated

6.3.1 Collect Known Data

The eight permeability profiles are given by Figure 6-4, Figure 6-5, and Figure 6-6. The well depths are given by Figure 6-7 and the well locations are given by Figure 6-8. This data was inputted into the geostatistical software, Stanford Geological Modeling Software (SGeMS). Figure 6-10 and Figure 6-11 show the location of the wells in SGeMS. Note that the larger grid represents the entire reservoir domain, while the smaller grid that contains wells #3-5 represents the platform 2 region. In this example, we developed the variogram using all the wells in the reservoir domain, but we only simulated permeability realizations in the platform 2 region.

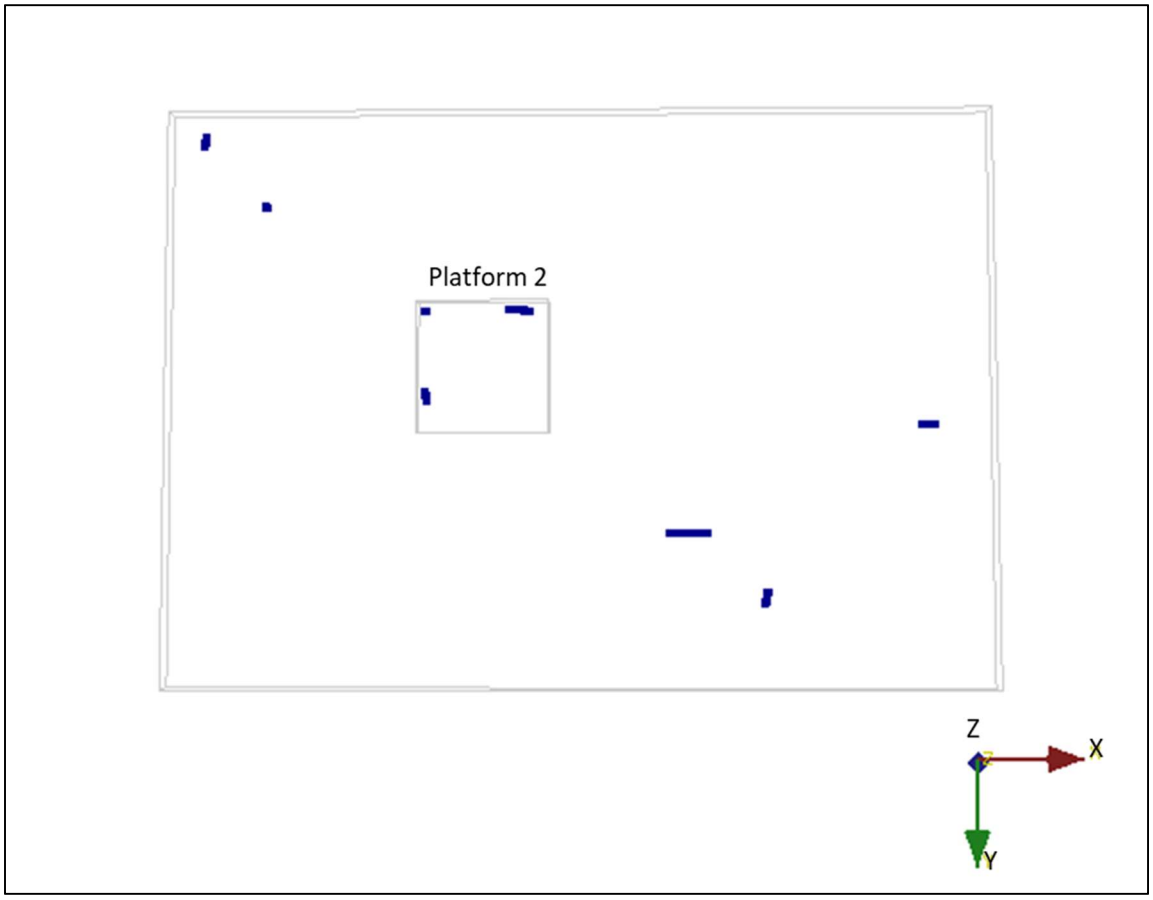

Figure 6-10: The location of the known wells in an XY plane (SGeMS input)

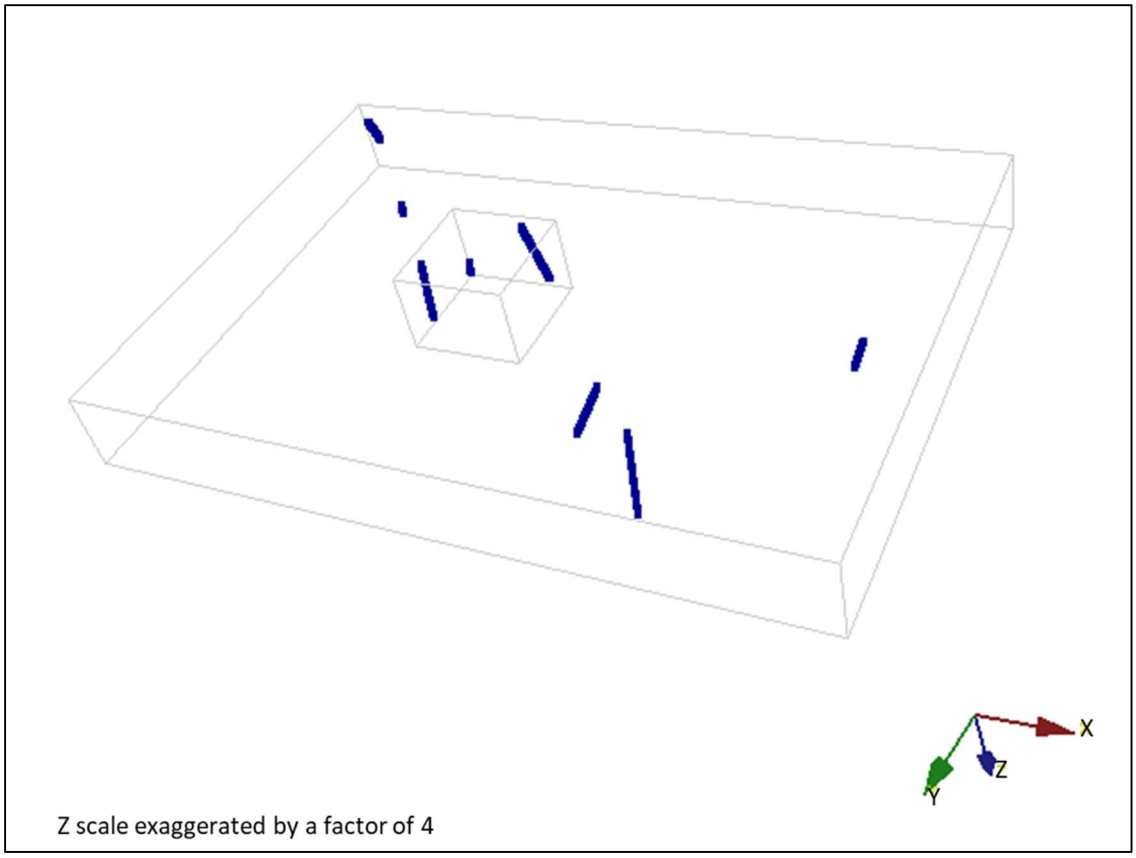

Figure 6-11: The location of the eight known wells in a Z plane (SGeMS input)

6.3.2 Create Variograms

The permeability realizations were developed using a spatial interpolation method called kriging. Kriging estimates the value of a property at an unknown location as the weighted average of the property values at the known locations see Eq. 6-1

$$k^* = \sum_{i=1}^{n} \lambda_i \, k_i \qquad (6\text{-}1)$$

The weights that are assigned to the known data points are based on an algorithm that is designed to impose minimum variance and unbiasedness. The algorithm is shown in Eq. 6-2. Please note that each form of kriging has slight variations to Eq. 6-1 and 6-2.

$$\begin{bmatrix}\text{Covariance among}\\ \text{known data points}\end{bmatrix}[\lambda] = \begin{bmatrix}\text{Covariance between known}\\ \text{and unknown data}\end{bmatrix} \tag{6-2}$$

The covariance values between any two points can be found using a variogram once the distance between the points is known. A variogram is plot of semi-variance versus lag distance that mathematically describes how similar two points are based on separation distance. Semi-variance (γ) between two points X and Y can be calculated as shown in Eq. 6-3. A sample variogram is shown in Figure 6-12.

$$\gamma(\mathrm{X},\mathrm{Y}) = \frac{1}{2}\mathrm{E}[(X-Y)^2] \tag{6-3}$$

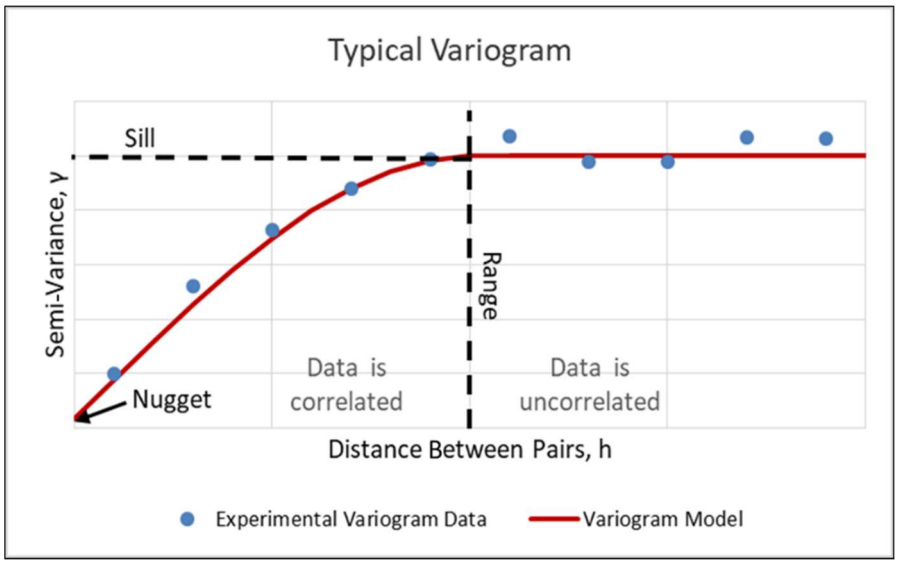

Figure 6-12: Sample Variogram

The covariance between two points can easily be calculated from the variogram once the separation distance between the two points is known. Eq. 6-4 shows the relationship between the semi-variance, variance, and covariance. Please note that C(0) is the covariance between two points with no separation distance, which, by definition is the variance of the data and is equal to the sill of the variogram (see Figure 6-12).

$$\gamma(\mathrm{X},\mathrm{Y}) = C(0) - C(X,Y) \qquad (6\text{-}4)$$

Please note that in this example, indicator kriging was used during the spatial interpolation. This means that the raw permeability measurements were not directly used. Instead, the data had to be transformed based on indicator thresholds. The random indicator variable $I(Z_k; x)$ is associated with the random function $Z(x)$ for the threshold value Z_k as shown in Eq 6-5:

$$I(Z_k; x) = \begin{cases} 0 \text{ if } Z(x) > Z_k \\ 1 \text{ if } Z(x) \leq Z_k \end{cases} \quad (6\text{-}5)$$

Ten thresholds were selected within the range of the permeability measurements for this example. Table 6-2 shows the thresholds that were selected and their cumulative probabilities.

Table 6-2: Indicator thresholds used for example

Permeability Threshold (mD)	Cumulative Probability
0.10	0.01
0.15	0.29
0.20	0.57
1	0.58
10	0.63
100	0.83
500	0.93
1500	0.98
1900	0.98
2000	1.00

In order to create the variogram, a series of experimental variograms were made in different azimuths (rotation about the Z-axis) and dips (rotation about the X-axis) to identify the directions of anisotropy. By identifying the direction of maximum variogram range (Figure 6-13) and the magnitude of the maximum, medium and minimum ranges (Figure 6-14), an ellipsoid that describes the variogram range was developed and used for interpolation.

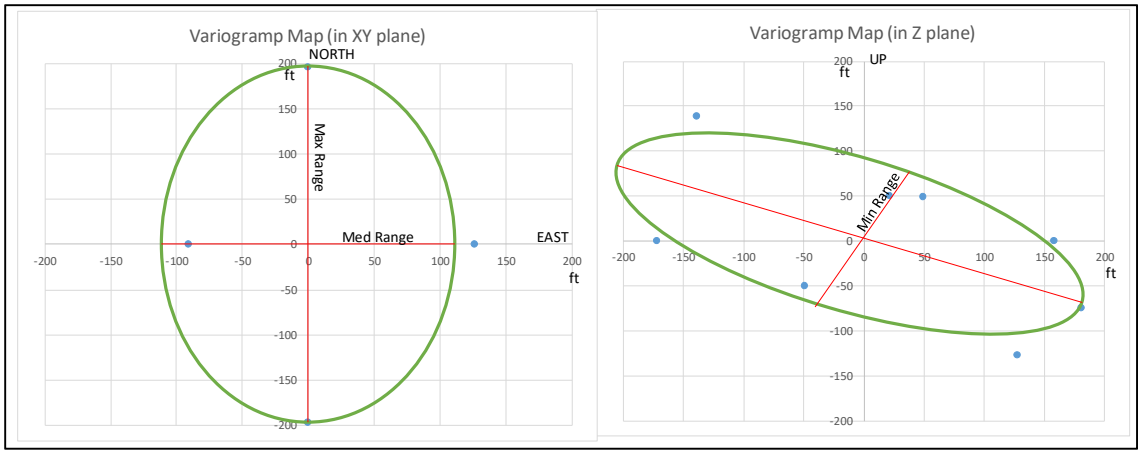

Figure 6-13: Variograms maps used to locate the anisotropy directions

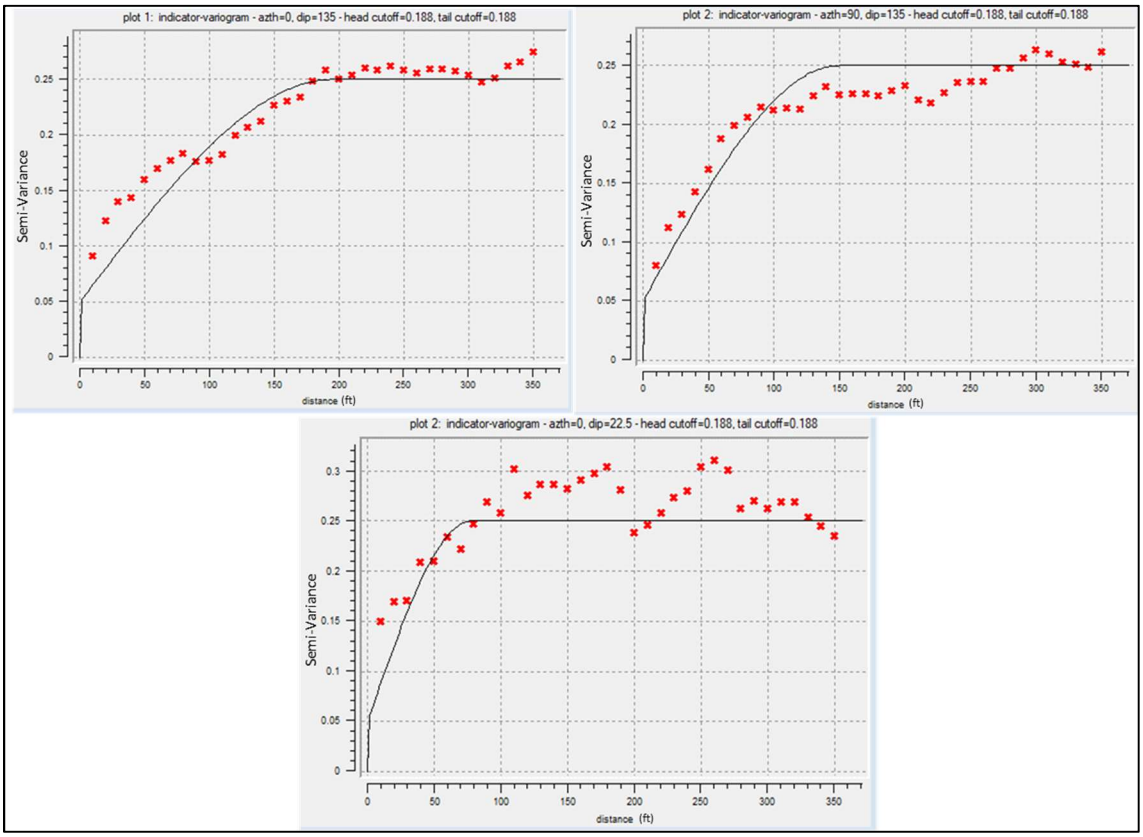

Figure 6-14: Variograms with the maximum (top left), medium (top right) and minimum (bottom) ranges

6.3.3 Create Reservoir Permeability Realizations

Once the variogram was modeled, we proceeded to create permeability realizations for the reservoir. As mentioned, we will use sequential indicator simulation (SIS) to carry out the spatial interpolation of permeability in the reservoir. Sequential indicator simulation (SIS) is a conditional simulation that uses indicator kriging. Indicator kriging was chosen over other kriging techniques because it does not assume a Gaussian distribution and thus can preserve connectivity between extreme values (this is important for permeability). Also, conditional simulation was chosen instead of directly using indicator kriging because indicator kriging only would create a single deterministic permeability realization as opposed to many equally probable realizations. A single deterministic solution would be overly smooth and not capture the variability of permeability in the reservoir. Once the data has been transformed into indicator thresholds (Eq. 6-5) and the variogram has been modelled, the method to carry out sequential indicator simulation (SIS) is as follows:

1. At an unknown location, estimate the cumulative probability of each threshold by carrying out indicator kriging (indicator kriging uses the same procedure as simple kriging as shown in Eq. 6-1 and Eq. 6-2, but the transformed property values and indicator variograms are used).
2. Compute a cumulative density function (CDF) using the cumulative probabilities at each threshold.
3. Sample a value from the CDF that was created for the unknown location and include this point as a part of the conditioning data (or known data points).

4. Repeat steps 1-3 until all locations have been estimated.

The dimensions of the reservoir that contain all eight wells was 50,000'x35,000'x1400'. It was computationally expensive to create realizations for the entire reservoir with a small resolution. Instead, permeability realizations were created within a block of the reservoir that contained the platform 2 wells that was 8000'x8000'x1400' (Figure 6-15).

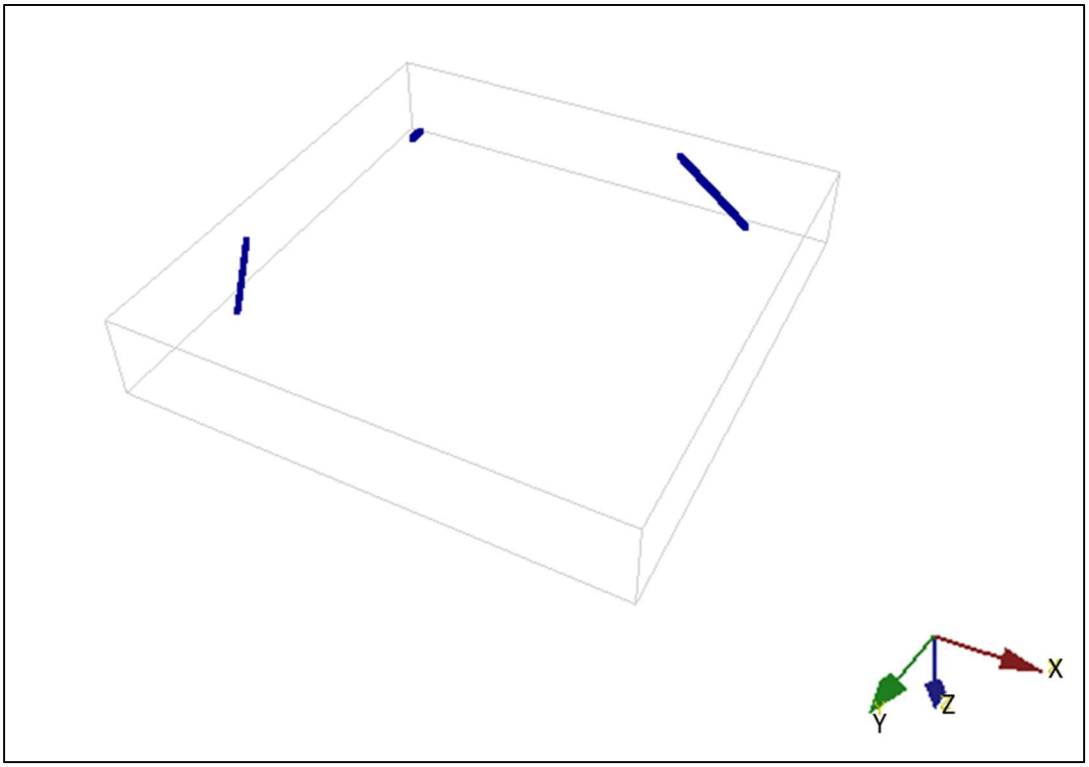

Figure 6-15: Block of the reservoir that SIS (sequential indicator simulation) was carried out on

Aside from deciding on the total size of the reservoir to simulate, we must also determine the size of and number of the smaller grids that make up the total reservoir grid. The maximum variogram range is 200'. This means that we cannot use grids that are larger than 200' (points that are separated by distances larger than the variogram range are completely uncorrelated – see Figure 1-3). On the other hand, when we model the negative skin due to wormholes in the reservoir simulator, the grids must be large enough to allow an equivalent wellbore radius that does not exceed the grid's pressure equivalent radius. To solve this issue, sequential indicator simulation (SIS) was carried out on a fine grid, 20'x20'x20' (so that the variogram and hard data can be useful in the interpolation), then the grids were upscaled to 20'x200'x200' (to allow the reservoir simulation to model the wormholes). Figure 6-16 shows a permeability realization created with sequential indicator simulation (SIS) on the fine scale grid. Figure 6-17 shows the same realization that has been upscaled to the larger grid size.

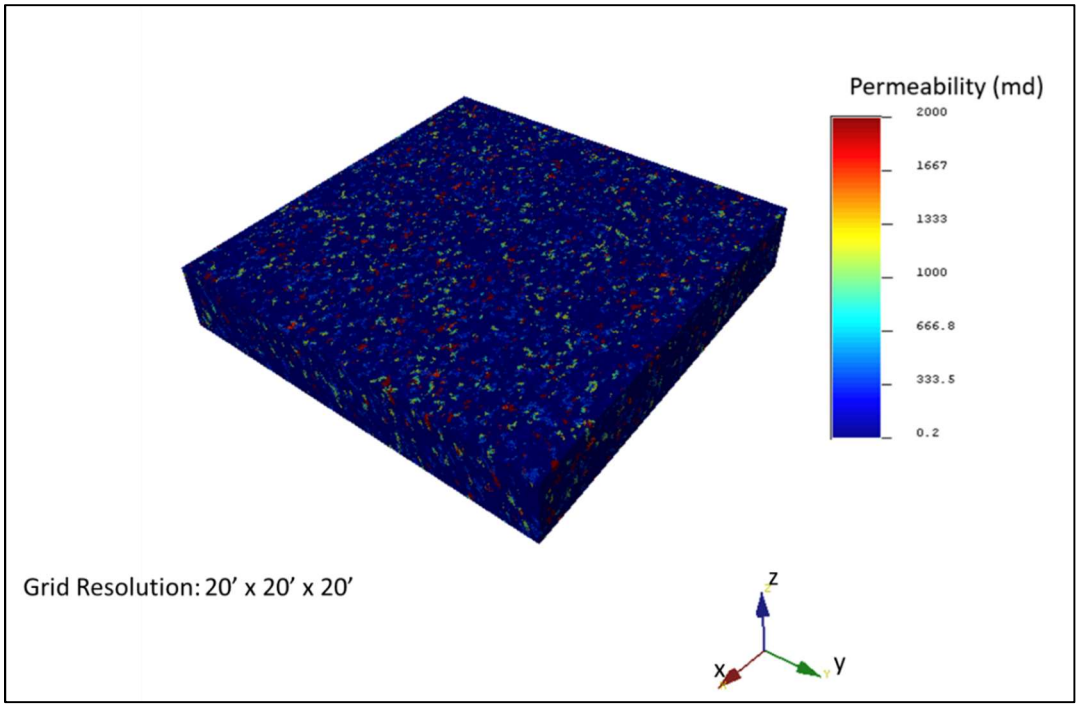

Figure 6-16: A permeability realization on the fine scale grid

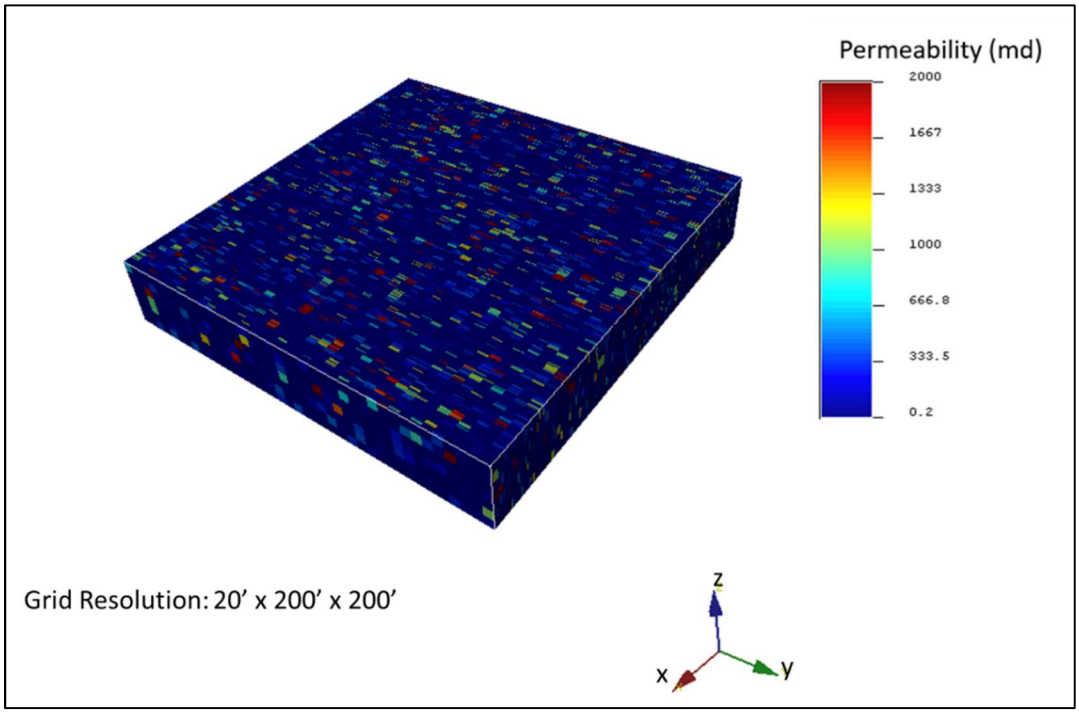

Figure 6-17: A permeability realization on the coarse scale grid

6.3.4 Determine Near Wellbore Permeability

The 1500' long, 55° deviated well to be simulated is located in the platform 2 reservoir and is shown in Figure 6-18.

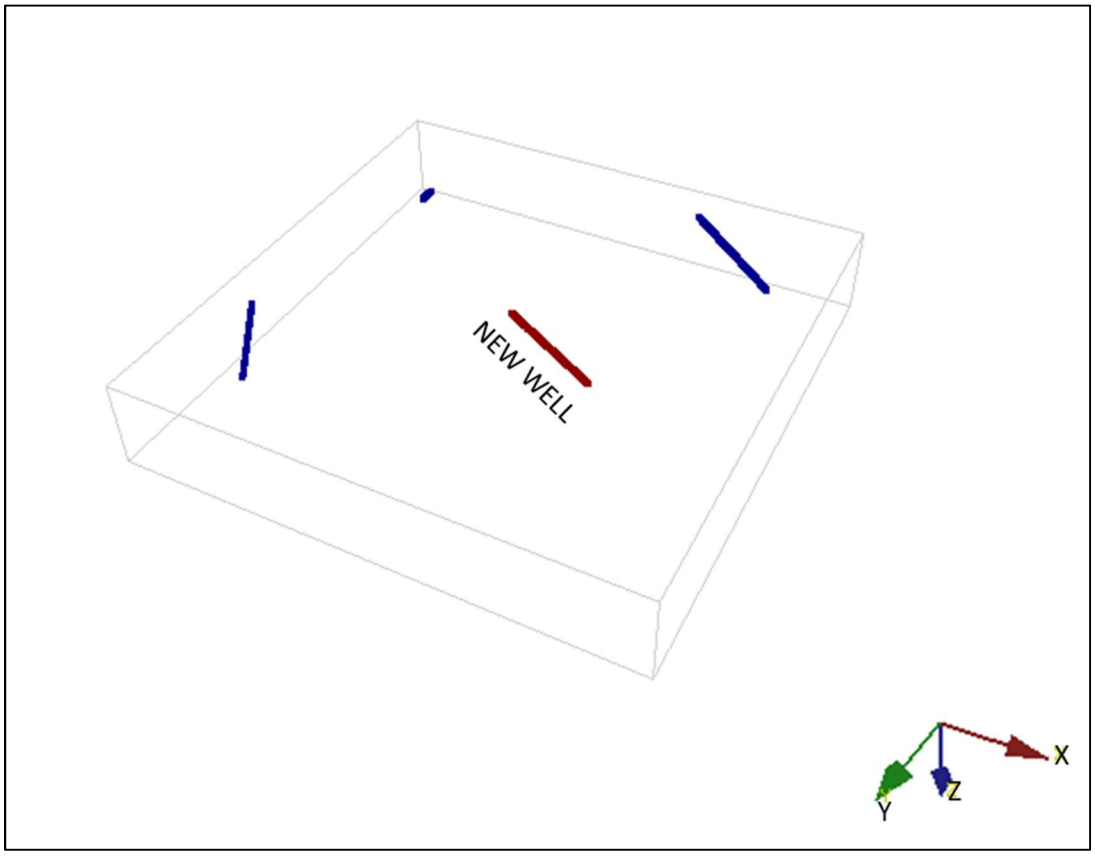

Figure 6-18: Location of the well that is being simulated relative to the other platform 2 wells (in SGeMS)

The permeability of the grids that our new well passes through can be directly read from the permeability realization results. However, the permeability of the grids that the well is located in is not the same as the near wellbore permeability. As can be seen in cartoon on the left side of Figure 6-19, a grid that the well passes through may have grids

surrounding that grid of very different permeabilities. The cartoon only shows neighboring grids in 2D but there are even more grids above and below the grid that the well passes through. The flow rate that enters the well at any given grid is not only a function of that grid's permeability but also the surrounding grids. However, when we use inflow performance relationship equations we treat the well as though it is producing from a laminated reservoir as shown by the cartoon on the right side of Figure 6-19. We can use a reservoir simulation to determine the flow rate in each grid for a given drawdown pressure and use these results to calculate the near wellbore permeability.

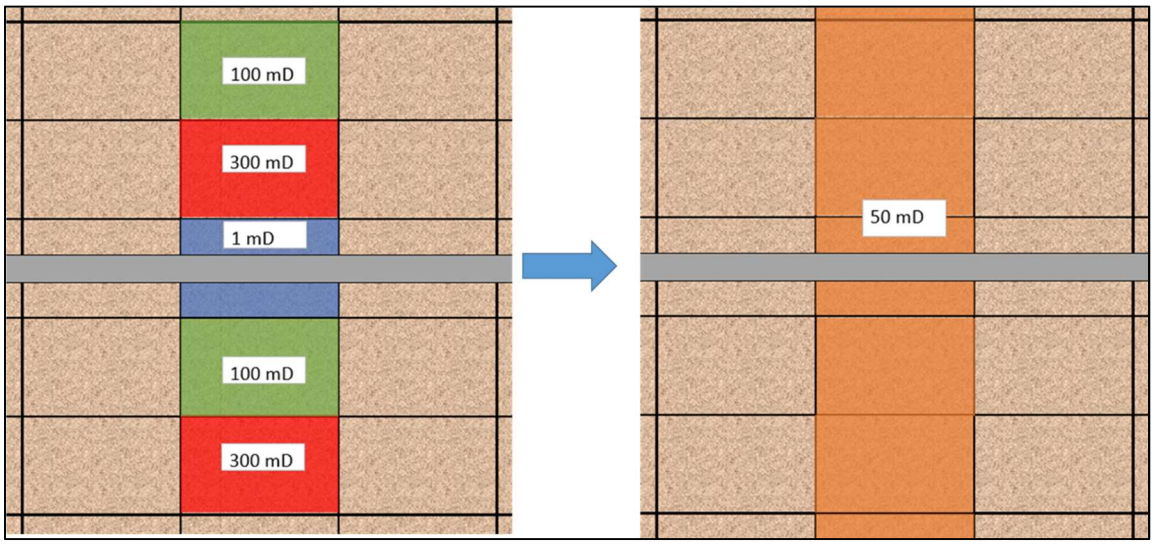

Figure 6-19: Cartoon showing the difference between the grid permeability and near wellbore permeability

The reservoir simulator that was used in this study was ECLIPSE Industry-Reference Reservoir Simulator. The well input data and the reservoir permeability realization of the permeability distribution were input into the reservoir simulator, and

then the production was simulated for a set time (1 year) with a fixed bottom hole pressure of 5000psi (an initial drawdown pressure of approximately 300psi). Production was simulated for 1 year because it was noticed that the productivity index (total well flow rate ÷ average drawdown pressure) becomes constant after this time, this means that we can use a steady state inflow equation. We can use the flow rate and wellbore pressure at each grid, along with the average reservoir pressure and an IPR for a horizontal gas well (see Eq. 6-6), to determine the near wellbore permeability. Figure 6-20 shows a flow profile and the permeability realization that is created based on the reservoir simulation.

$$q_g = \frac{kL(p_e^2 - p_{wf}^2)}{1424\overline{Z}\overline{\mu_g}T\left(\ln\left[\frac{hI_{ani}}{r_w(I_{ani}+1)}\right] + \frac{\pi y_b}{hI_{ani}} - 1.224 + s\right)} \tag{6-6}$$

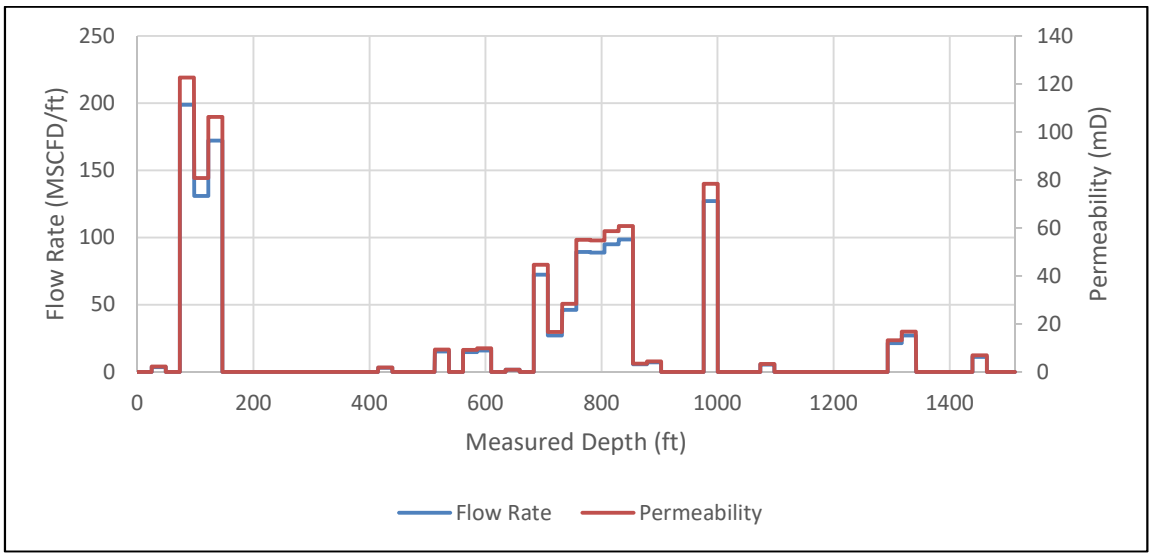

Figure 6-20: A flow rate and permeability profile for the well based on a permeability realization of the reservoir

Table 6-3, Table 6-4, and Figure 6-21 show the properties that were used for the reservoir simulation. Many of the parameters such as porosity, compressibility, anisotropy ratio, and pressures were taken from Whitson and Kuntadi (2005), which describes a reservoir simulation that was done for the Khuff formation (the same formation that the North Field wells are drilled into).

Table 6-3: Reservoir model description

Property	**Unit**	**Value**	**Comment**
Reservoir size	ft	8000x8000x1400	
Number of grids		400x40x7	
Fluid components		Gas and water only	Eclipse E100 simulator was used, so it is not necessary to specify the composition of the gas
Porosity		10% and 15%	The reservoir is broken into 4 layers K1-K4, K1 (200ft) & K4 (400ft) are given 10% porosity, K2 (400ft) and K3 (400ft) are given 15% porosity.
kh/kv		10	
Rock compressibility	psi^{-1}	5.00E-06	
Water compressibility	psi^{-1}	2.64E-06	
Datum depth	ft	9000	
Reservoir pressure at datum depth	psi	5300	

Table 6-3: Continued

Property	Unit	Value	Comment
Reservoir temperature at datum depth	°F	220	
Gas / water contact depth	ft	12,000	No aquifer and no water injection, gas production only
Depth of well heel	ft	9100	
Well control method		Bottom hole pressure	
Bottom hole pressure	psi	5000	
Wellbore diameter	in	7	
Well skin factor		50	Initial Skin taken from Van Vliet et al. (2011)

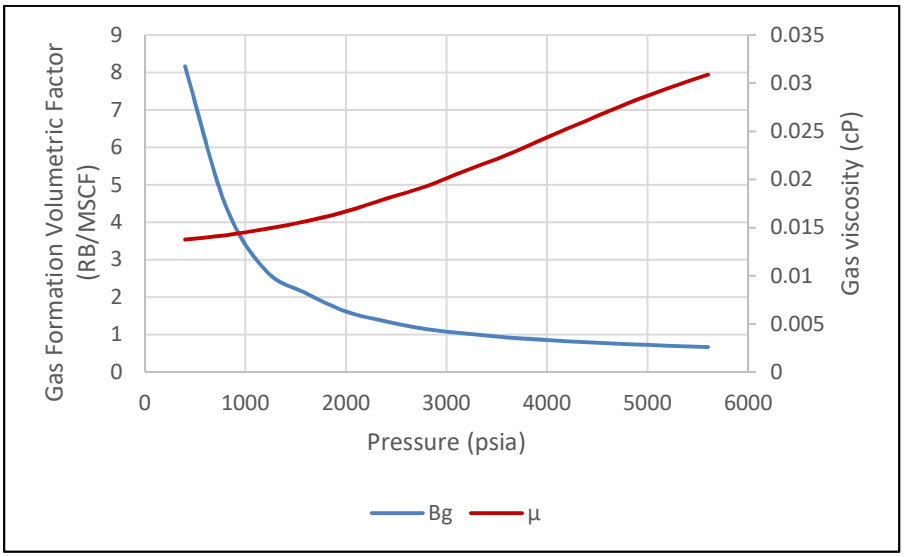

Figure 6-21: PVT data for the reservoir simulation (Adapted from Whitson and Kuntadi 2005)

Table 6-4: Relative permeability data (Adapted from Petterson, 2006)

Sg	krg	krw	capillary pressure (psi)
0.00	0.00	1.00	0.0
0.04	0.00	0.90	0.2
0.10	0.02	0.80	0.5
0.20	0.10	0.50	1.0
0.30	0.24	0.40	1.5
0.50	0.42	0.21	2.5
0.60	0.50	0.11	3.0
0.70	0.81	0.00	3.5
0.78	1.00	0.00	3.9

6.3.5 Calculate Skin Profiles

The next stage was to begin searching for the optimal diverter size for the well based on this permeability realization. In order to do this, we first determined the skin profile of the well based on different diverter batch sizes. As discussed earlier, we have used Horizontal Well Acid Simulator (HWAS), with modifications to include the PLA skin factor developed in this dissertation. Five acid stages and four diversion stages were used. The total acid injected in each case was1bbl/ft of 15% HCl acid (1500bbl). All acid stages were pumped at 20bpm, and all diverter stages were pumped at 10bpm. The parameters that were used for the near wellbore simulation are as shown in Table 6-5.

Table 6-5: Parameters used for HWAS simulation

Parameters	Units	Value	Comments
Well completion	Cased and Perforated		
Placement method	Bullheading		
Reservoir type	Gas		
Total reservoir compressibility	psi^{-1}	1.5×10^{-4}	
Reservoir fluid viscosity	cP	0.03	
Wellbore radius	ft	0.29	
Permeability ratio (kh/kv)		10	
Damaged zone radius	ft	1.5	
Permeability impairment ratio (ks/k)		0.01	
Perforation length	in	15	
Perforation diameter	in	0.39	Similar completion to the other eight wells
Perforation phasing	deg	120	
Shot density	spf	3	
Specific gravity of diverting agent		1.24	
Acid concentration in acid stages		15%	
Specific cake resistance	ft/lb	9.00E+13	Based on values used to match field cases

The acid efficiency parameters that were used for the near wellbore simulation are given in Table 6-6.

Table 6-6: Optimal points used for wormhole propagation calculations

Optimal Pore Volume to Break Through	Optimal Interstitial Velocity	Min Perm that this optimal point refers to	Max Perm that this optimal point refers to
$PV_{bt\text{-}opt}$	$V_{i\text{-}opt}$	k_{min}	k_{max}
	cm/min	mD	mD
0.94	1.80	0	10
0.98	2.04	11	100
1.18	1.88	101	200
1.40	1.33	201	2000

Figure 6-22 shows an example of the skin profile of the well. Figure 6-23 shows how the total skin factor calculated by Eq. 3-4 varied with the diverter batch size for this permeability profile.

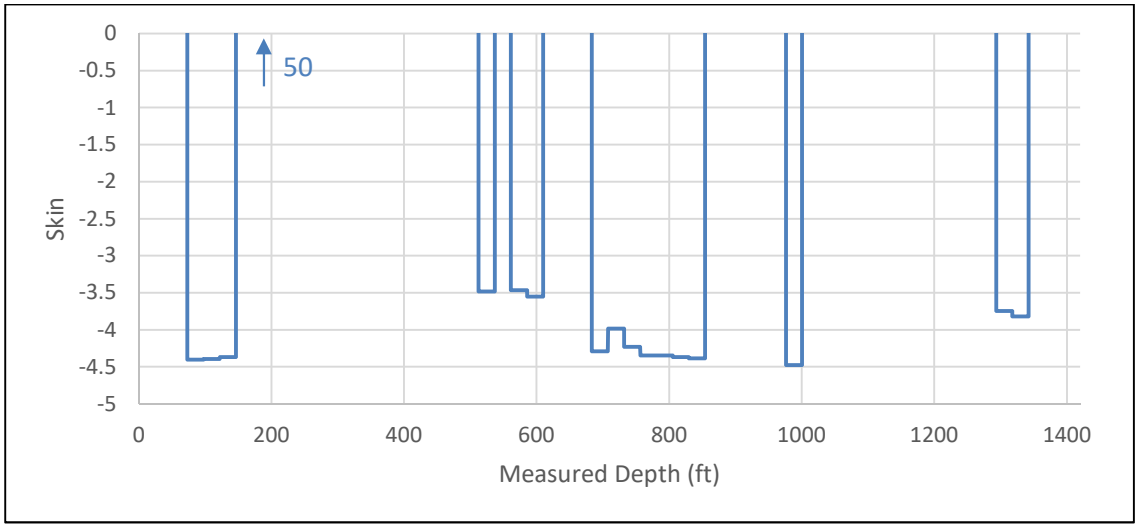

Figure 6-22: Example of a skin profile of the well

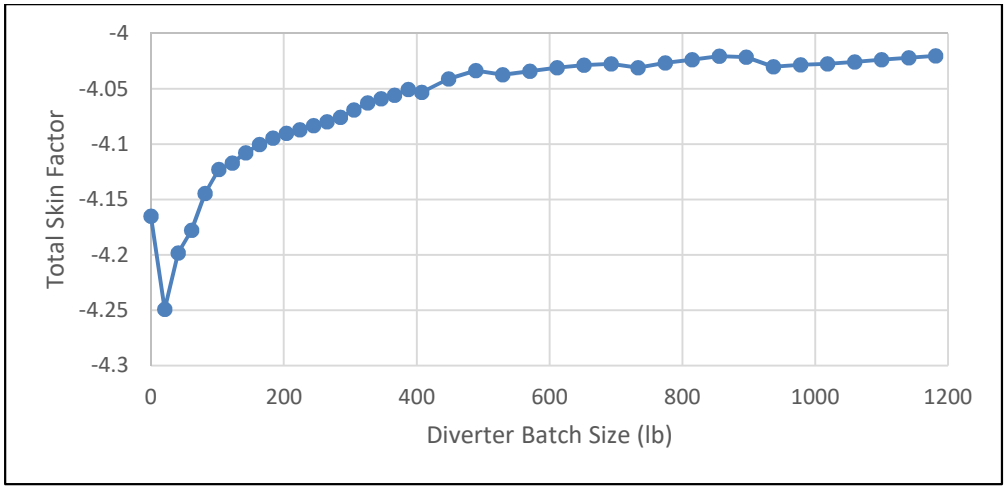

Figure 6-23: Total skin factor for a range of diverter batch sizes

It should be noted that there is a maximum diverter batch size, use of diverter sizes above which may not be practical. When the diverter is pumped into a well, it creates resistance to flow wherever it is deposited, this in turn increases the bottom hole pressure if a constant rate is being applied. If the pumping bottom hole pressure increases above the fracturing pressure, the acid will hydraulically fracture the formation (this is undesirable because a large amount of acid will flow through the fracture and not evenly across the well). In practice, this is avoided by lowering the injection rate, however, if the injection rate must be lowered significantly it may impact acid efficiency because wormholing efficiency is a function of the injection rate. The maximum diverter batch size that will be used for this case is 1200 lb PLA/stage. As an example, when this maximum batch size is used in this well with the permeability realization shown in Figure 6-20, the acid injection rate would have to be lowered from 20 bpm to 8 bpm to avoid fracturing the rock. The necessary reduction in flow rate was found by running HWAS with constant pressure at the fracture pressure and the fracture gradient was assumed to be 0.7 psi/ft.

6.3.6 Calculate Long Term Cumulative Production

Following this, we simulated the reservoir again, but now we included the skin profiles that were generated. Three years of production were simulated. The flow rate of the well was controlled by bottom hole pressure and a constant bottom hole pressure of 4000psi was used throughout the three year period (this equates to an initial drawdown pressure of approximately 1300psi). The same reservoir properties were used as described in the first reservoir simulation (to determine the near wellbore permeability) – see Table 6-3, Table 6-4, and Figure 6-21. Each skin profile that was used along the well resulted in a different cumulative production. By plotting the cumulative production versus batch size, one can clearly determine which diverter batch size is optimal, as seen in Figure 6-24.

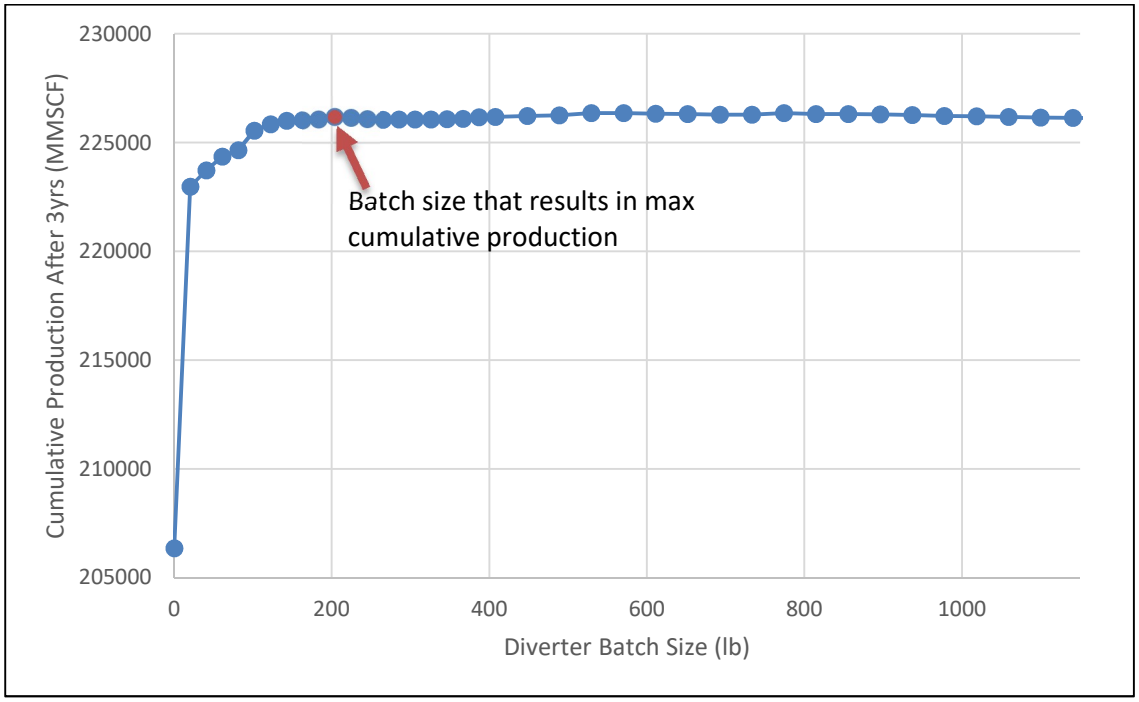

Figure 6-24: Selection of the optimal batch size based on cumulative production

Please note that we have chosen to define the optimal batch size as the batch size that results in the maximum cumulative production. The wells in this reservoir are high production gas wells with nominal production rates of 200 MMSCFD (Clancey et al., 2008). This means that a small improvement could be very profitable. For example if the 3 year cumulative production of the well is 2,000,000 MMSCF, a 0.01% increase would result in an increased profit of $600,000USD if gas is sold at $3/MSCF. In wells that do not produce as much, selection of the optimal diverter size or even the choice of whether to use diverter may require inclusion of economic calculations that consider the cost of the treatment.

When we compare Figure 6-23 with Figure 6-24, one point of controversy is that there are several diverter batch sizes that resulted in a worse (less negative) skin factor compared to having no diverter, but still resulted in a larger cumulative production. According to the inflow performance relationship that was used (see Eq. 6-6), as the skin factor becomes more negative, the well can produce more fluid per unit pressure drawdown. However, this inflow performance relationship model assumes a drainage pattern that is radial close to the well and becomes linear far from the well as shown in Figure 6-25. Figure 6-26 shows that the flow pattern is not simply linear and radial. Figure 6-26 shows the production streamlines after 3 years of production with a constant drawdown pressure of 4000psi; the streamlines were generated based on the permeability realization shown in Figure 6-17 and the same reservoir properties given earlier (Table 6-3). Since the reservoir permeability varies throughout the reservoir and is not laminated, the gas does not travel in straight paths but instead it will flow based the permeability of

the surrounding formation and find the paths of least resistance. The difference in the flow path explains why the inflow performance relationship is unable to determine the skin profile that leads to the maximum cumulative well production.

Please note that the streamlines were generated using Schlumberger ECLIPSE FRONTSIM streamline simulator.

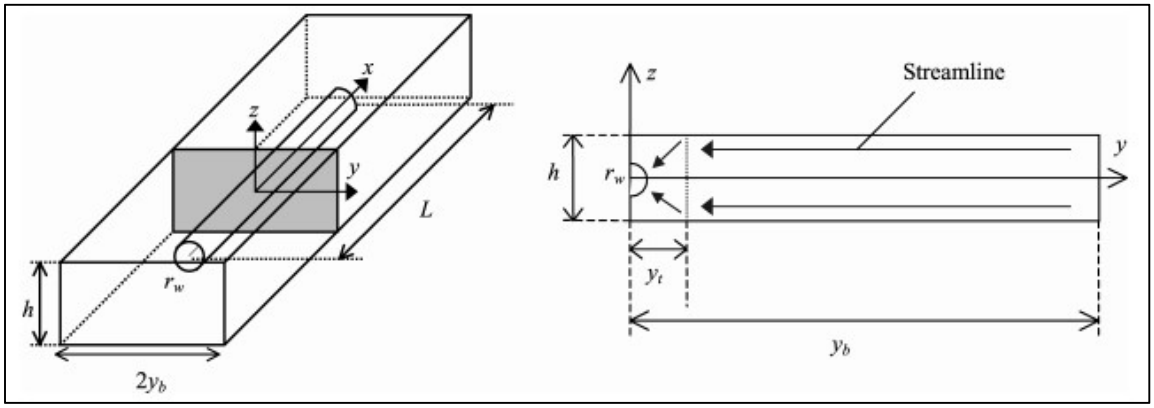

Figure 6-25: Drainage pattern assumed by Furui et al. IPR equation for horizontal wells (Adapted from Furui et al., 2003)

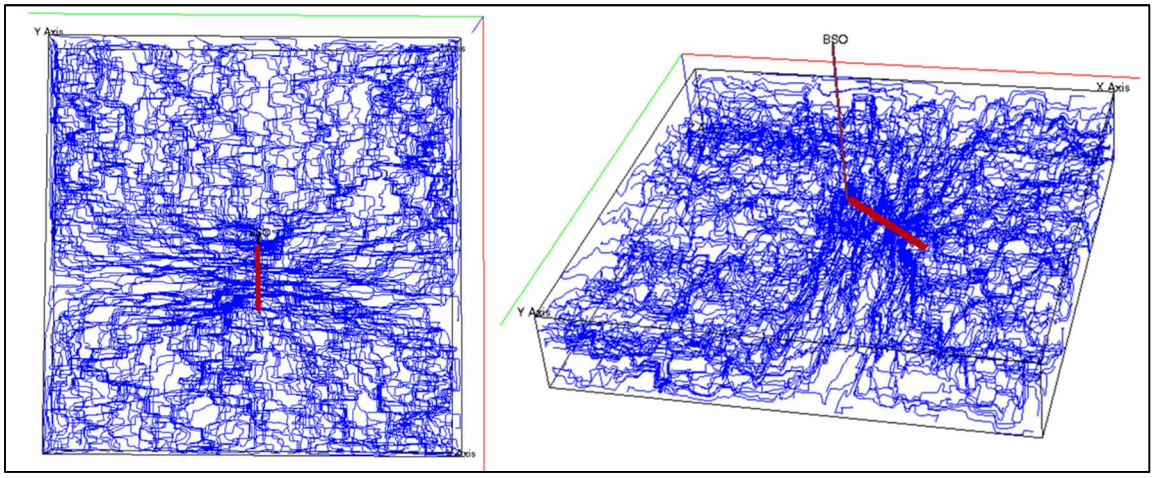

Figure 6-26: Streamlines for the example well after 3 years of production (left: XY plane view, right: 3D view)

Furthermore, a similar phenomenon where minimizing the total skin factor did not lead to maximum cumulative production was observed by Postl et al. (2009). In the study conducted by Postl et al. (2009), they attempted to find the treatment that would be able to maximize the cumulative production of a North Field, Qatar well shown in Figure 6-27. This figure shows that there is one zone that contains a significantly higher permeability than the rest of the well, but that the other zones still have significant porosity.

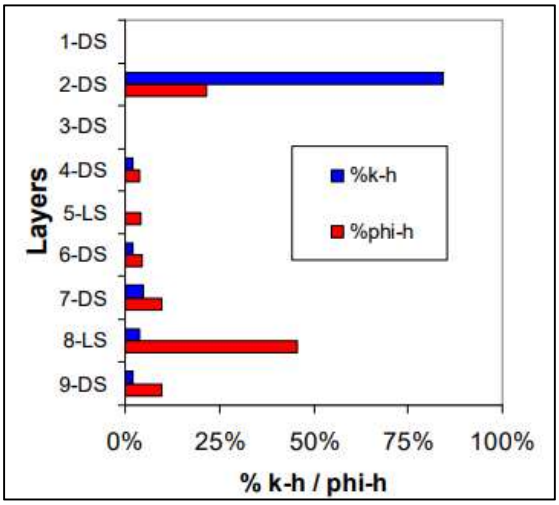

Figure 6-27: Permeability and porosity of the well investigated by Postl et al. (Adapted from Postl et al., 2009)

Similar to our observations in Chapter 6 (Sensitivity Analysis), they noticed that in order to minimize the skin factor it is better to apply most of the acid in the high permeability zones (i.e., no diversion). However, if they wanted to maximize connectivity to the reservoir porosity, acid needs to be distributed differently – see Figure 6-28.

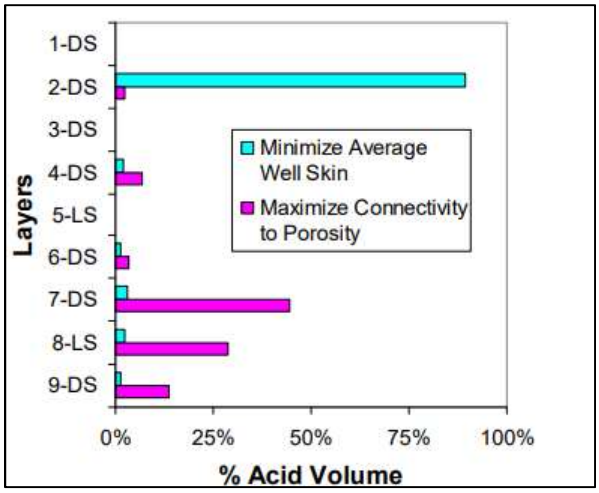

Figure 6-28: Acid placement needed to minimize the total skin factor and to maximize connectivity to the well (Adapted from Postl et al., 2009)

The long-term performance of the well was simulated both for the well treated to attain the minimum negative skin and for the well treated to attain maximum connectivity to the reservoir. Figure 6-29 shows that in order to maintain a constant well production, having a better distributed treatment led to a smaller reduction of the flowing bottom hole pressure. This indicates that connectivity to the porosity of the well can allow better drainage of the reservoir.

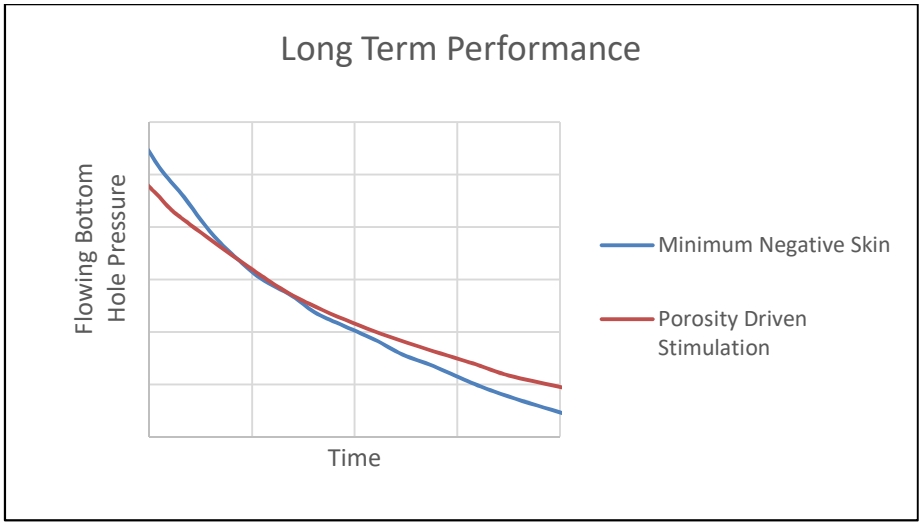

Figure 6-29: Long Term Well Performance (Adapted from Postl et al., 2009)

Their results agree with the findings of this study, and show that being better connected to the reservoir's porosity plays a role in determining the cumulative production of the well. Thus, even if the total skin factor is reduced (made less negative), if the diversion treatment allows better connectivity to the well, the net effect may be a higher cumulative production, as observed in Figure 6-24. However, connectivity to the well is clearly not the only factor that impacts the cumulative well production, because in many cases, applying diverting agent can create a more uniform flow profile, but it does not improve the overall cumulative production. Also, as we use larger diversion batch sizes, the skin profile becomes more uniform (see section 6.3), but there is some limit to which adding more diverter stops increasing the cumulative production of the well. This suggests that both the total skin factor and the connectivity to the reservoir porosity play roles in determining the cumulative production of the well.

6.3.7 Repeat Until Average Optimal Batch Size Converges

The stages that were described in sections 6.3.3-6.3.6 applied to a single permeability realization of the reservoir. We then repeated these steps for several realizations and find an average optimal diverter batch size. In this case, iterations were stopped after the cumulative average converged within ±10lb, see Figure 6-30.

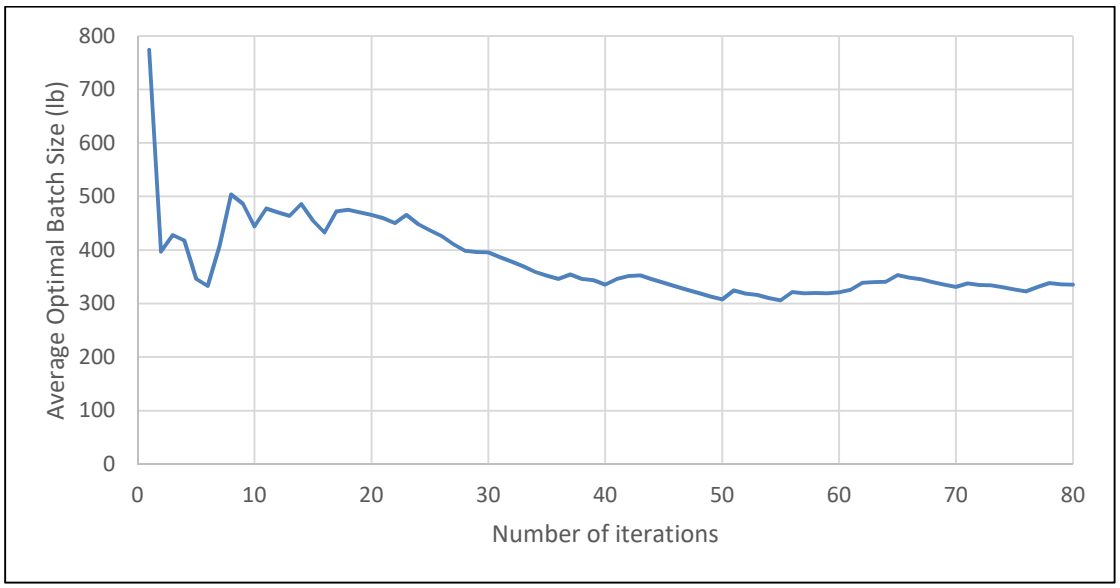

Figure 6-30: Cumulative average optimal batch size versus number of iterations

Finally, Figure 6-31 shows a histogram of the optimal batch sizes from the various iterations. This histogram shows that the mode of the optimal diverter batch sizes is close to the mean, and that 73% of the values lie between 0-400lb diverter.

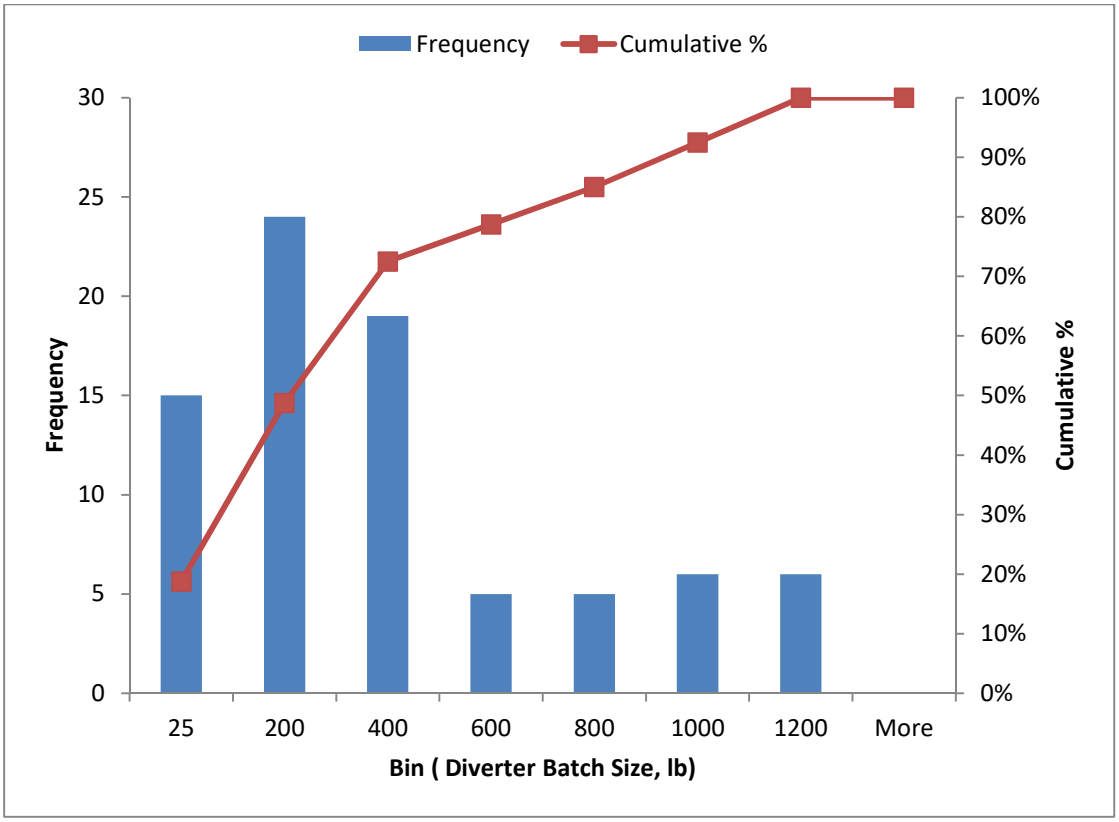

Figure 6-31: Histogram of the optimal diverter batch sizes

6.4 Distribution of the High Permeability Zones

One of the advantages of the proposed method to design diversion treatments using geostatistical tools is that it allows investigation of what conditions could lead to diversion being useful and, just as importantly, when diversion would not be useful. By comparing the permeability profiles or treatment inputs that lead to large increases or no increase in cumulative production when diversion is applied, we can develop trends based on the examples. This can be very useful information, because even if a production log has not been carried out on the well that is being stimulated, one may have an idea of the location of the high permeability zones based on drilling and completion data, for example, using

mud losses while drilling. Furthermore, if a permeability profile is obtained through production logging, then assessments could be made about whether diversion is likely to be effective even before simulations are run, just based on the shape of the permeability profile.

One of the trends that was observed is that the location of the high permeability zones can impact the effectiveness of a diversion treatment. If the high permeability streaks occur close to the toe of the well, the diversion treatment tends not to be effective in improving the cumulative production. One way of quantifying this trend is to calculate the percentage of permeability x well length within the third of the well closest to the toe, we will refer to this as $kl_{1/3}$. Figure 6-32 shows four permeability profile realizations for the example well, in each case, $kl_{1/3}$ was high (>50%), and there was minimal improvement in the cumulative production of the well when diversion was used in any of these cases (≤1% improvement).

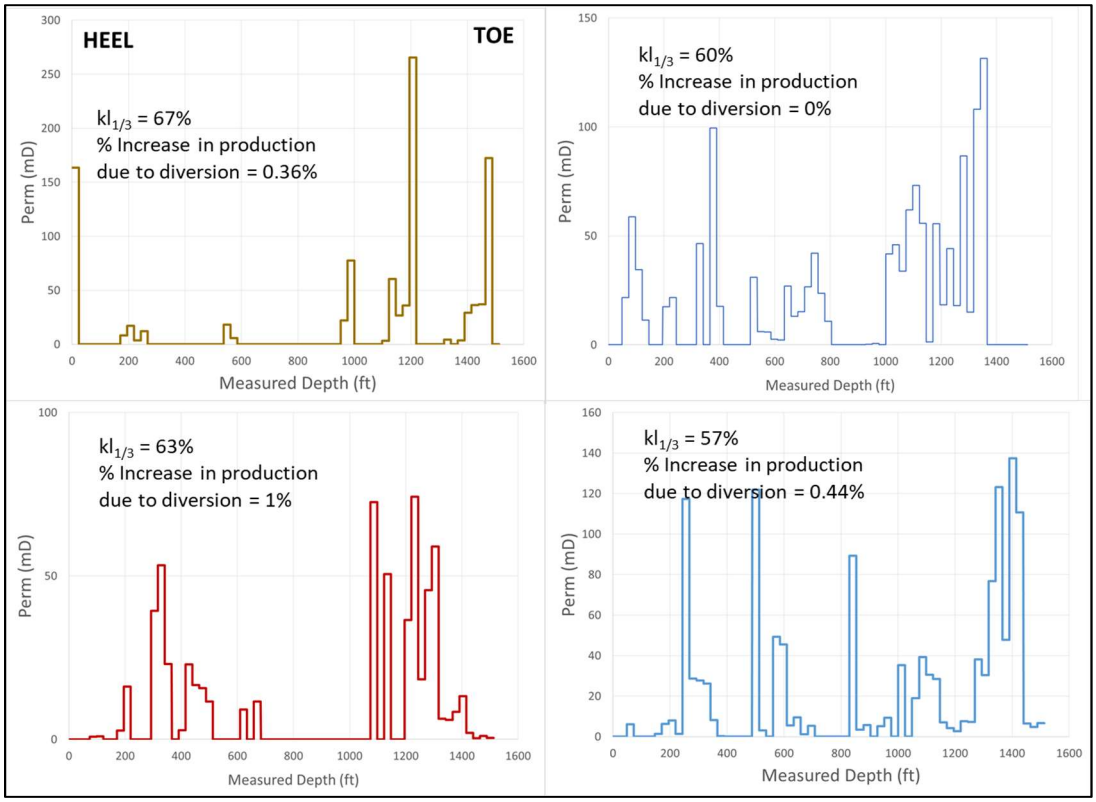

Figure 6-32: Examples of wells with high permeability streaks close to the toe of the well

This finding makes sense because the toe of the well is typically harder to treat than the heel. Thus, if the high permeability streak is located close to the toe, the acid can more easily treat the toe, and less acid is consumed in the heel of the well, i.e., even without chemical diversion, the acid is more evenly distributed along the well, making diversion unnecessary.

Similarly, well permeability profiles that contain several well distributed and similarly sized permeability peaks, tend to have no increase in cumulative production when diverter is applied. Figure 6-33 shows four examples that each have at least 3 isolated high permeability zones, in each case diversion had a minimal increase in

cumulative production for the permeability profiles illustrated in Figure 6-33 (≤1% improvement). An isolated high permeability zone is a section of the well where the permeability is greater than half of the maximum permeability for that well and is separated from other high permeability peaks.

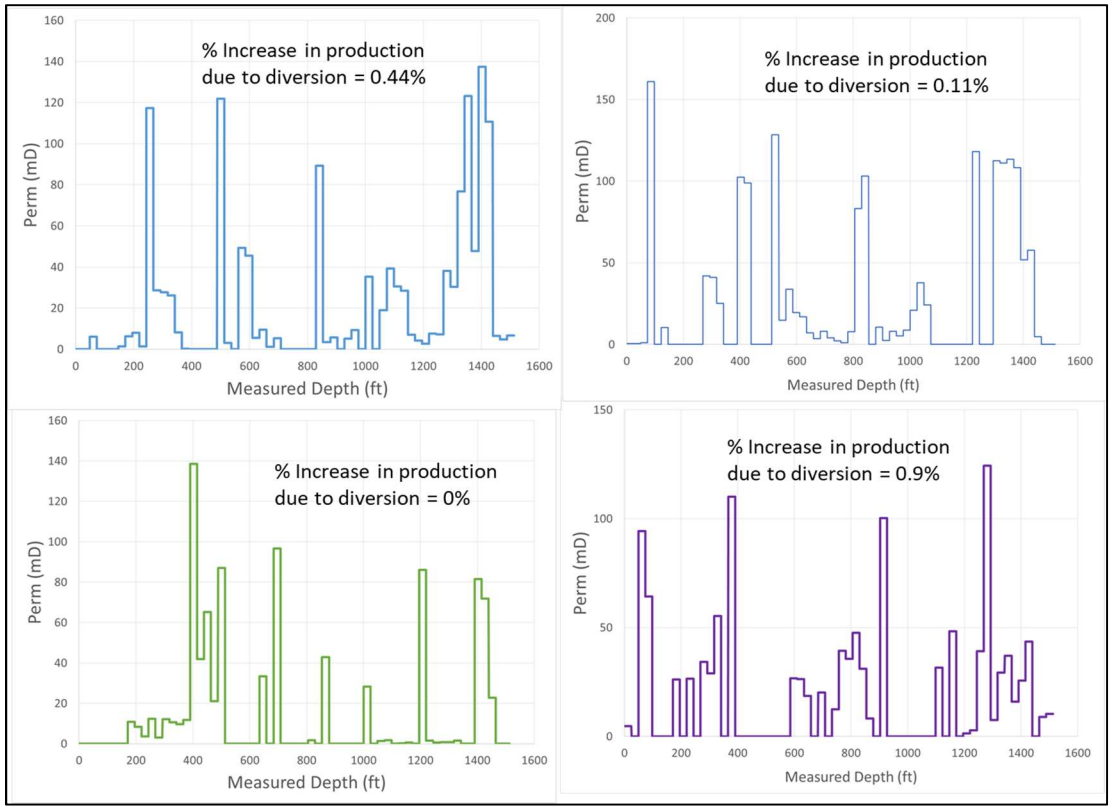

Figure 6-33: Examples of wells with several well distributed high permeability zones

On the contrary, diversion treatments tend to have the most benefit on permeability profiles that have only one or two high permeability zones located close to the heel or middle of the well, and several other lower permeability zones scattered along the well. In these cases, without diversion, a large volume of the acid tends to flow into and stimulate

the high permeability zones at the expense of the other, lower permeability zones. This leads to the well having a poor connection to the reservoir's porosity. When diversion is used in these cases, some of the acid is redistributed to the lower permeability zones, allowing a more uniform skin profile and production from more of the well. For the pure limestone examples studied, diversion treatments were typically able to increase the 3yr cumulative production in the range of 0-15%. In the profiles shown in Figure 6-34 below, diversion was able to increase the 3yr cumulative production by at least 10%. In each case $kl_{1/3}$ is less than 10% and there are no more than 3 isolated high permeability peaks.

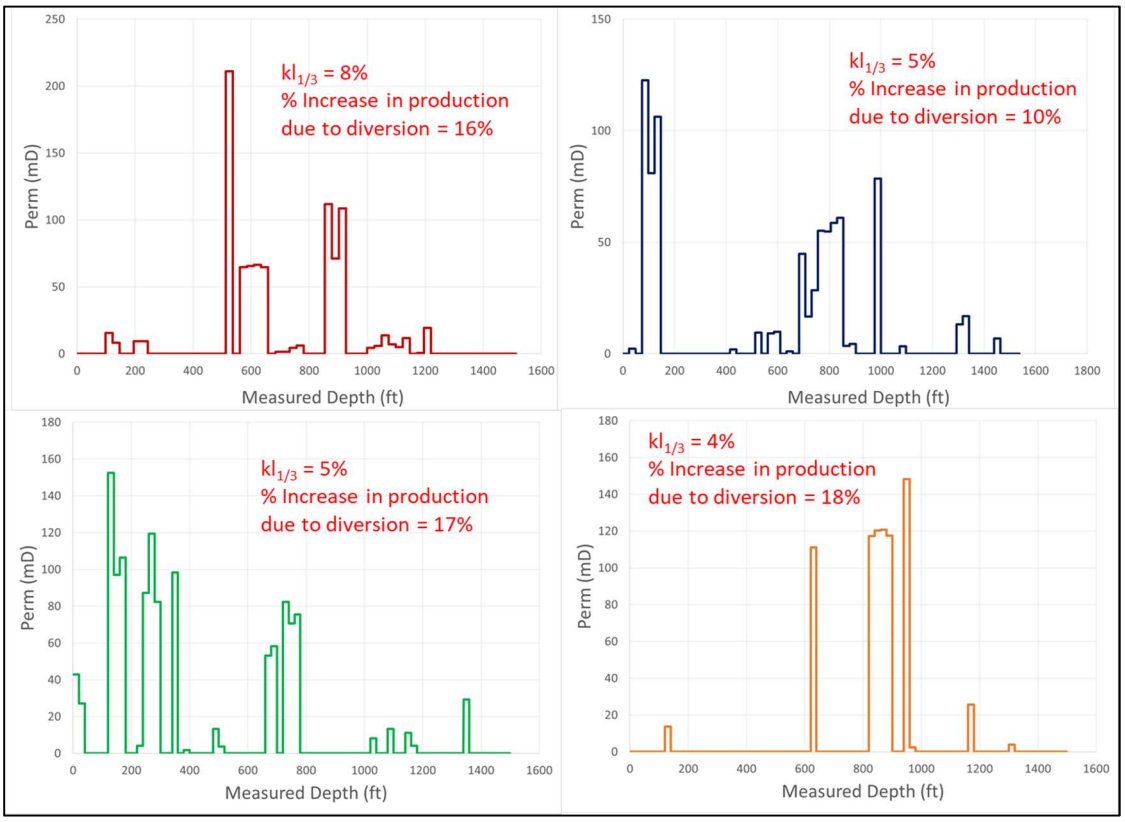

Figure 6-34: Examples of permeability profiles that led to diversion treatments being successful

6.5 Example 2: Mixed Lithology

In the previous example, we assumed that the lithology was consistently limestone. Based on descriptions of the North Field formation by several authors (Abou-Sayed et al., 2007, Clancey et al., 2009, Thabet et al., 2009), the North Field reservoir that we are simulating has laminations of dolomite and limestone, see Figure 6-3. The lithology has a significant impact on the acid efficiency parameters that are used to estimate the size of the acid induced wormholes. Figure 6-35 shows how different the optimal pore volume to breakthrough and interstitial velocity can be in the two lithologies.

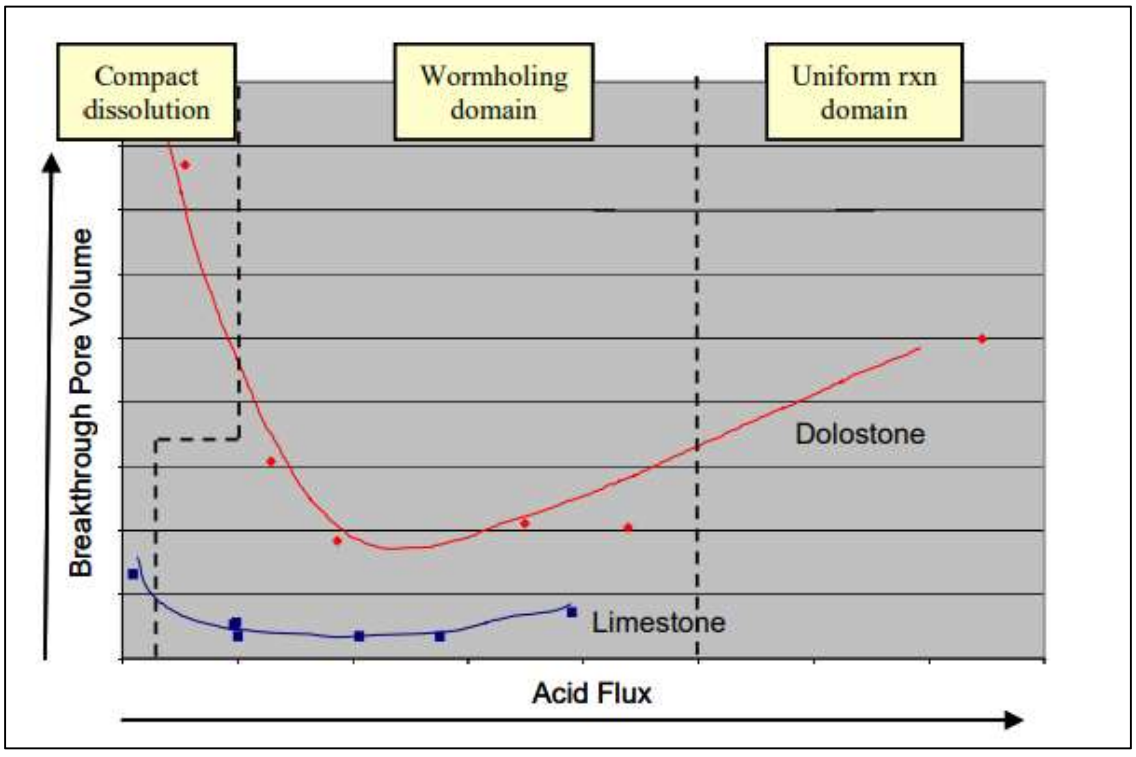

Figure 6-35: Acid efficiency curves for different lithology based on North Field Cores (Adapted from Abou-Sayed 2007)

This could have a significant impact on the diversion treatment. Since acid creates wormholes more efficiently in limestone than in dolomite, it could lead to preferential acid flow into limestone regions. This could leave long sections of dolomite, some which may even have significant permeability with little to no stimulation.

6.5.1 Problem Description

In this example, the impact of varying lithology was investigated by applying relevant acid efficiency data when determining the skin profile along the well.

Table 6-7 shows the optimal acid efficiency parameters that were used in this example. For limestone, the data from Table 4-5 were averaged; and the data for dolomite was taken from Ali and Nasr-El-Din (2018).

Please note that the acid efficiency parameters relating to limestone (Table 4-5) were based on limestone cores that were assumed to be analogous to Middle Eastern limestone formations. In the absence of any Middle Eastern dolomite acid efficiency parameters, we have used acid efficiency data from published data for Silurian dolomite.

Table 6-7: Optimal acid efficiency parameters used for wormhole propagation calculations

Lithology	Optimal Pore Volume to Break Through	Optimal Interstitial Velocity
	$PV_{bt\text{-}opt}$	$V_{i\text{-}opt}$
		cm/min
Limestone	1.13	1.76
Dolomite	3.30	3.29

We are told that the limestone and dolomite in this field are often laminated in inter-bedded layers (Abou-Sayed 2007). The thickness of these layers vary from well to well on the same platform. In this example, we assumed a simple distribution of the two lithologies; we assumed that they alternate every 100ft of vertical depth (174ft measured depth) as shown in Figure 6-36.

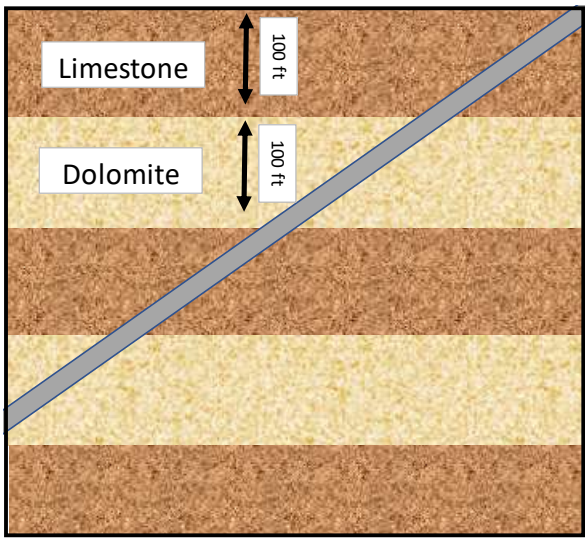

Figure 6-36: Lithology distribution for this example

In this example, we used the same permeability profiles that were generated in the last example. We are using the same well locations and well data, so these realizations are applicable to this case. There is no need to re-create variograms or carry out additional sequential indicator simulations (SIS) for a number of iterations, unless the cumulative average optimal diverter batch size does not converge within an acceptable tolerance. The simulation parameters in Table 6-5 were used with the acid efficiency parameters from Table 6-7.

6.5.2 Results

Figure 6-37 shows the cumulative average of the batch sizes for this example. Similar to the pure limestone example, the cumulative average converged within ±10lb after eighty iterations. Additionally, the optimal batch size did not vary from the previous example when there was pure limestone.

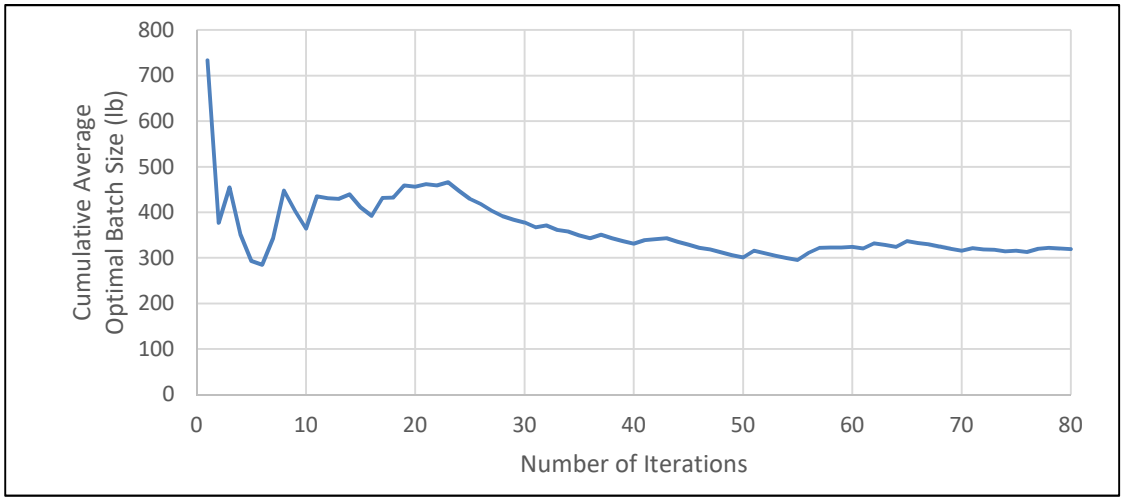

Figure 6-37: Example 2 cumulative average optimal batch size versus number of iterations

Figure 6-38 shows a histogram of the results. Like the previous example, the mode was similar to the mean, and a majority of the results (64%) were within the range of 0-410 lb. However, the optimal batch size is more scattered about the mode in this case i.e. there are more cases that require larger diverter batch sizes to obtain the maximum cumulative production. Moreover there are some cases where diversion resulted in a larger improvement in production when there was pure limestone as compared to when there was a mixed lithology (an example of this is shown and discussed in the following subsection: Discussion). Several publications simply list the presence of mixed lithology as a reason for requiring diversion treatments. Intuitively, one might expect this to be true since the lithology impacts where acid naturally tends to enter the formation. However, this was not so for many of the realizations studied in this example. The upcoming sections (Discussion and Relationship Between Permeability, Lithology and Diverter Usefulness) discuss the conditions where the presence of a second lithology make diversion useful.

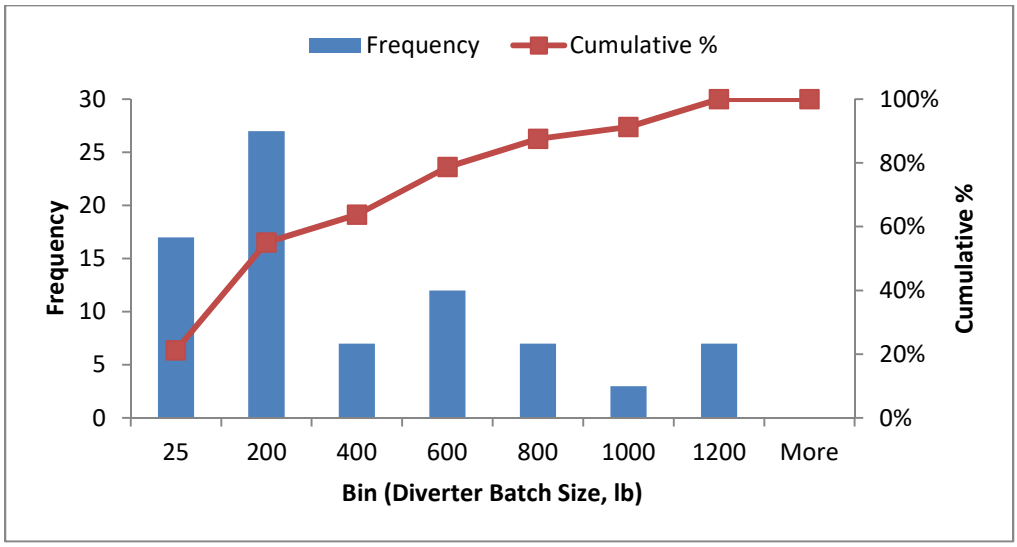

Figure 6-38: Example 2 histogram of optimal diverter batch sizes

6.5.3 Discussion

To understand, why having a mixed lithology did not create a greater need for diversion in this case, consider one of the permeability realizations that is shown in Figure 6-39 below. If we assume that the lithology was pure limestone, diversion could improve the 3yr cumulative production by 6.1%, but when we assume that there is both limestone and dolomite, distributed as discussed earlier, diversion does not improve the cumulative production of the well.

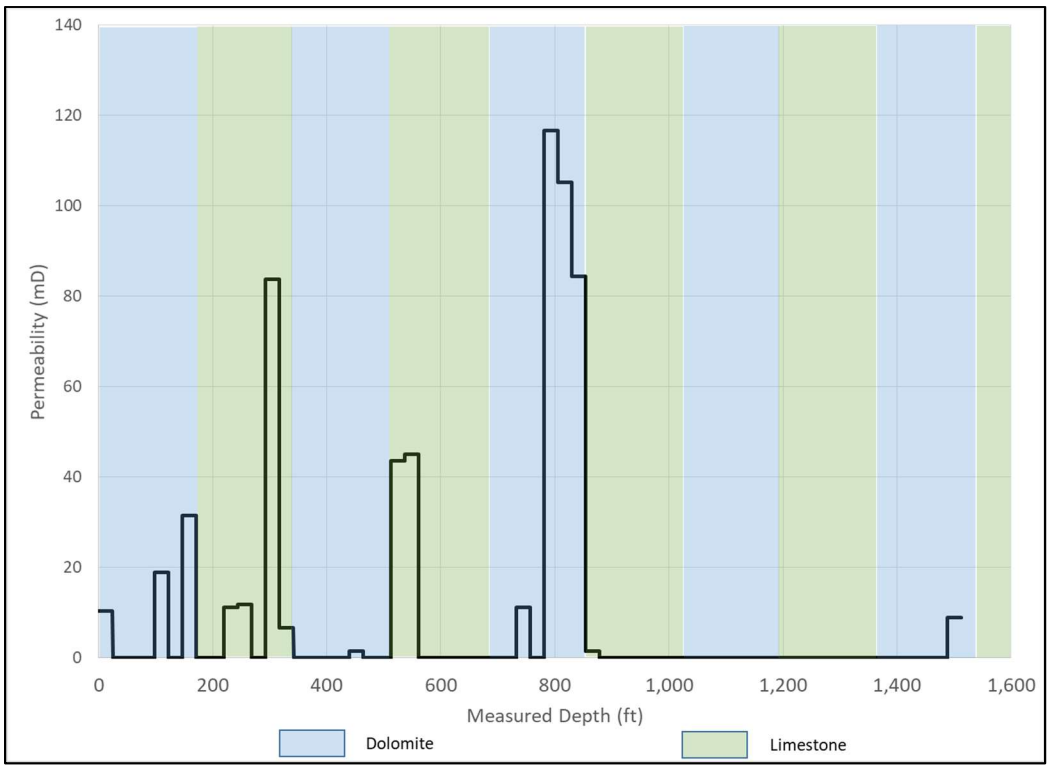

Figure 6-39: Example of a near wellbore permeability realization of the well

Figure 6-40 shows the skin profile that was created when no diverter was used on the well with the permeability profile described by Figure 6-39. Figure 6-40 also shows

the skin profile if the well did not have a mixed lithology, i.e., if the well had pure limestone as in example 1.

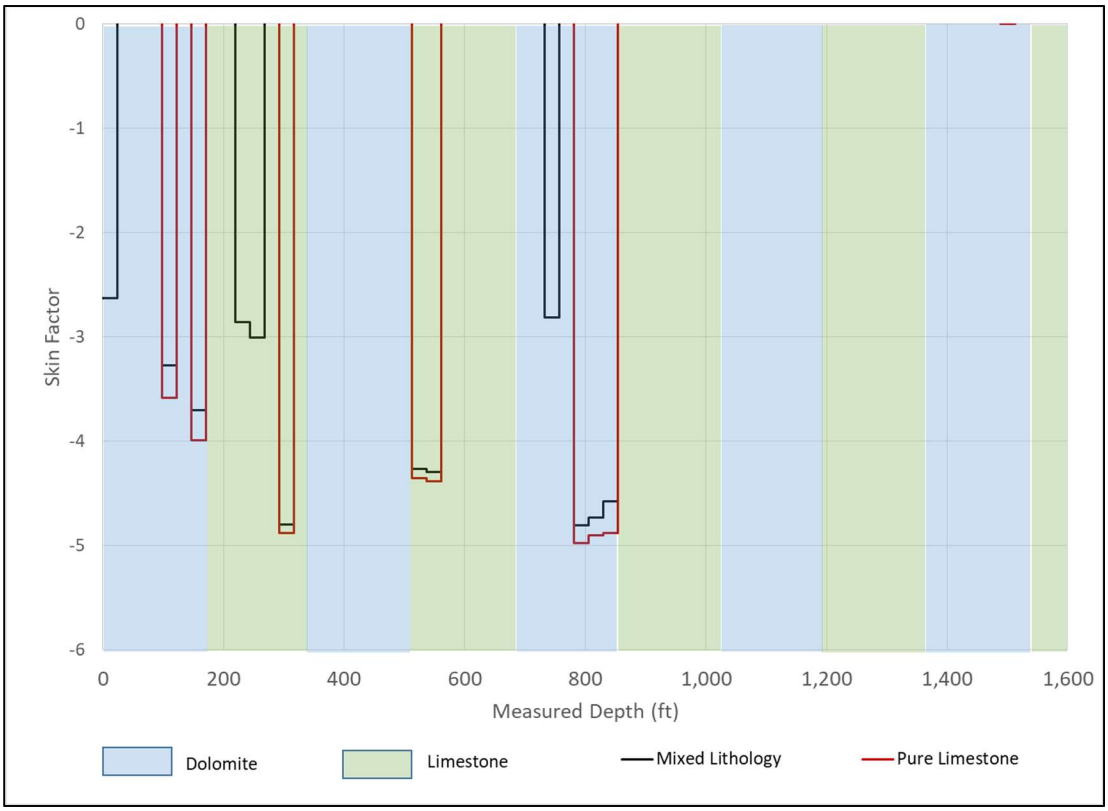

Figure 6-40: Example of a skin profile of the well with mixed lithology when no diverter is used

Figure 6-40 shows that when we assume a mixed lithology along the well, there are several zones that were treated that would not have been treated if we assumed a constant lithology along the well. In this case, the highest permeability streak was within a dolomite zone (see Figure 6-39). Though the flow rate into the reservoir is highest in the high permeability zone, since the acid efficiency is low in the high permeability zone, the skin

factor is limited. This allows several other zones to be treated without diverter being applied and explains why the use of diverter was less effective in this case.

This case demonstrates that it is not only important if there are multiple lithologies but what their permeability is, this issue is further investigated using more examples in section 6.5.

6.6 Relationship between Permeability, Lithology and Diverter Usefulness

In the example presented earlier, the lithology was layered in equally spaced sections (100ft of vertical depth). Thus, there was no relationship between the lithology and the permeability. In many cases, there is a relationship between lithology and permeability. The diagenesis process of dolomitization very often has distinct impacts on both the porosity and permeability, leading the dolomite zones to either be much higher or lower permeability than the neighboring limestone sections. For example, when calcium carbonate in the form of calcite is replaced by dolomite, magnesium ions are incorporated into the crystal lattice, while calcium ions are released. The equation can be expressed as seen in Eq. 6-7.

$$2CaCO_3 + Mg^{2+} \rightarrow CaMg(CO_3)_2 + Ca^{2+} \quad (6\text{-}7)$$

Because of the difference in the size of the calcium and magnesium ions, there is a reduction in the size of the solid minerals which increases the porosity by 13% (Chen et al., 1985) and, by extension, increases the permeability. The North Field, Qatar reservoir

that was used in this study is an example of a reservoir that contains high permeability dolomite, see Figure 6-27, the high permeability streak shown is dolomite (labelled as 'DS').

On the contrary, carbonate ions are also commonly supplied in the dolomitizing fluid; therefore, an alternate dolomitization model can be expressed by Eq. 6-8.

$$CaCO_3 + Mg^{2+} + CO_3^{2-} \rightarrow CaMg(CO_3)_2 \quad (6\text{-}8)$$

If dolomitization occurs through the reaction shown above, the volume of solid minerals increases by 75% (Saller and Henderson, 1998), this significantly decreases the porosity and permeability compared to the parent limestone.

Furthermore, even when all of the limestone precursors have been dolomitized, additional dolomite can still be precipitated in the pores directly from the fluid according to Eq. 6-9. This process is called over-dolomitization (Halley and Schmoker, 1983). The precipitated dolomite acts like a cement, filling the pores and reducing the formation's porosity and permeability.

$$Ca^{2+} + Mg^{2+} + 2CO_3^{2-} \rightarrow CaMg(CO_3)_2 \quad (6\text{-}9)$$

Hence, it is very plausible and common to have dolomite facies that are either very high or very low permeability relative to the neighboring limestone facies. If the dolomite zones are either high or low permeability with respect to the neighboring limestone zones,

there could be an impact on the effectiveness of the diversion treatment. For instance, consider the permeability profile shown in Figure 6-41 below; let us consider that all of the low permeability zones (<10mD) were dolomite but that the high permeability zones were limestone.

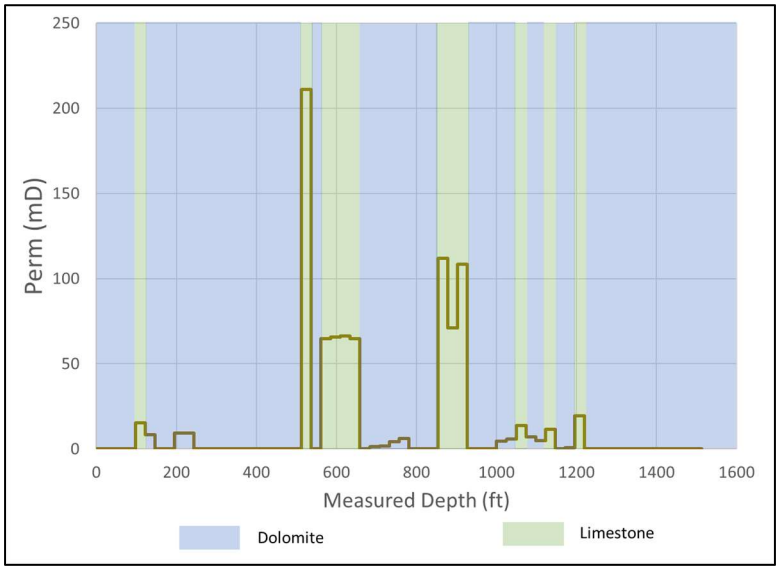

Figure 6-41: An example of a permeability profile realization with low permeability dolomite zones

This configuration of the lithology results in a diversion treatment that improves the 1yr cumulative well production by 17.9%. On the other hand, if all of the high permeability zones were dolomite instead (and all of the low permeability zones, <10mD, were limestone), then diversion only improves the 1yr cumulative production by 6.8%. When the high permeability zones are limestone, larger volumes of the acid flow into the limestone zones because of its higher reactivity and permeability. This leads to several other zones which could potentially contribute to the well's production being under or

unstimulated. The use of diversion helps to redistribute flow along the well and improves the well's connection with the reservoir porosity. In the case that the high permeability zones are dolomite, even without using chemical diversion, the higher reactivity of the limestone formation facilitates more uniform distribution of acid. Thus, diversion treatments are less effective.

This phenomenon can be seen in Figure 6-42. The plot compares the acid distribution along the well when only acid is used to stimulate the well (i.e., no diverter). The plot demonstrates that even without diverter, more acid tends to flow into low permeability zones if the high permeability zones are dominated by dolomite (see the two circled zones). When acid flows into a limestone formation it forms wormholes more efficiently, this lowers the skin factor and encourages more acid to flow into the formation where the wormholes are formed. Thus more acid will tend to flow into low permeability limestone formations as opposed to low permeability dolomite formations. In the same way, for the high permeability zones, if the formation is dolomite, worm holing efficiency will be lower than if the high permeability zone was limestone. This will cause the wormholes to grow at a slower rate and less acid will flow into the high permeability dolomite formation as compared to if the same zone was made of limestone. This suggests that these formations, where the dolomite tends to be lower permeability, acid will not flow into the low permeability zone as easily and wells in these formations stand to benefit more from diversion treatments.

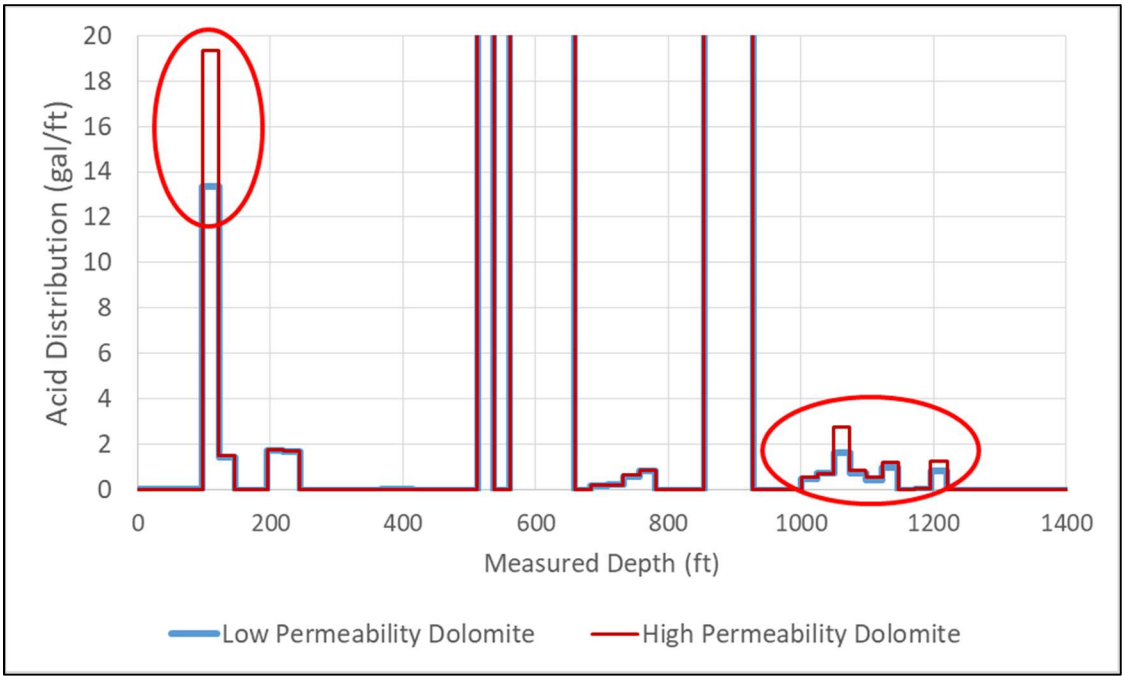

Figure 6-42: Acid distribution for the two lithology distributions when no diverter was applied

It should be noted that this trend still occurs even when there is not an initially high skin factor. In the examples that were carried out in this study there was significant formation damage (Van Vliet et al., 2011). An initial skin factor of 50 was used in the simulations; this skin factor was created by having a zone of impaired permeability around the well. A simulation was repeated to investigate the acid distribution along the well with the same permeability realization used in Figure 6-40 but with no formation damage. Figure 6-43 show the result of this simulation and shows that even without formation damage, when there is high permeability dolomite and low permeability limestone, more acid tends to flow into the formation at the zones of low permeability even without any diversion, though the differences in flow distribution shown are small.

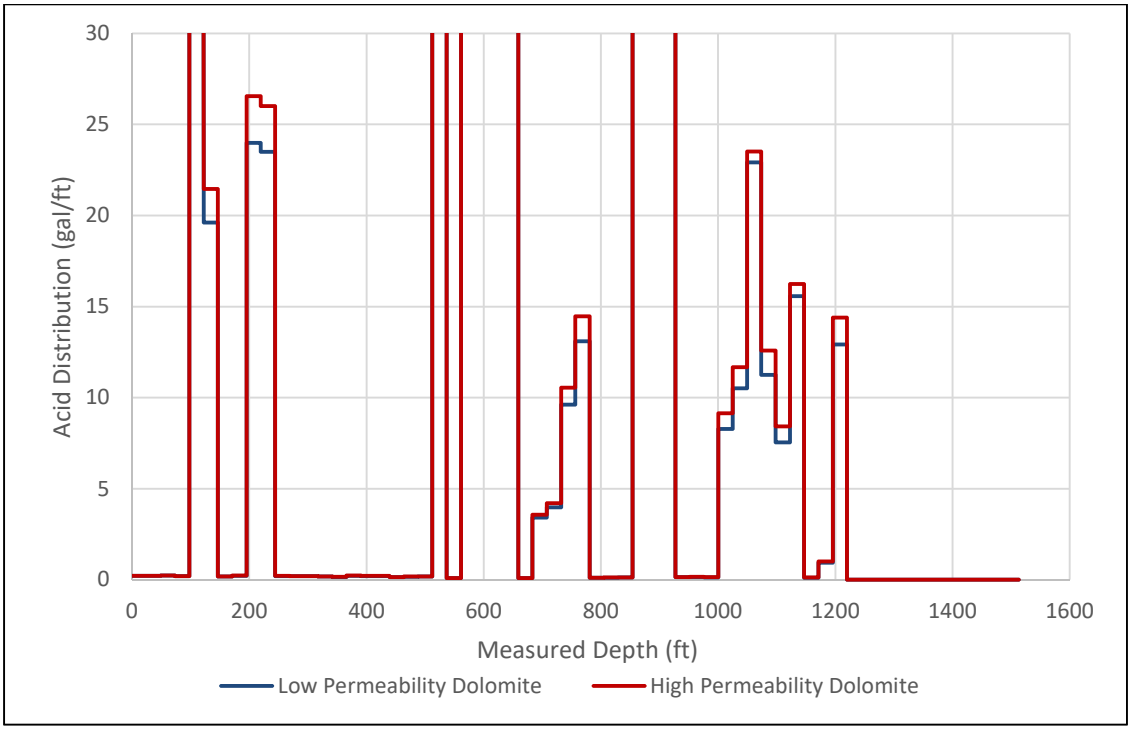

Figure 6-43: Acid distribution for the two lithology distributions when no diverter was applied and there is no formation damage

This trend has been observed for a number of different permeability profiles. Figure 6-44 shows four examples, including the example described above, where the low permeability zones (k<10mD) are dolomite while the high permeability zones (k>10mD) are limestone. In each case, diversion significantly increased the 1yr cumulative production.

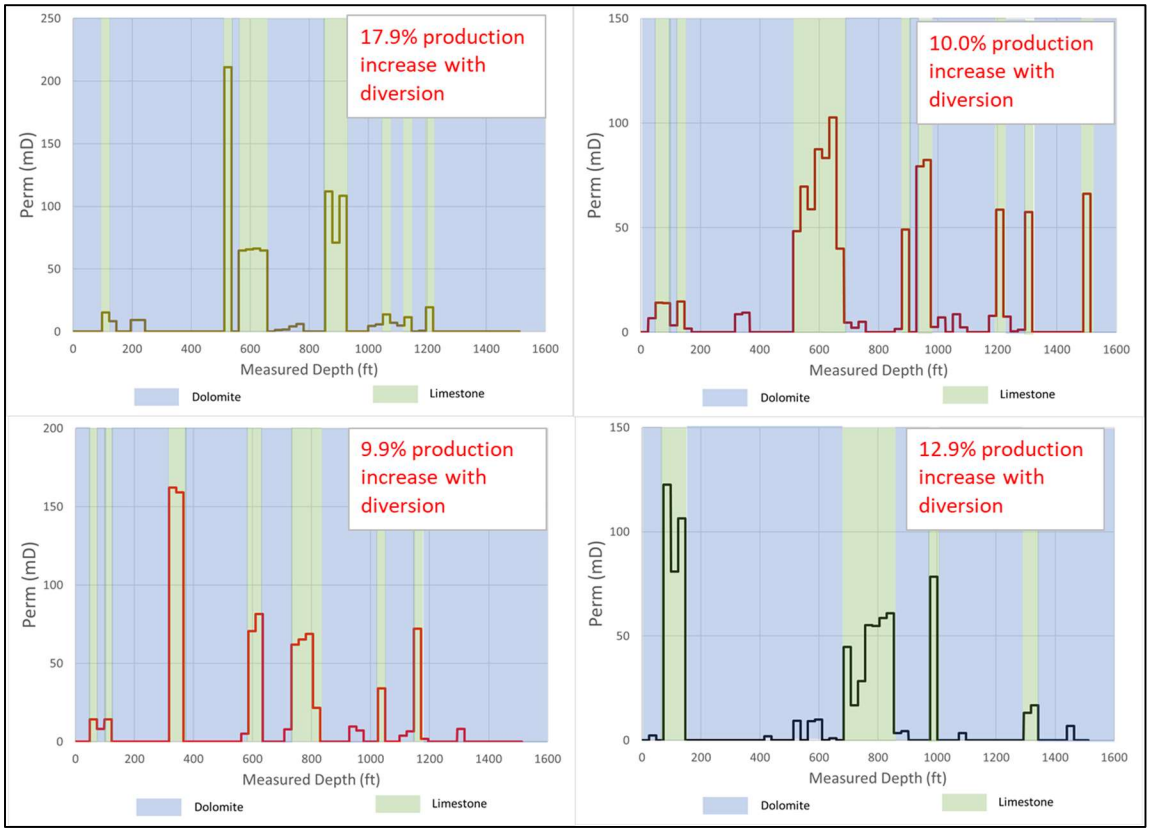

Figure 6-44: Examples of permeability profiles with low permeability dolomite

Figure 6-45 shows that when diversion is applied to the same permeability profiles, but where the dolomite zones were high permeability instead, there were significantly smaller increases in the cumulative production.

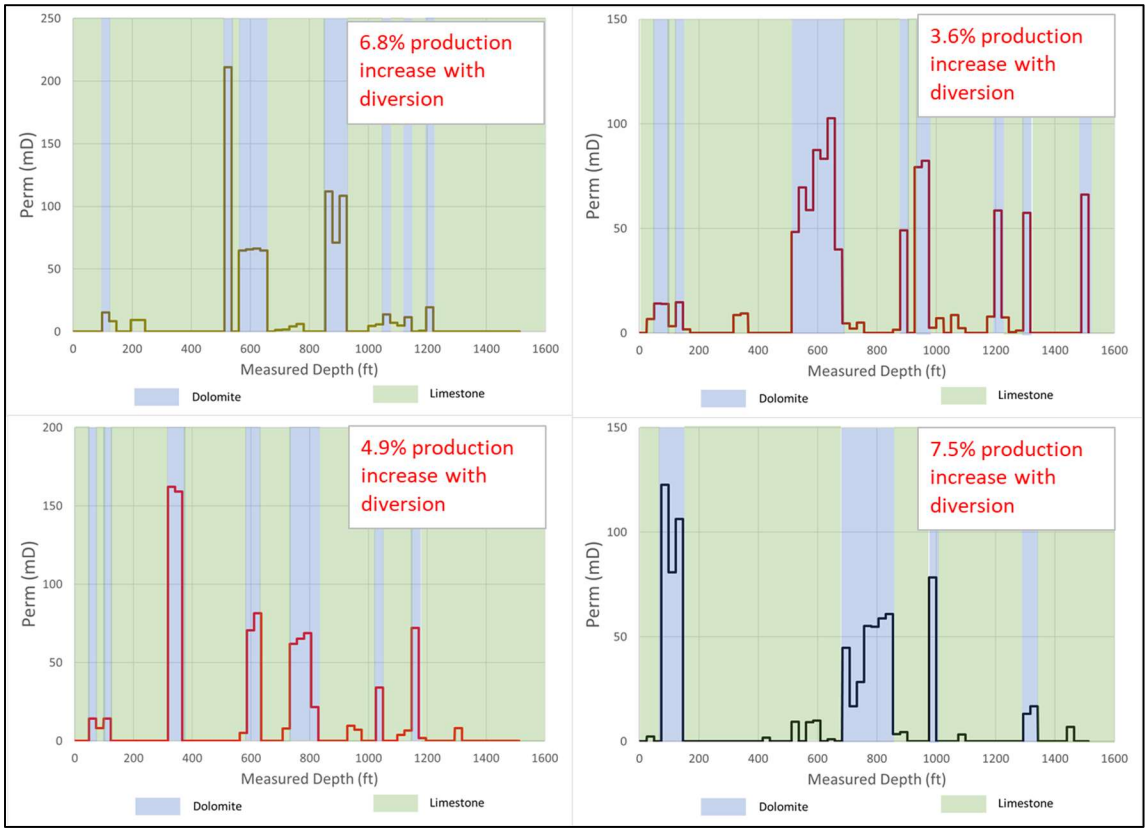

Figure 6-45: Examples of the same permeability profiles with high permeability dolomite

6.7 Abnormally Pressured Reservoirs

One issue that has not yet been discussed but can also play an important role in diversion is reservoir pressures. In thick carbonate reservoirs, the pressure drop between the wellbore and formation can vary significantly along the completed intervals for several reasons. For instance, uneven depletion in the reservoir can occur due to variability in permeability, unequal support by gas caps or water aquifers, or impermeable layers within the pay zone.

In the North Field, Qatar reservoir, which has been used for a number of examples and studies in this dissertation, it is difficult to fully stimulate wells that are completed in all of the layers of the reservoir because the different layers in the reservoir have different reservoir pressures (Postl et al., 2009, Whitson and Kuntadi 2005). There is an impermeable layer of anhydrite separating the bottom layer from the top zones. Many wells are completed in either the upper or lower sections of the reservoir only leading to different drainage rates and different reservoir pressures in the two sections. However, some of the wells are completed in the top and bottom zones. Chemical diversion has been successfully applied to overcome the issues of the differentially depleted reservoir (Shuchart et al., 2009).

Having differential drawdown pressures during stimulation and during production can lead to layers of the well not producing as much as it is capable of, despite having high permeability. During stimulation, it is easier to stimulate the lower pressure zones of the reservoir, but during well production, the higher pressured zones have larger

drawdown pressures and can be high producing zones. In these cases, it can be very important for the long-term productivity of the well to stimulate the well uniformly.

A simple example is used to illustrate how chemical diversion can be used to redistribute acid along a well in an abnormally pressured reservoir and thus provide a uniform treatment. Consider a well that has four zones; two of the zones are high permeability zones, and two are low permeability zones. The reservoir pressures are as described in Figure 6-46 below:

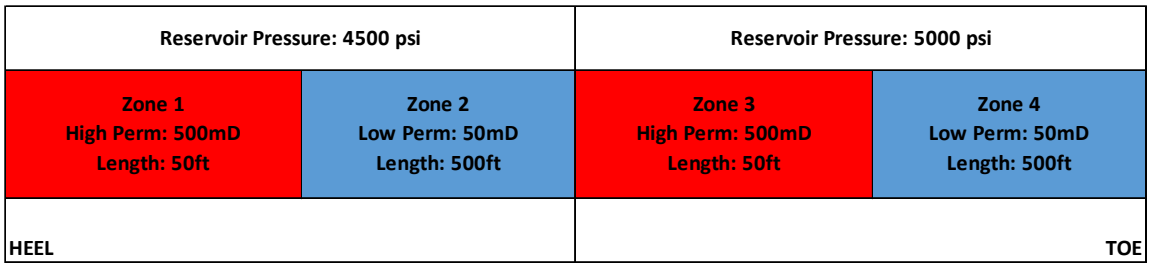

Figure 6-46: Example well with differential reservoir pressure

In this example, the difference between the acid injection pressure and the reservoir pressure was greater closer to the heel, where the reservoir pressure is 4500psi. However, during production, the difference between the reservoir pressure and the wellbore pressure was largest close to the toe, where the reservoir pressure is 5000psi. This makes the section closer to the heel easier to treat, but the section closer to the toe, more valuable to the production rate of the well. Table 6-8 shows the parameters that will be used to simulate a treatment of the reservoir using the near wellbore simulator, HWAS (Horizontal Well Acidizing Simulator).

Table 6-8: Parameters used in HWAS simulation of abnormal pressured reservoir

Parameters	Units	Value
Well Completion		Open Hole
Placement Method		Bullheading
Reservoir Type		Oil
Reservoir Fluid Viscosity	cP	1
Wellbore Radius	ft	0.29
Porosity		15%
PLA Concentration	lb/1000 gal	75
Damage Penetration	ft	1.5
Permeability Impairment Ratio		0.05
Specific Gravity of Diverting Agent		1.24
Acid Concentration in Pure Acid Stages		15%
Total Acid Injection Volume	bbl/ft	1.5
Total Diverting Agent	lb	346
Specific Cake Resistance	ft/lb	9.0e13
Optimal Pore Volume to breakthrough		0.5
Optimal Interstitial Velocity	cm/min	1.75

Figure 6-47 shows a comparison of the skin factor profiles for the well whether PLA diversion is used or not. Without diversion, only the section of the well closer to the heel that has a lower reservoir pressure was properly treated. The section of the well closer to the toe has a higher reservoir pressure and is thus more difficult to treat. The high

permeability streak is still treated but is does not achieve as low a skin factor as the high perm streak in the low reservoir pressure zone (-4 compared to -5.5). The low permeability section in the high pressure zone did not have its formation damage skin removed. On the contrary, when diversion is applied, most of the formation damage has been removed regardless of the reservoir pressure and the two high permeability zones obtain similar skin factors.

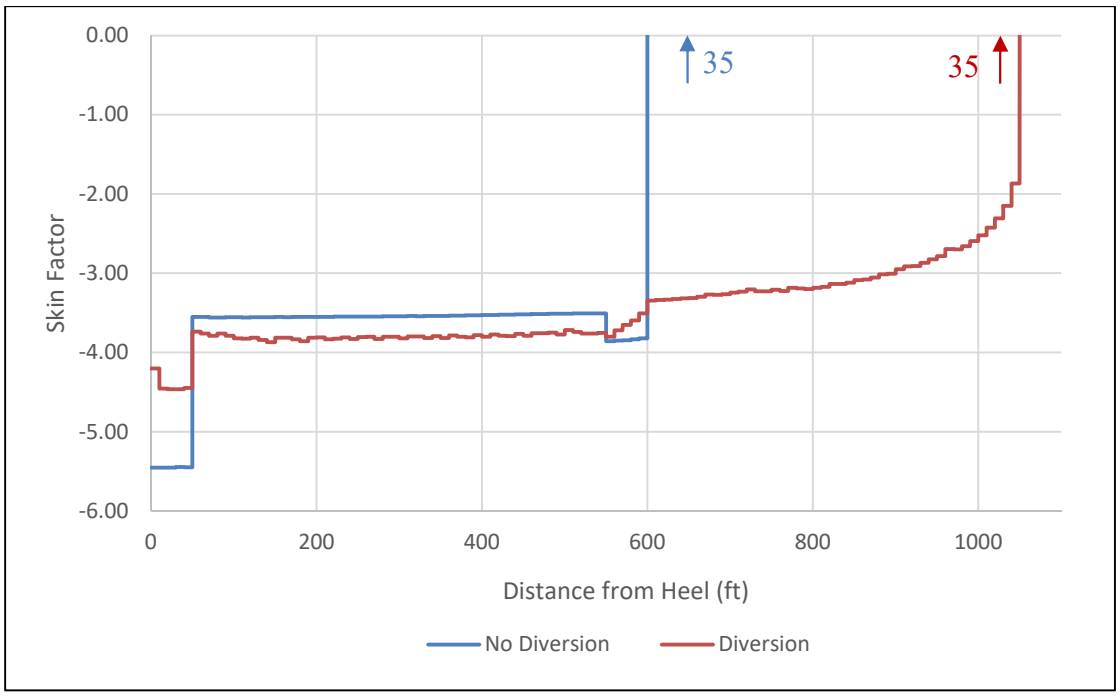

Figure 6-47: Skin factor profile for abnormal pressured reservoir example

When the well is produced with a bottom hole pressure of 4450psi (at the heel of the well), the well has a 44% higher production rate with diversion as compared to without. Figure 6-48 shows the production profile with respect to distance along the well. This figure shows that the low permeability zone with high reservoir pressure (600ft-1100ft)

was higher when diversion was applied, this allowed the well to have a higher production rate.

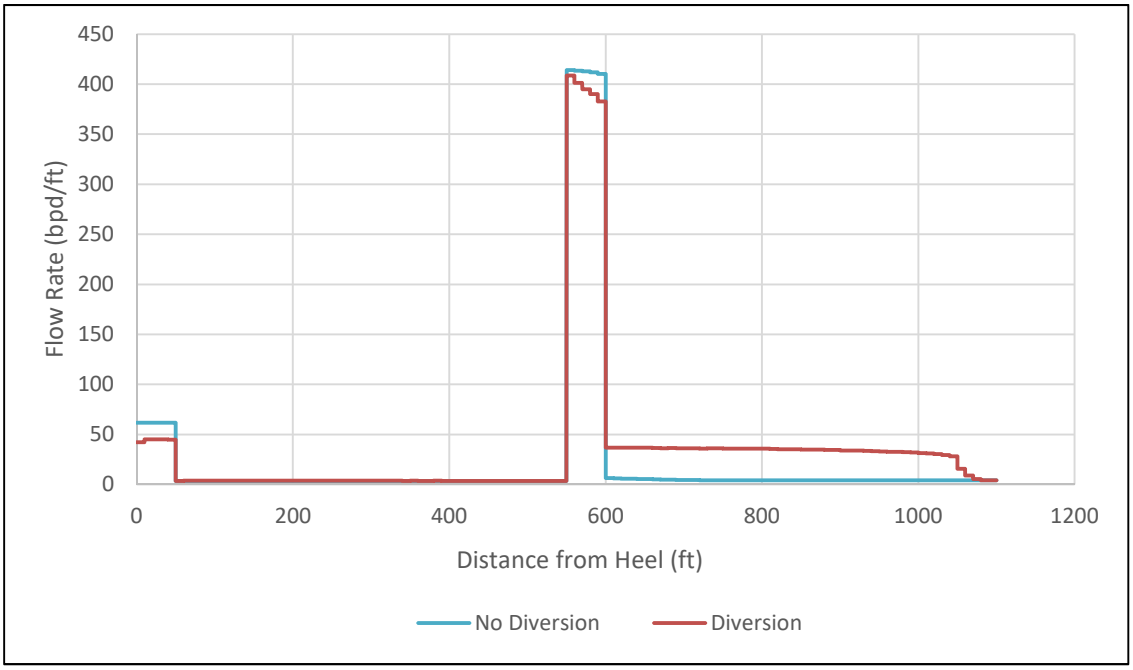

Figure 6-48: Production profile for abnormal pressured reservoir example

6.8 Conclusions

The method that has been proposed to determine the optimal batch size was implemented in an example reservoir that uses real well logs. The method was able to identify the most likely batch size, since the cumulative average optimal batch size converged within a tight tolerance. Furthermore, aside from being a useful tool for designing stimulation treatments, this tool has the potential for studying the effects of various design parameters on the value of diversion.

Having a large variation in the permeability or a mixed lithology along the well is not sufficient to deduce that applying chemical diversion could improve the well's long-term productivity. By investigating the effect of diversion on various permeability realizations using the PLA skin factor model, our near wellbore stimulation simulator, and a reservoir simulator, it has been shown that there are permeability and lithology trends that tend to result in effective diversion. When the permeability streaks are located close to the toe or if there are several equally sized permeability streaks along the well, diversion tends to be ineffective in increasing the well's cumulative production. When there are one or two high permeability streaks that are located away from the toe, the diversion treatment tends to be effective. If the high permeability streaks are limestone, as opposed to dolomite, the diversion treatment tends to be more effective in increasing the well cumulative production. Finally, diversion may be useful for improving the long-term productivity of a well if it is abnormally pressured, considering that the reservoir pressures may change or equalize over time. Diversion treatments can help ensure a uniform treatment along the well in these scenarios.

7. CONCLUSIONS

Some conclusions that can be drawn for this study are as follows:

- When PLA enters a wormhole, it creates pressure drop by forcing the fluid to flow in the rock matrix instead of flowing through the wormhole, provided that the PLA cake permeability is lower than the matrix permeability.
- The same mass of PLA creates a more uniform skin profile along the well if it forms a filter cake on the sand face, compared to if it enters the wormholes.
- Increasing the concentration or the diverter's specific cake resistance can create a more uniform skin profile, but it can come at the cost of worsening the total skin factor for the well.
- Using multiple diverter stages is better than applying all of the diverter in a single stage, as this allows an improved acid distribution and could facilitate higher acid injection rates in between diversion stages.
- Applying diversion to a well can improve the well's long term cumulative production by improving the well's connectivity to the reservoir porosity, even though it may worsen the total skin factor.
- Finding the average optimal diverter batch size for multiple possible and equally probable realizations of permeability profiles along the well is a viable method of designing a diversion treatment.
- For the well and reservoir that were investigated in the diverter batch optimization study, the optimal diverter batch size was approximated 320lb PLA.

- The presence of a large variation in the permeability or a mixed lithology along the well is not sufficient to deduce that applying chemical diversion will improve the well's long-term productivity.
- When the permeability streaks are located close to the toe, or if there are several equally sized permeability streaks along the well, diversion tends to be ineffective in increasing the well's cumulative production.
- When there are only one or two high permeability streaks that are located away from the toe, the diversion treatment tends to be effective.
- If the high permeability streaks are limestone, as opposed to dolomite, the diversion treatment tends to be more effective in increasing the well's cumulative production.
- Diversion may be useful for improving the long-term productivity of a well if the reservoir is abnormally pressured, considering that the reservoir pressures may change or equalize over time.

REFERENCES

Abou-Sayed, I., Shuchart, C. E., Choi, N. H., Clancey, B. M., & Bene, T. F. (2007, January 1). Well Stimulation Technology for Thick, Middle East Carbonate Reservoirs. International Petroleum Technology Conference. doi:10.2523/IPTC-11660-MS

Ahmed, Z., Al-Muhanna, D., A-Enezi, A., Prakash, R., Salem, A., & Mahmoud, W. (2018, January 29). High Rate Matrix Acidizing Technique Using Innovative Diverter Technologies to Restore and Improve Well Performance in North Kuwait Jurassic Gas NKJG. Society of Petroleum Engineers. doi:10.2118/189409-MS

Ali, M. T., & Nasr-El-Din, H. A. (2019, February 1). A Robust Model To Simulate Dolomite-Matrix Acidizing. Society of Petroleum Engineers. doi:10.2118/191136-PA

Alsaheb, R. A. A., Aladdin, A., Othman, N., Malek, R. A., Mei Leng, O., Aziz, R. & El Enshasy, H. (2015, January 1). Recent applications of polylactic acid in pharmaceutical and medical industries. Journal of Chemical and Pharmaceutical Research. 2015. 51-63.

Burton, R. C., Nozaki, M., Zwarich, N. R., & Furui, K. (2018, September 24). Improved Understanding of Acid Wormholing in Carbonate Reservoirs Through Laboratory Experiments and Field Measurements. Society of Petroleum Engineers. doi:10.2118/191625-MS

Chen, Y.H., Liu, Y. & Sun, S. (1985). Change for pore volume in dolomitization. Exp. Pet. Geol. 7, 29–37

Clancey, B. M., Manuel, M., Bene, T. F., Khemakhem, A. S. D., Garcia, E. M., & Benesch, J. M. (2008, January 1). Optimized Big Bore Gas Wells For Qatar North Field. International Petroleum Technology Conference. doi:10.2523/IPTC-12458-MS

Cohen, C. E., Tardy, P. M. J., Lesko, T. M., Lecerf, B. H., Pavlova, S., Voropaev, S. V., & Mchaweh, A. (2010, January 1). Understanding Diversion with a Novel Fiber-Laden Acid System for Matrix Acidizing of Carbonate Formations. Society of Petroleum Engineers. doi:10.2118/134495-MS.

Doerler, N., & Prouvost, L. P. (1987, January 1). Diverting Agents: Laboratory Study and Modeling of Resultant Zone Injectivities. Society of Petroleum Engineers. doi:10.2118/16250-MS

Eckerfield, L. D., Zhu, D., Hill, A. D., Robert, J. A., & Bartko, K. M. (2000, September 1). Fluid Placement Model for Horizontal-Well Stimulation. Society of Petroleum Engineers. doi:10.2118/65408-PA

Economides, M.J., Hill, A.D., Ehlig-Economides, E., Zhu, D. (2013) Petroleum Production Systems, second edition. New Jersey: Pearson Education, Inc.

Furui, K., Zhu, D., & Hill, A. D. (2002, January 1). A Rigorous Formation Damage Skin Factor and Reservoir Inflow Model for a Horizontal Well. Society of Petroleum Engineers. doi:10.2118/74698-MS

Furui, K., Burton, R. C., Burkhead, D. W., Abdelmalek, N. A., Hill, A. D., Zhu, D., & Nozaki, M. (2012, March 1). A Comprehensive Model of High-Rate Matrix-Acid Stimulation for Long Horizontal Wells in Carbonate Reservoirs: Part I--Scaling Up Core-Level Acid Wormholing to Field Treatments. Society of Petroleum Engineers. doi:10.2118/134265-PA.

Ghommem, M., Qiu, X., Brady, D., Al-Tajar, F., Crary, S., & Mahjoub, A. (2016, September 26). Monitoring of Matrix Acidizing by Using Resistivity Measurements. Society of Petroleum Engineers. doi:10.2118/181414-MS

Gonzalez, D., Ulloa, J., Safari, R., Al-Rawi, A., & Babey, A. (2017, November 13). State of the Art Biodegradable Diversion Technology Applied on Tight Carbonates Reservoir Leads to Maximized Production. Society of Petroleum Engineers. doi:10.2118/188632-MS

Glasbergen, G., Todd, B. L., Van Domelen, M. S., & Glover, M. D. (2006, January 1). Design and Field Testing of a Truly Novel Diverting Agent. Society of Petroleum Engineers. doi:10.2118/102606-MS

Glasbergen, G., Yeager, V. J., Reyes, R. P., & Everett, D. M. (2009, January 1). Fluid Diversion Monitoring: the Key to Treatment Optimization. Society of Petroleum Engineers. doi:10.2118/122353-MS

Grabski, E.R. (2012). Matrix Acidizing Core Flooding Apparatus: Equipment and Procedure Description. Master of Science, Texas A&M University, College Station.

Grace, H.P. (1953) Resistance and Compressibility of Filter Cake. Chemical Engineering Progress, 49, 303-318.

Guinn, J. H. & Wright, W. S. (1968, June 7) Well Treating Methods Using Temperature Surveys. US Patent No.: 3,480,079.

Hajj, J. A., Wilms, C., Delaney, P., Harami, K. K., Herms, A., & Garcia, G. D. (2009, January 1). The Continuous Improvement of Formation Evaluation Data Assurance. A Case Study from Offshore Qatar. International Petroleum Technology Conference. doi:10.2523/IPTC-13687-MS

Halley, R.B. & Schmoker, J.W. (1983). High-porosity Cenozoic carbonate rocks of south Florida: progressive loss of porosity with depth. AAPG Bull. 67, 191–200

Hong, K. C., & Millhone, R. S. (1977, December 1). Injection Profile Effects Caused by Gravity Segregation in the Wellbore. Society of Petroleum Engineers. doi:10.2118/6129-PA

Harrison, N. W. (1972, May 1). Diverting Agents-History and Application. Society of Petroleum Engineers. doi:10.2118/3653-PA

Hill, A. D., & Galloway, P. J. (1984, July 1). Laboratory and Theoretical Modeling of Diverting Agent Behavior. Society of Petroleum Engineers. doi:10.2118/11576-PA

Hill, A. D., Sepehrnoori, K., & Wu, P. Y. (1994, May 1). Design of the HCl Preflush in Sandstone Acidizing. Society of Petroleum Engineers. doi:10.2118/21720-PA

Hill, A. D., & Zhu, D. (1996, May 1). Real-Time Monitoring of Matrix Acidizing Including the Effects of Diverting Agents. Society of Petroleum Engineers. doi:10.2118/28548-PA

Huang, J., Safari, R., & Fragachan, F. E. (2018, October 16). Applications of Self-Degradable Particulate Diverters in Wellbore Stimulations: Hydraulic Fracturing and Matrix Acidizing Case Studies. Society of Petroleum Engineers. doi:10.2118/191408-18IHFT-MS

Jin, Y., Wan, Y. & Liu, Z. (2017, January 1). Surface polish of PLA parts in FDM using dichloromethane vapour. MATEC Web of Conferences. doi:10.1051/matecconf/20179505001.

Jones, A. T., & Davies, D. R. (1998, August 1). Quantifying Acid Placement: The Key to Understanding Damage Removal in Horizontal Wells. Society of Petroleum Engineers. doi:10.2118/50975-PA

Kalfayan, L. J., & Martin, A. N. (2009, January 1). The Art and Practice of Acid Placement and Diversion: History, Present State, and Future. Society of Petroleum Engineers. doi:10.2118/124141-MS

King, G. E., & Hollingsworth, F. H. (1979, January 1). Evaluation Of Diverting Agent Effectiveness And Cleanup Characteristics Using A Dynamic Laboratory Model - High Permeability Case. Society of Petroleum Engineers. doi:10.2118/8400-MS

Lagrone, K. W., & Rasmussen, J. W. (1962, January 1). Better Completion by Controlled Fracture Placement Limited-entry Technique. American Petroleum Institute.

Malik, A. R., Yaseen, A. H., Ogundare, T. M., Asiri, M. A., Younis, A. A., Driweesh, S. M., Shammari, N. S. & Ahmed, D. (2017, March 6). First Worldwide Successful Implementation of Coiled Tubing Compatible Novel Fiber Laden Diverter for Matrix Stimulation Using a New Generation High Rate Fiber Optic Real-Time Telemetry System. Society of Petroleum Engineers. doi:10.2118/183765-MS

Malik, A. R., Asiri, M. A., Ogundare, T. M., & Khalifa, M. (2018, January 29). Successful Implementation of Multi-Modal, Self-Assembling, Self-Degradable and Environmentally Friendly Solids Particulates as Diverter in Acid Stimulation Treatments in Carbonate Reservoirs. Society of Petroleum Engineers. doi:10.2118/189420-MS.

Matheron, G. (1965). The theory of Regionalized Variables and Its Applications. Paris School of Mines, Cah. Cent. Morphologic Math., Fontainbleau, France.

McLeod, H. O., & Coulter, A. W. (1969, August 1). The Stimulation Treatment Pressure Record An Overlooked Formation Evaluation Tool. Society of Petroleum Engineers. doi:10.2118/2287-PA

Mishra, V., Zhu, D., Hill, A. D., & Furui, K. (2007, January 1). An Acid Placement Model for Long Horizontal Wells in Carbonate Reservoirs. Society of Petroleum Engineers. doi:10.2118/107780-MS

Mogensen, K., & Hansen, J. H. (2007, January 1). A Dynamic Model for High-Rate Acid Stimulation of Very Long Horizontal Wells. Society of Petroleum Engineers. doi:10.2118/110135-MS

Chang, F. F., Qiu, X., & Nasr-El-Din, H.A. (2007, January 1). Chemical Diversion Techniques Used for Carbonate Matrix Acidizing: An Overview and Case Histories. Society of Petroleum Engineers. doi:10.2118/106444-MS

Nozaki, M., & Hill, A. D. (2010, August 1). A Placement Model for Matrix Acidizing of Vertically Extensive, Heterogeneous Gas Reservoirs. Society of Petroleum Engineers. doi:10.2118/124881-PA

Paccaloni, G. (1979, November 26). Matrix stimulation planning. Part 2. Field history verifies control, evaluation. Oil and Gas Journal, United States.

Paccaloni, G., & Tambini, M. (1993, March 1). Advances in Matrix Stimulation Technology. Society of Petroleum Engineers. doi:10.2118/20623-PA

Paccaloni, G. (1995, August 1). A New, Effective Matrix Stimulation Diversion Technique. Society of Petroleum Engineers. doi:10.2118/24781-PA

Petterson, O. (2006) Basics of Reservoir Simulation with the Eclipse Reservoir Simulator. Dept. of Mathematics, Univ. of Bergen

Postl, D., Ellison, T. K., Chang, D.-L., Shuchart, C. E., Mols, A. L., Nor, N., Al-Kharaz, H.A.R., Valle, A., Sieben, C.J., Chintaluri, R., Wang, Z., Sanchez, L., Farah, A. M. (2009, January 1). Optimization of Carbonate Stimulation based on Long-Term Well Performance Predictions. International Petroleum Technology Conference. doi:10.2523/IPTC-13622-MS

Prouvost, L.P., and Economides, M.J., (1987, May 1). Real Time Evaluation of Matrix Acidizing Treatments. Journal of Petroleum Science and Engineering, 1, No. 2, 145-154

Reddy, B. R., & Cortez, J. (2014, February 1). Activator Development for Controlling Degradation Rates of Polymeric Diverting Agents. Society of Petroleum Engineers. doi:10.2118/164117-PA.

Ruth, B.F., Montillon, G.H., Montonna, R.E. (January 1933) Studies in Filtration –I. Critical Analysis of Filtration Theory. Ind. Eng. Chem. 1933, 25(1), pp 76-82. doi: 10.1021/ie50277a018.

Safari, R., Shahri, M. P., Smith, C., & Fragachan, F. (2017, October 4). Analysis and Design Method for Particulate Diversion in Carbonate Acidizing. Society of Petroleum Engineers. doi:10.2118/187525-MS.

Saller, A.H. & Henderson, N. (2001). Distribution of porosity and permeability in platform dolomites: insight from the Permian of West Texas: reply. AAPG Bull. 85, 530–532.

Sasongko, H., Zhu, D., & Hill, A. D. (2011, January 1). Simulation of Acid Jetting Treatments in Long Horizontal Wells. Society of Petroleum Engineers. doi:10.2118/144200-MS

Sau, R., Shuchart, C., Clancey, B., Lecerf, B., & Pavlova, S. (2015, December 6). Qualification and Optimization of Degradable Fibers for Re-Stimulation of Carbonate Reservoirs. International Petroleum Technology Conference. doi:10.2523/IPTC-18352-MS.

Shuchart, C. E., Jackson, S., Mendez-Santiago, J., Choi, N. H., Montgomery, J. K., Khemakhem, A. S. D., Sieben, C. J., Clancey, B. M., Chintaluri, R., Farah, A. M. & Wang, Z. (2009, January 1). Effective Stimulation of Very Thick, Layered Carbonate Reservoirs Without the Use of Mechanical Isolation. International Petroleum Technology Conference. doi:10.2523/IPTC-13621-MS

Shahri, M. P., Huang, J., Smith, C. S., & Fragachán, F. E. (2016, November 7). Recent Advancements in Temporary Diversion Technology for Improved Stimulation Performance. Society of Petroleum Engineers. doi:10.2118/182883-MS

Shahri, M. P., Huang, J., Smith, C. S., & Fragachán, F. E. (2017, October 9). An Engineered Approach to Design Biodegradables Solid Particulate Diverters: Jamming and Plugging. Society of Petroleum Engineers. doi:10.2118/187433-MS

Shirley, R., & Hill, A. D. (2019, March 22). General Guidelines for Batch Treatments of Polylactic Acid for Diversion in Multistage Matrix Acidizing Treatments. International Petroleum Technology Conference. doi:10.2523/IPTC-19227-MS

Shirley, R. M., & Hill, A. D. (2019, March 29). Experimental Investigation of Particulate Polylactic Acid Diversion in Matrix Acidizing. Society of Petroleum Engineers. doi:10.2118/193565-MS

Taha, R., Hill, A. D., & Sepehrnoori, K. (1986, July 1). Simulation of Sandstone-Matrix Acidizing in Heterogeneous Reservoirs. Society of Petroleum Engineers. doi:10.2118/13218-PA

Taha, R., Hill, A. D., & Sepohrnoori, K. (1989, February 1). Sandstone Acidizing Design With a Generalized Model. Society of Petroleum Engineers. doi:10.2118/16885-PA

Tan, X., Payne, C., & Panga, M. (2018, February 7). Modeling the Effectiveness of Diverters for Matrix Acidizing Based on Filter Cake Characteristics. Society of Petroleum Engineers. doi:10.2118/189473-MS.

Thabet, E. A., Brady, M. E., Parsons, C. A., Byrne, S., Voropaev, S. V., Lesko, T. M., Mchaweh, A. (2009, January 1). Changing the Game In The Stimulation of Thick Carbonate Gas Reservoirs. International Petroleum Technology Conference. doi:10.2523/IPTC-13097-MS.

Van Domelen, M. S. (2017, March 27). A Practical Guide to Modern Diversion Technology. Society of Petroleum Engineers. doi:10.2118/185120-MS.

Van Vliet, J., Reid, A., Haibi, S., Ross, F., Hajj, J., & Wilms, C. (2011, January 1). Achieving Effective Acid Stimulation of Thick Carbonate Gas Reservoirs in Qatar's North Field. World Petroleum Congress.

Whitson, C. H., & Kuntadi, A. (2005, January 1). Khuff Gas Condensate Development. International Petroleum Technology Conference. doi:10.2523/IPTC-10692-MS

Willberg, D. and Dismuke, K. (2009, January 27). Self-destructing filter cake. US Patent No. 7,482,311.

Zhou, Z., & Rossen, W. R. (1995, March 1). Applying Fractional-Flow Theory to Foam Processes at the "Limiting Capillary Pressure." Society of Petroleum Engineers. doi:10.2118/24180-PA

Zhu, D., Hill, A. D., & da Motta, E. P. (1998, January 1). On-site Evaluation of Acidizing Treatment of a Gas Reservoir. Society of Petroleum Engineers. doi:10.2118/39421-MS